NACA RM A51G31a

NACA

RESEARCH MEMORANDUM

SUMMARY OF RESULTS OF A WIND-TUNNEL INVESTIGATION OF NINE RELATED HORIZONTAL TAILS

By Jules B. Dods, Jr., and Bruce E. Tinling

Ames Aeronautical Laboratory
Moffett Field, Calif.

NATIONAL ADVISORY COMMITTEE
FOR AERONAUTICS

WASHINGTON

October 12, 1951

NATIONAL ADVISORY COMMITTEE FOR AERONAUTICS

RESEARCH MEMORANDUM

SUMMARY OF RESULTS OF A WIND-TUNNEL INVESTIGATION OF NINE RELATED HORIZONTAL TAILS

By Jules B. Dods, Jr., and Bruce E. Tinling

SUMMARY

The results of a wind-tunnel investigation of a series of models of nine related horizontal tails have been summarized to provide basic design information; to indicate the effects of aspect ratio, sweepback, and changes in the Mach number; and to provide experimental values of the lift and hinge-moment parameters for comparison with values computed by a method employing lifting-surface theory. The models had aspect ratios from 2 to 6, angles of sweepback of the quarter-chord line from 5.7° to 45°, a taper ratio of 0.5, and had 30-percent chord, sealed, plain flaps. The Mach number was varied from 0.12 to 0.94 for Reynolds numbers of 2, 3, or 4 million. Also, a constant-chord airfoil having the NACA 64A010 section and completely spanning the wind tunnel was tested at a Mach number of 0.12. This airfoil had the same section and flap-chord ratio as the nine horizontal-tail models.

Satisfactory correlation was obtained between the low-speed experimental values of the lift and hinge-moment parameters and the computed values. Extension of the method employing lifting-surface theory to high subsonic Mach numbers through an application of the Prandtl-Glauert rule yielded variations of the lift parameters with Mach number which were in good agreement with the experimental results at Mach numbers less than that for lift divergence. The predicted values of the hinge-moment parameters, however, did not agree with the experimental results at Mach numbers approaching the divergence Mach number.

INTRODUCTION

An investigation of the aerodynamic characteristics of horizontal tails has been undertaken by the NACA to provide basic design information

and to provide experimental results which could be used to determine the accuracy of theoretical procedures for estimating the lift and hinge-moment parameters. References 1, 2, and 3 have presented detailed results of tests, conducted in the Ames 7- by 10-foot wind tunnels and the Ames 12-foot pressure wind tunnel, of a series of horizontal-tail models having aspect ratios from 2 to 6 and either having the hinge line normal to the plane of symmetry or having 35° or 45° of sweepback of the quarter-chord line. A comparison of the lift and hinge-moment parameters evaluated from theory with those obtained experimentally was presented in reference 4.

The purposes of the present report are: to combine the basic design information available in references 1, 2, and 3; to summarize the experimental and the theoretical variations of the lift and hinge-moment parameters with aspect ratio and sweepback at a low Mach number; and to show the effects of changes of the Mach number on these parameters for three of the models.

NOTATION

Coefficients

C_{h_e} elevator hinge-moment coefficient $\left(\frac{\text{elevator hinge moment}}{2qM_A}\right)$

c_{h_e} section hinge-moment coefficient $\left(\frac{\text{section hinge moment}}{q(c_e')^2}\right)$

C_L lift coefficient $\left(\frac{\text{lift}}{qS}\right)$

c_l section lift coefficient $\left(\frac{\text{section lift}}{qc}\right)$

$\frac{\Delta p}{q}$ pressure coefficient across the elevator nose seal

$$\left(\frac{\text{pressure below seal - pressure above seal}}{\text{free-stream dynamic pressure}}\right)$$

Symbols

A aspect ratio $\left(\frac{2b^2}{S}\right)$

a speed of sound, feet per second

b lateral dimension of the semispan models, measured perpendicular to the plane of symmetry, feet

b' lateral dimension of the constant-chord model, feet

c chord of the models measured parallel to the plane of symmetry, feet

c' chord of the models measured perpendicular to the sweep reference line of the swept-back models (c' equivalent to c for the unswept models), feet

$\bar{c}$ mean aerodynamic chord $\left(\frac{\int_0^b c^2 dy}{\int_0^b c\, dy}\right)$, feet

c_e' chord of the elevator behind the hinge line measured perpendicular to the hinge line, feet

M Mach number $\left(\frac{V}{a}\right)$

M_A moment about the hinge line of the elevator area behind the elevator hinge line, feet cubed

q free-stream dynamic pressure, pounds per square foot

R Reynolds number $\left(\frac{\rho V \bar{c}}{\mu}\right)$

S semispan horizontal-tail area, square feet

V velocity of air, feet per second

y lateral distance normal to the plane of symmetry, feet

α corrected angle of attack, degrees

α_o corrected section angle of attack, degrees

α_u uncorrected angle of attack, degrees

δ_e elevator deflection measured in a plane normal to the elevator hinge line, degrees

δ_t tab deflection measured in a plane normal to the tab hinge line, degrees

Λ angle of sweepback of line joining quarter-chord points of wing section, degrees

λ taper ratio (ratio of tip chord to root chord)

μ absolute viscosity, slugs per foot-second

ρ density of air, slugs per cubic foot

Parameters

$$C_{h_\alpha} = \left(\frac{\partial C_{h_e}}{\partial \alpha}\right)_{\delta_e=o} ; \quad c_{h_{\alpha_o}} = \left(\frac{\partial c_{h_e}}{\partial \alpha_o}\right)_{\delta_e=o} \quad \text{(measured through } \alpha=0 \text{ or } \alpha_o=0)$$

$$C_{h_\delta} = \left(\frac{\partial C_{h_e}}{\partial \delta_e}\right)_{\alpha=o} ; \quad c_{h_\delta} = \left(\frac{\partial c_{h_e}}{\partial \delta_e}\right)_{\alpha_o=o} \quad \text{(measured through } \delta_e=0)$$

$$C_{L_\alpha} = \left(\frac{\partial C_L}{\partial \alpha}\right)_{\delta_e=o} ; \quad c_{l_{\alpha_o}} = \left(\frac{\partial c_l}{\partial \alpha_o}\right)_{\delta_e=o} \quad \text{(measured through } \alpha=0 \text{ or } \alpha_o=0)$$

$$C_{L_\delta} = \left(\frac{\partial C_L}{\partial \delta_e}\right)_{\alpha=o} ; \quad c_{l_\delta} = \left(\frac{\partial c_l}{\partial \delta_e}\right)_{\alpha_o=o} \quad \text{(measured through } \delta_e=0)$$

The subscripts outside of the parentheses represent the factors held constant for the measurement of the parameters.

MODELS

The horizontal-tail models tested during this investigation each had a taper ratio (ratio of tip chord to root chord) of 0.5. The aspect ratios, angles of sweepback, and elevator hinge locations for these models are given in the following table:

Aspect ratio	Sweepback (deg)		Hinge-bracket location, percent semispan	
	Reference line	Hinge line	7- by 10-foot wind-tunnel models	12-foot pressure wind-tunnel models
2	16.7	0	82	- - - - - - -
2	45.0	35.1	82	- - - - - - -
3	11.3	0	82	- - - - - - -
3	35.0	26.6	82	- - - - - - -
3	45.0	38.7	--	50.2 and 90.6
4.5	7.6	0	82	28, 81 and 95
4.5	35.0	29.5	82	34, 80 and 96
6	5.7	0	82	- - - - - - -
6	35.0	31.0	38 and 82	- - - - - - -

The geometry of each model is shown in figure 1. In addition to the horizontal-tail models, a 3-1/2-foot-chord airfoil with no sweepback that completely spanned the 7-foot dimension of the 7- by 10-foot wind tunnel was tested. This airfoil had the NACA 64A010 section and a 30-percent-chord, sealed, plain flap. The coordinates of the NACA 64A010 airfoil section are presented in table I. The horizontal-tail models which had no sweepback of the hinge line had the NACA 64A010 section parallel to the plane of symmetry. The horizontal-tail models which had either 35° or 45° of sweepback had this section perpendicular to the sweep reference line. The sweep reference line was chosen as that line which joined the quarter-chord points of the NACA 64A010 airfoil sections. The models with the hinge line normal to the plane of symmetry (referred to in this report as the unswept models) had some sweepback of the sweep reference line. To be strictly consistent, the NACA 64A010 airfoil sections should have been placed normal to the sweep reference lines of the unswept models. However, since the angle of sweepback involved was small, the aerodynamic effects resulting from this inclination of the NACA 64A010 airfoil section to the sweep reference line were probably negligible.

The tip shape of each model was formed by rotating the airfoil section about a chord line inboard of the tip a distance equal to one-half the maximum thickness of the tip airfoil section.

All the models had 30-percent-chord, sealed, plain elevators and two of the models (fig. 1(e)) were equipped with tabs. The 30-percent-chord ratio of the elevator was maintained in the planes of the NACA 64A010 airfoil sections. The details of the elevator balance chambers are shown in figure 1. The elevator hinges divided the balance chamber into separate sections. Seals were fitted closely at the ends of each section to reduce the leakage to a minimum.

TESTS

Models of all the tails, with the exception of the tail having an aspect ratio of 3 and 45° of sweepback, were tested at low Mach numbers in the Ames 7- by 10-foot wind tunnels at a Reynolds number of 3 million. The tests in the Ames 12-foot pressure wind tunnel of the horizontal-tail models having an aspect ratio of 4.5 were conducted at a Reynolds number of 2 million, and the tests of the model having an aspect ratio of 3 and 45° of sweepback were conducted at a Reynolds number of 4 million. The maximum test Mach numbers were 0.88 and 0.94 for the unswept and the swept-back horizontal tails, respectively.

The semispan models were mounted vertically with the wind-tunnel floor serving as a reflection plane as shown for typical models in figure 2. The turntables upon which the models were mounted were directly connected to the force-measuring apparatus. The elevator hinge moments were measured with resistance-type electric strain gages which were beneath the turntable cover plates.

CORRECTIONS TO DATA

All the data have been corrected for the effects of tunnel-wall interference. The corrections to the data from the 7- by 10-foot wind tunnels were computed by the methods of references 5 and 6. The corrections to the data from the 12-foot pressure wind tunnel were computed by the methods of references 7 and 8. In the application of the method of reference 7, the theoretical span loadings for incompressible flow were calculated by the method of reference 9.

RESULTS AND DISCUSSION

The results of low-speed tests of the 3-1/2-foot-chord airfoil having the NACA 64A010 section and having a 30-percent-chord, sealed, plain flap are presented in figure 3. The results of tests of the nine related semispan model horizontal tails having the same airfoil section and differing only in aspect ratio and sweepback are presented in figures 4 to 20. The lift and hinge-moment characteristics are summarized in figures 21 to 24. The effectiveness of a tab in reducing the elevator hinge moments for a range of Mach numbers is presented in figure 25 for the models having aspect ratios of 4.5. An index of the figures presenting the results is given in the appendix.

Information not presented herein but which is available in references 1, 2, and 3 shows the effects of standard leading-edge roughness, the effects of removal of the elevator nose seal, the effects of variation of the Reynolds number, and the pitching-moment characteristics. In addition, the drag characteristics are available in references 2 and 3 for the three models tested in the 12-foot pressure wind tunnel. The pressure distribution at the midsemispan and the tab hinge moments have also been given in reference 2 for the two models having an aspect ratio of 4.5.

The following discussion covers first the effects of sweepback and aspect ratio at a low Mach number, and then the effects of changes of the Mach number for the three models which were tested throughout the subsonic Mach number range.

Effect of Sweepback and Aspect Ratio at Low Mach Numbers

Lift and hinge-moment parameters.- The data presented in figures 3 through 11 were obtained in the 7- by 10-foot wind tunnels. These results are summarized in figure 21 to show the effects of variations of sweepback and aspect ratio upon the lift parameters C_{L_α} and C_{L_δ}, and on the hinge-moment parameters C_{h_α} and C_{h_δ}. For convenience, the numerical values are also listed in table II. These data summarized in figure 21 and presented in table II were obtained at low subsonic Mach numbers. Because of the nonlinearities in the lift and hinge-moment data, the slope parameters are valid only for a small range of angles of attack and of elevator deflections near 0°. The theoretical values presented were calculated by the method recommended in reference 4. The correlation between the parameters as evaluated from theory and by experiment is considered to be reasonably good. As shown in figure 21, the lift and hinge-moment parameters have an orderly variation with

both aspect ratio and sweepback. The lift parameters C_{L_α} and C_{L_δ} increased as the aspect ratio was increased and were reduced in magnitude as the angle of sweepback became larger. The numerical values of the hinge-moment parameters C_{h_α} and C_{h_δ} became more negative with increasing aspect ratio. The numerical values of C_{h_α} also became more negative with increasing sweepback. The values of C_{h_δ}, however, were reduced in magnitude with increasing sweepback. The experimental lift and hinge-moment parameters from the Ames 12-foot pressure wind tunnel for Mach numbers comparable to those of the 7- by 10-foot wind tunnels are listed in table II. The lift and hinge-moment parameters from the Ames 12-foot pressure tunnel are in satisfactory agreement with those from the 7- by 10-foot wind tunnel with the exception of the value of C_{h_α} for the unswept model having an aspect ratio of 4.5. This difference between the values of C_{h_α} from the two facilities exists only at angles of attack near zero. Between 2° and 4° angle of attack, the value of C_{h_α} is -0.0020 from either wind tunnel (figs. 8(b) and 16(a)).

Pressure coefficients across the elevator nose seal.- The pressure coefficients across the elevator nose seal presented in parts (c) of figures 3 to 11 are useful in the design of sealed, internal, aerodynamically balanced elevators.[1] The rate of change of pressure coefficient across the elevator nose seal with elevator deflection was nearly independent of aspect ratio for both the unswept and the swept-back horizontal-tail models. A sizable difference was noted, however, in the rate of change of pressure coefficient across the elevator nose seal with elevator deflection between the unswept and the swept-back models. For example, it was about 25 percent less for the models with 35° of sweepback than for the models without sweep. From the limited information available for the 45° swept-back model it appears that an additional 15-percent reduction should be expected at this higher angle of sweepback. The models without sweepback having aspect ratios of 3, 4.5, and 6, and also the swept-back model having an aspect ratio of 6 tested in the 7- by 10-foot wind tunnels had abrupt losses of balancing pressures at moderate elevator deflections. (See figs. 6(c), 8(c), 10(c), and 11(c).) The reason for these losses of balancing pressure is not known. Tests in the 12-foot pressure tunnel of the models having aspect ratios of 4.5 did not show such an abrupt loss of balancing pressure. Attempts to explain this discrepancy have shown that it cannot be definitely ascribed to the difference in balance-chamber volumes or to the number of compartments in the balance chambers.

[1]For a discussion of the design procedure see reference 10.

Effects of Mach Number

The results of tests of three models in the Ames 12-foot pressure wind tunnel are presented in figures 12 to 20. The variations of the lift and hinge-moment parameters C_{L_α}, C_{L_δ}, C_{h_α}, and C_{h_δ} with Mach number are presented in figures 22 and 23. These figures also show the theoretical effects of compressibility on the lift and hinge-moment parameters calculated from the method recommended in reference 4, modified by application of the Prandtl-Glauert rule. The details of this procedure are given in reference 3.

Measurements of the static pressure on the walls of the tunnel test section taken during the tests of the model having an aspect ratio of 3 and 45° of sweepback indicated that for some test conditions the local Mach number was greater than 1.0 at the wall opposite the upper surface of the model. The data obtained under these conditions are indicated by dotted lines because their validity is questionable.

Lift.- The lift parameters C_{L_α} and C_{L_δ} are presented as functions of Mach number in figure 22. Comparison of the theoretical and experimental values of the lift parameters indicates good agreement up to the Mach number where a reduction in elevator or stabilizer effectiveness occurred with further Mach number increase. This Mach number will be referred to as the divergence Mach number.

The divergence Mach numbers for C_{L_α} were approximately 0.85 and 0.93 for the unswept and the 35° swept-back horizontal tails, respectively. The Mach number for divergence of the elevator-effectiveness parameter C_{L_δ} was approximately 0.85 for both the 35° swept-back and the unswept horizontal tails which had aspect ratios of 4.5. With further increase of Mach number, the rate of decrease of C_{L_δ} was much greater for the unswept horizontal tail than for the horizontal tail having 35° of sweepback. The lift-effectiveness parameters of the 45° swept-back horizontal tail having an aspect ratio of 3 continued to increase with increasing Mach number up to the maximum test Mach number, 0.94.

Hinge moment.- The variations of the hinge-moment parameters C_{h_α} and C_{h_δ} with Mach number are presented in figure 23. These data show that except for the horizontal tail having 45° of sweepback, application of the Prandtl-Glauert rule to calculate the hinge-moment parameters does not yield reliable results at the higher Mach numbers. For the two horizontal tails having an aspect ratio 4.5, the predicted variation with Mach number of C_{h_α} and C_{h_δ} does not agree with the test results at Mach numbers approaching that for lift divergence. It should also be noted (see figs. 16 and 19) that the measured values of

C_{h_α} and C_{h_δ} are not truly indicative of the hinge-moment characteristics at Mach numbers near that for divergence of the elevator-effectiveness parameter C_{L_δ}, since, at these Mach numbers, the slopes of the hinge-moment curves vary considerably with angle of attack and with elevator deflection.

The variations of the hinge-moment coefficient with Mach number for various elevator deflections or angles of attack are summarized in figure 24. These data show that the Mach numbers at which abrupt changes in the elevator hinge-moment coefficients occurred were dependent upon the angle of attack and the elevator deflection. Comparison of the data from tests of the three model horizontal tails indicates that an increase of sweepback delayed these abrupt changes to higher Mach numbers.

Balancing pressure coefficient across the elevator seal.- The variation of the pressure coefficient across the elevator nose seal with elevator deflection is shown in figures 14, 17, and 20. Measured through 0° elevator deflection, the rate of change of pressure coefficient across the elevator nose seal became greater with increasing Mach number. However, the range of elevator deflections for which the rate of change of pressure coefficient across the elevator nose seal with elevator deflection was markedly positive progressively diminished as the Mach number was increased. These results indicate that the balancing effect obtained from a sealed internal aerodynamic balance would become greater as the Mach number is increased. However, the range of elevator deflections for which a large balancing effect would be realized would diminish with increasing Mach number.

Tab effectiveness.- The tab-effectiveness data from tests of the horizontal tails having aspect ratios of 4.5 are summarized in figure 25 where the increment in elevator hinge-moment coefficient due to tab deflection is presented as a function of Mach number. These data show that, for 0° elevator deflection, the effectiveness of the tab was little affected by increases in the Mach number over the range investigated. At negative elevator deflections of 6° or greater, however, the tab was not effective when deflected more than 10° at a Mach number of about 0.88 for the unswept horizontal tail, and at a Mach number of about 0.94 for the horizontal tail with 35° of sweepback.

Ames Aeronautical Laboratory
National Advisory Committee for Aeronautics
Moffett Field, Calif.

APPENDIX

INDEX TO THE DATA IN THIS REPORT

LIFT AND HINGE-MOMENT CHARACTERISTICS

Model	Results presented	M	R (million)	Figure number
Two-dimensional	c_l vs α_o	0.12	3.0	3(a)
	c_{h_e} vs α_o			3(b)
	$\Delta p/q$ vs δ_e			3(c)
A,2;unswept	C_L vs α	.14		4(a)
	C_{h_e} vs α			4(b)
	$\Delta p/q$ vs δ_e			4(c)
A,2;Λ, 45°	C_L vs α			5(a)
	C_{h_e} vs α			5(b)
	$\Delta p/q$ vs δ_e			5(c)
A,3;unswept	C_L vs α	.17		6(a)
	C_{h_e} vs α			6(b)
	$\Delta p/q$ vs δ_e			6(c)
A,3;Λ,35°	C_L vs α			7(a)
	C_{h_e} vs α			7(b)
	$\Delta p/q$ vs δ_e			7(c)
A,4.5;unswept	C_L vs α	.21		8(a)
	C_{h_e} vs α			8(b)
	$\Delta p/q$ vs δ_e			8(c)
A,4.5;Λ, 35°	C_L vs α			9(a)
	C_{h_e} vs α			9(b)
	$\Delta p/q$ vs δ_e			9(c)

LIFT AND HINGE-MOMENT CHARACTERISTICS (CONTINUED)

Model	Results presented	M	R (million)	Figure number
A,6;unswept	C_L vs α	0.23	3.0	10(a)
	C_{h_e} vs α			10(b)
	$\Delta p/q$ vs δ_e			10(c)
A,6; Λ, 35°	C_L vs α			11(a)
	C_{h_e} vs α			11(b)
	$\Delta p/q$ vs δ_e			11(c)
A,3; Λ, 45°	C_L vs α	.25	4.0	12(a)
		.60		12(b)
		.80		12(c)
		.85		12(d)
		.90, .92		
		.94		12(e)
	C_{h_e} vs α	.25		13(a)
		.60		13(b)
		.80		13(c)
		.85		13(d)
		.90		13(e)
		.92, .94		13(f)
	$\Delta p/q$ vs δ_e	.25		14(a)
		.60		14(b)
		.80		14(c)
		.85		14(d)
		.90, .92, .94		14(e)
A.4.5;unswept	C_L vs α	.21	2.0	15(a)
		.60		15(b)
		.80		15(c)
		.85		15(d)
		.88		15(e)
	C_{h_e} vs α	.21		16(a)
		.60		16(b)
		.80		16(c)
		.85		16(d)
		.88		16(e)

LIFT AND HINGE-MOMENT CHARACTERISTICS (CONCLUDED)

Model	Results presented	M	R (million)	Figure number
A.4.5;unswept	$\Delta p/q$ vs δ_e	0.21	2.0	17(a)
↓	↓	.60	↓	17(b)
↓	↓	.80	↓	17(c)
↓	↓	.85	↓	17(d)
↓	↓	.88	↓	17(e)
A,4.5;Λ,35°	C_L vs α	.21	↓	18(a)
↓	↓	.60	↓	18(b)
↓	↓	.85	↓	18(c)
↓	↓	.90	↓	18(d)
↓	↓	.93	↓	18(e)
↓	↓	.94	↓	18(f)
↓	C_{h_e} vs α	.21	↓	19(a)
↓	↓	.60	↓	19(b)
↓	↓	.85	↓	19(c)
↓	↓	.90	↓	19(d)
↓	↓	.93	↓	19(e)
↓	↓	.94	↓	19(f)
↓	$\Delta p/q$ vs δ_e	.21	↓	20(a)
↓	↓	.60	↓	20(b)
↓	↓	.85	↓	20(c)
↓	↓	.90	↓	20(d)
↓	↓	.93	↓	20(e)
↓	↓	.94	↓	20(f)

SUMMARY FIGURES

Model	Results presented	Figure number
All	C_{L_α} and C_{L_δ} vs A	21(a)
All	C_{h_α} and C_{h_δ} vs A	21(b)
A,4.5;unswept	C_{L_α} and C_{L_δ} vs M	22
A,4.5;Λ, 35°		
A,3;Λ, 45°		
↓	C_{h_α} and C_{h_δ} vs M	23
	C_{h_e} vs M; $\delta_e = 0°$	24(a)
	C_{h_e} vs M; $\alpha = 0°$	24(b)
A,4.5; unswept	ΔC_{h_e} due to tab deflection vs M	25
A,4.5; Λ, 35°		

REFERENCES

1. Dods, Jules B., Jr.: Wind-Tunnel Investigation of Horizontal Tails.

   I - Unswept and 35° Swept-Back Plan Forms of Aspect Ratio 3. NACA RM A7K24, 1948.

   II - Unswept and 35° Swept-Back Plan Forms of Aspect Ratio 4.5. NACA RM A8B11, 1948.

   III - Unswept and 35° Swept-Back Plan Forms of Aspect Ratio 6. NACA RM A8H30, 1948.

   IV - Unswept Plan Form of Aspect Ratio 2 and a Two-Dimensional Model. NACA RM A8J21, 1948.

   V - 45° Swept-Back Plan Form of Aspect Ratio 2. NACA RM A9D05, 1949.

2. Tinling, Bruce E., and Dickson, Jerald K.: Tests of a Model Horizontal Tail of Aspect Ratio 4.5 in the Ames 12-Foot Pressure Wind Tunnel.

   I - Quarter-Chord Line Swept Back 35°. NACA RM A9G13, 1949.

   II - Elevator Hinge Line Normal to the Plane of Symmetry. NACA RM A9H11a, 1949.

3. Kolbe, Carl D. and Bandettini, Angelo: Investigation in the Ames 12-Foot Pressure Wind Tunnel of a Model Horizontal Tail of Aspect Ratio 3 and Taper Ratio 0.5 Having the Quarter-Chord Line Swept Back 45°. NACA RM A51D02, 1951.

4. Dods, Jules B., Jr.: Estimation of Low-Speed Lift and Hinge-Moment Parameters for Full-Span Trailing-Edge Flaps on Lifting Surfaces With and Without Sweepback. NACA TN 2288, 1951.

5. Swanson, Robert S., and Toll, Thomas A.: Jet-Boundary Corrections for Reflection-Plane Models in Rectangular Wind Tunnels. NACA Rep. 770, 1943. (Formerly NACA ARR 3E22)

6. Allen, H. Julian, and Vincenti, Walter G.: Wall Interference in a Two-Dimensional-Flow Wind Tunnel, with Considerations of the Effect of Compressibility. NACA Rep. 782, 1944. (Formerly NACA ARR 4K03)

7. Sivells, James C., and Deters, Owen J.: Jet-Boundary and Plan-Form Corrections for Partial-Span Models with Reflection Plane, End Plate, or No End Plate in a Closed Circular Wind Tunnel. NACA Rep. 843, 1946. (Formerly NACA TN 1077)

8. Herriot, John G.: Blockage Corrections for Three-Dimensional-Flow Closed-Throat Wind Tunnels, with Considerations of the Effect of Compressibility. NACA Rep. 995, 1950. (Formerly NACA RM A7B28)

9. DeYoung, John, and Harper, Charles W.: Theoretical Symmetric Span Loading at Subsonic Speeds for Wings Having Arbitrary Plan Form. NACA Rep. 921, 1948. (Formerly NACA TN's 1476, 1491, 1772)

10. Crane, Robert M., and Holtzclaw, Ralph W.: Wind-Tunnel Investigation of the Effects of Profile Modification and Tabs on the Characteristics of Ailerons on a Low-Drag Airfoil. NACA Rep. 803, 1944. (Formerly NACA ACR's 4A14, 4A15, 4H15)

TABLE I.- COORDINATES FOR THE NACA 64A010 AIRFOIL SECTION

[All dimensions in percent of chord]

Upper and Lower Surfaces

Station	Ordinate
0	0
.50	.804
.75	.969
1.25	1.225
2.50	1.688
5.00	2.327
7.50	2.805
10.00	3.199
15.00	3.183
20.00	4.272
25.00	4.606
30.00	4.837
35.00	4.968
40.00	4.995
45.00	4.894
50.00	4.684
55.00	4.388
60.00	4.021
65.00	3.597
70.00	3.127
75.00	2.623
80.00	2.103
85.00	1.582
90.00	1.062
95.00	.541
100.00	.021
L.E. radius, 0.687 T.E. radius, 0.023	

TABLE II.- SUMMARY OF LOW-SPEED EXPERIMENTAL AND THEORETICAL LIFT AND HINGE-MOMENT PARAMETERS
[NACA 64A010 airfoil section;[a] elevator-chord ratio, 0.30; taper ratio, $\lambda = 0.50$]

Model		Lift and hinge-moment parameters[b]							
Aspect ratio, A	Angle of sweep-back, Λ (deg)	C_{L_α}		C_{L_δ}		C_{h_α}		C_{h_δ}	
		Experiment	Theory	Experiment	Theory	Experiment	Theory	Experiment	Theory
2	16.7	0.040	0.043	0.029	0.024	-0.0002	-0.0001	-0.0071	-0.0079
2	45	.041	.040	.021	.020	-.0016	-.0016	-.0068	-.0054
3	11.3	.053	.055	.037	.033	-.0010	-.0011	-.0085	-.0086
3	35	.053	.052	.028	.028	-.0014	-.0021	-.0076	-.0069
3	45	[c].049	.048	[c].025	.023	[c]-.0028	-.0026	[c]-.0066	-.0056
4.5	7.6	.066 [c].063	.067	.045 [c].044	.040	-.0020 [c]-.0032	-.0023	-.0093 [c]-.0100	-.0093
4.5	35	.061 [c].059	.060	.032 [c].032	.031	-.0024 [c]-.0025	-.0033	-.0078 [c]-.0080	-.0074
6	5.7	.074	.075	.050	.045	-.0030	-.0033	-.0102	-.0099
6	35	.065	.065	.034	.033	-.0032	-.0040	-.0082	-.0076

[a]Experimentally, $c_{l_{\alpha_o}} = 0.108$; $c_{l_\delta} = 0.065$; $c_{h_{\alpha_o}} = -0.0057$; $c_{h_\delta} = -0.0114$

[b]Measured through 0° angle of attack and 0° elevator deflection.

[c]From 12-foot pressure wind-tunnel tests. (Other data from 7- by 10-foot wind tunnels.)

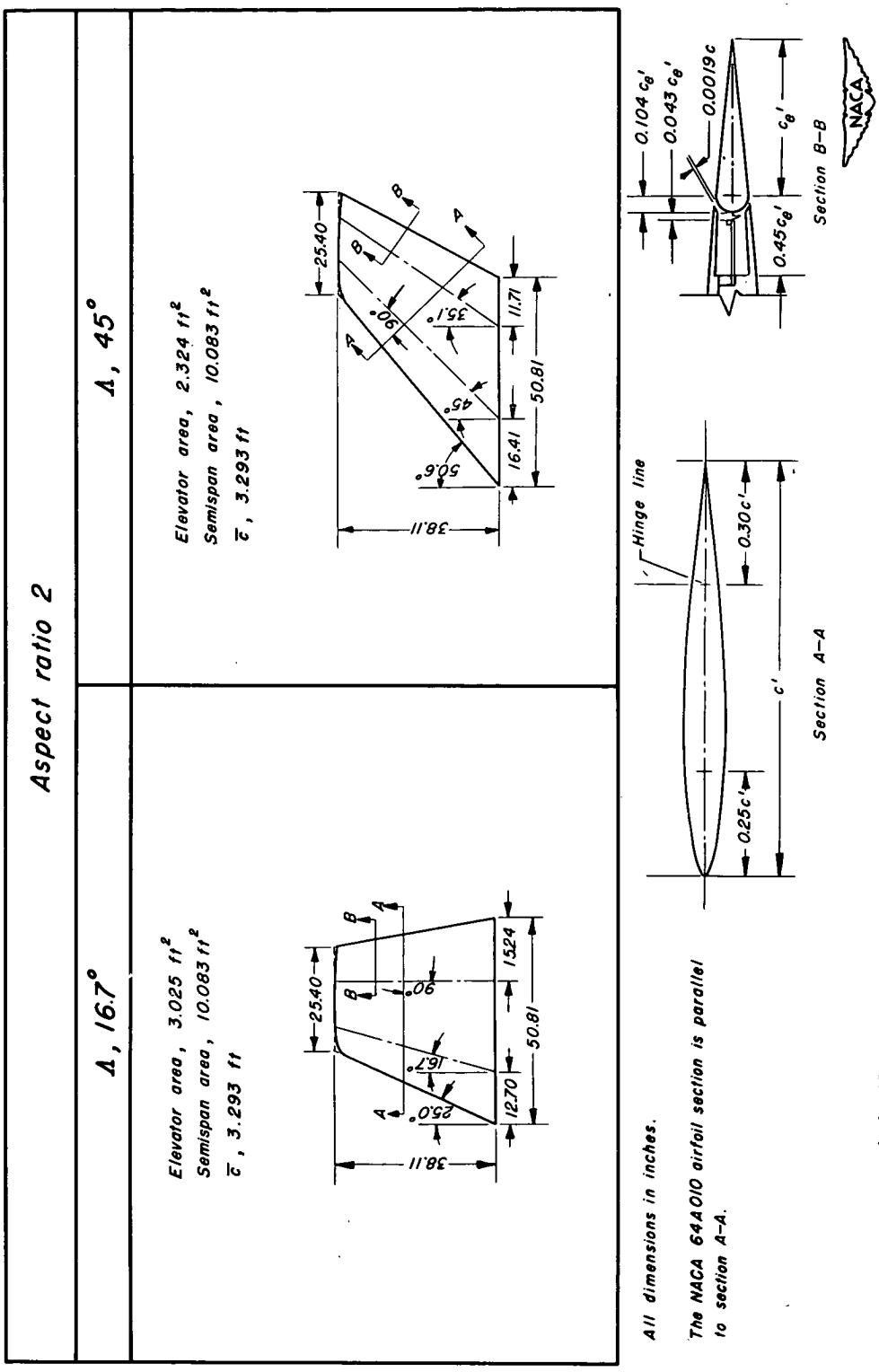

(a) 7-by 10-foot wind-tunnel models of aspect ratio 2 and taper ratio of 0.5; Λ, 16.7° and 45°.

Figure 1.—Geometry of the horizontal-tail models.

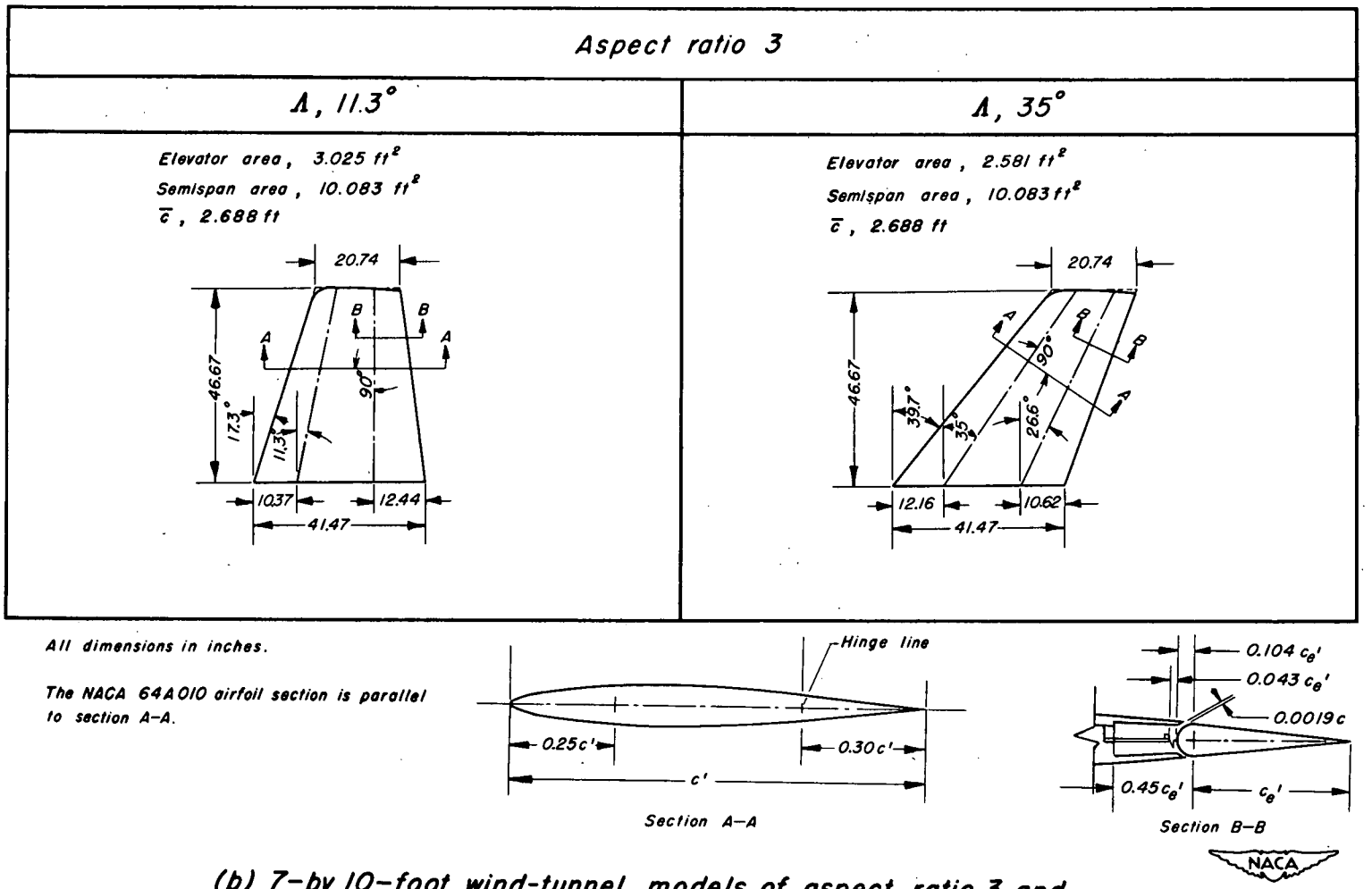

(b) 7-by 10-foot wind-tunnel models of aspect ratio 3 and taper ratio of 0.5; Λ, 11.3° and 35°.

Figure 1.—Continued.

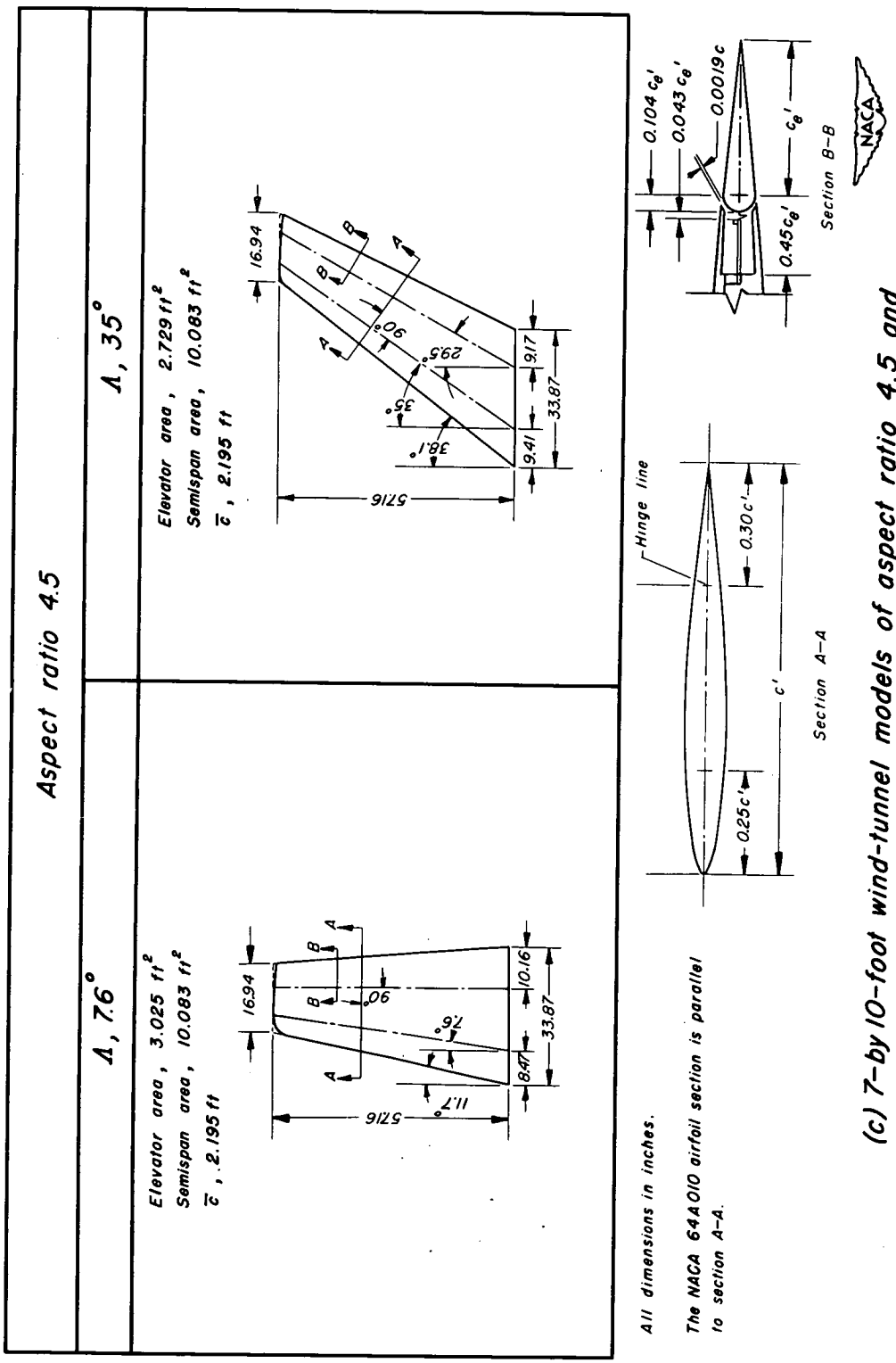

(c) 7-by 10-foot wind-tunnel models of aspect ratio 4.5 and taper ratio of 0.5; 4, 7.6° and 35°.

Figure 1.—Continued.

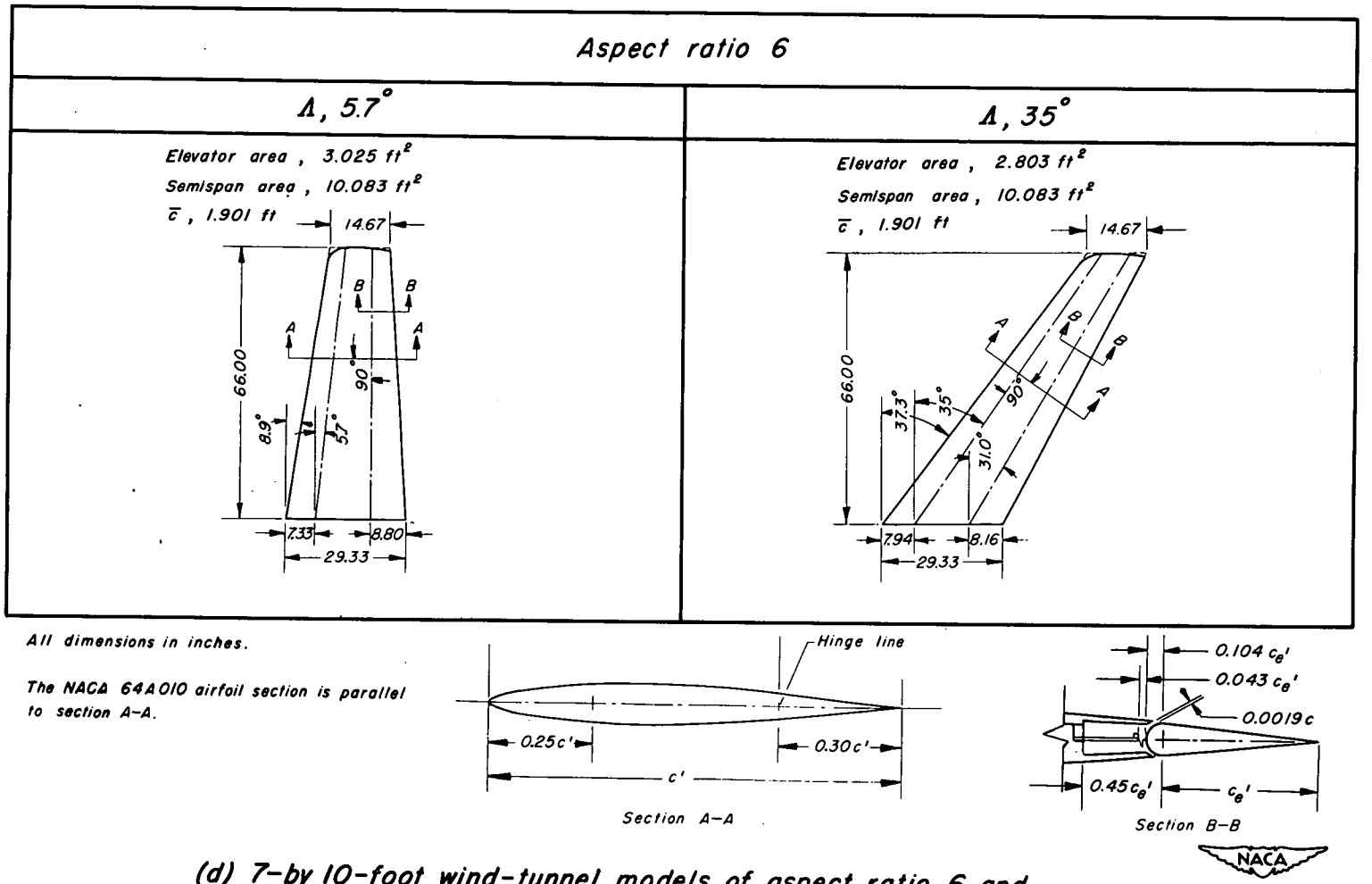

(d) 7-by 10-foot wind-tunnel models of aspect ratio 6 and taper ratio of 0.5; Λ, 5.7° and 35°.

Figure 1.—Continued.

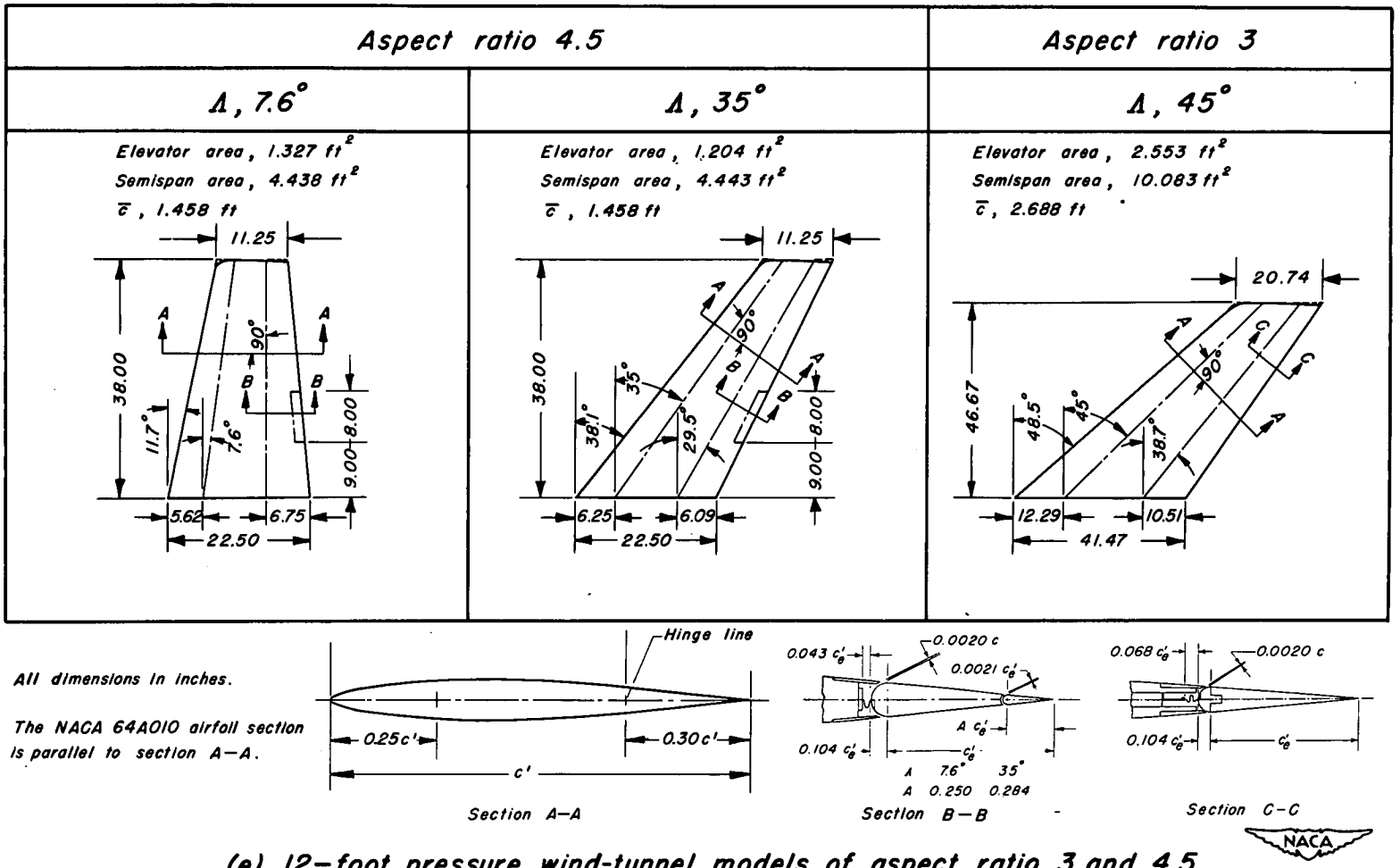

(e) 12-foot pressure wind-tunnel models of aspect ratio 3 and 4.5 and taper ratio of 0.5; Λ, 7.6°, 35°, and 45°.

Figure 1.—Concluded.

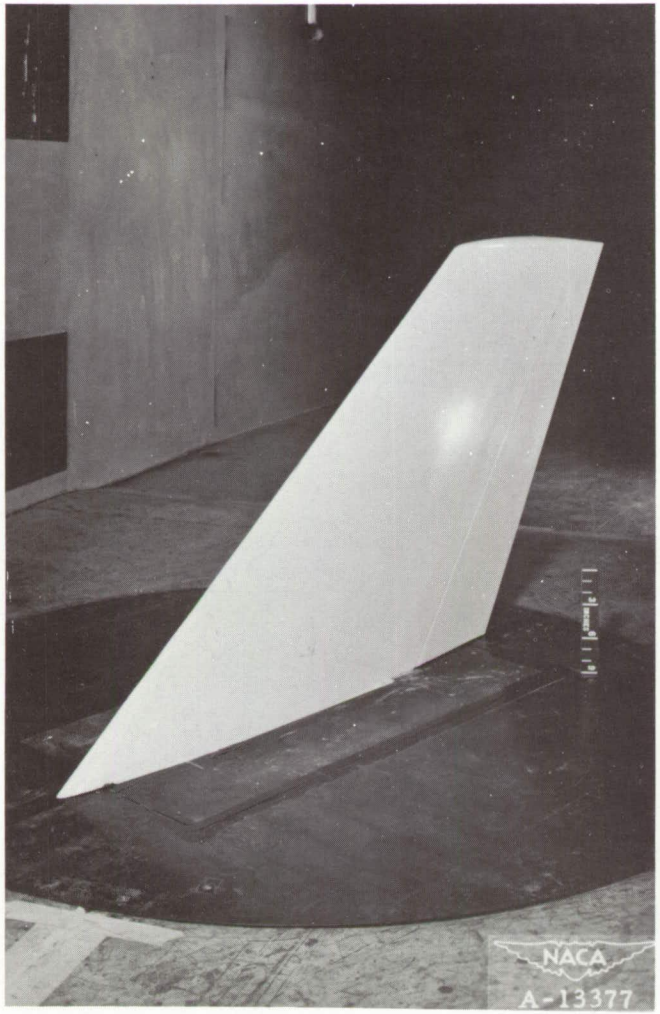

(a) The 45° swept-back model of aspect ratio 2 in the 7- by 10-foot wind tunnel.

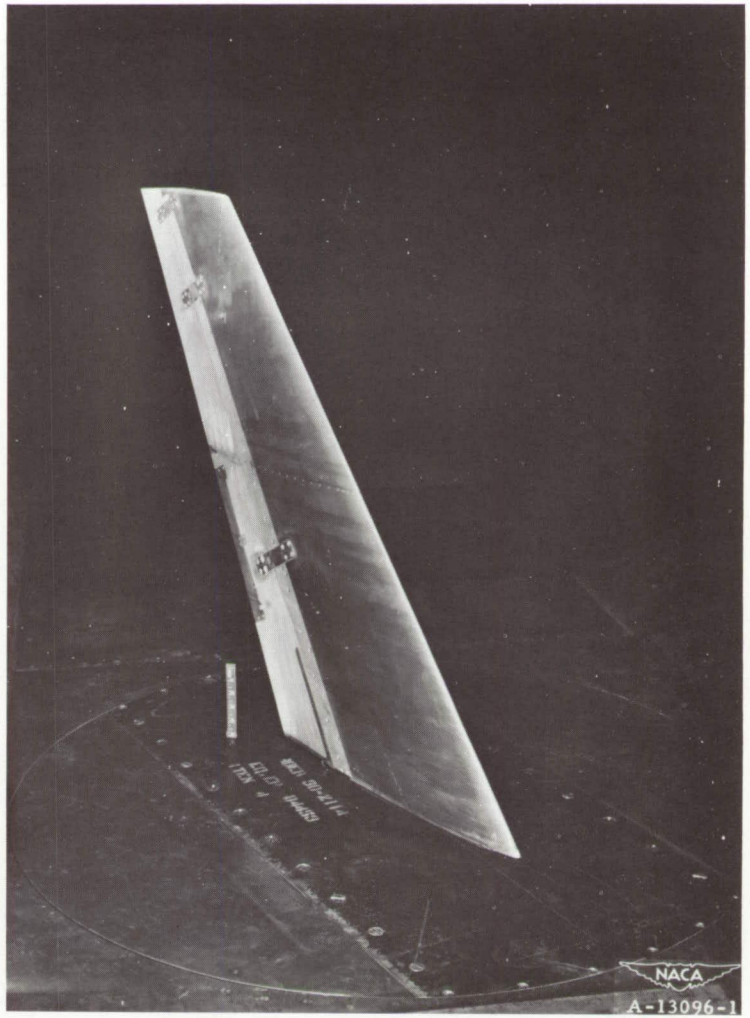

(b) The 35° swept-back model of aspect ratio 4.5 in the 12-foot pressure wind tunnel.

Figure 2.- Representative semispan horizontal-tail model installations.

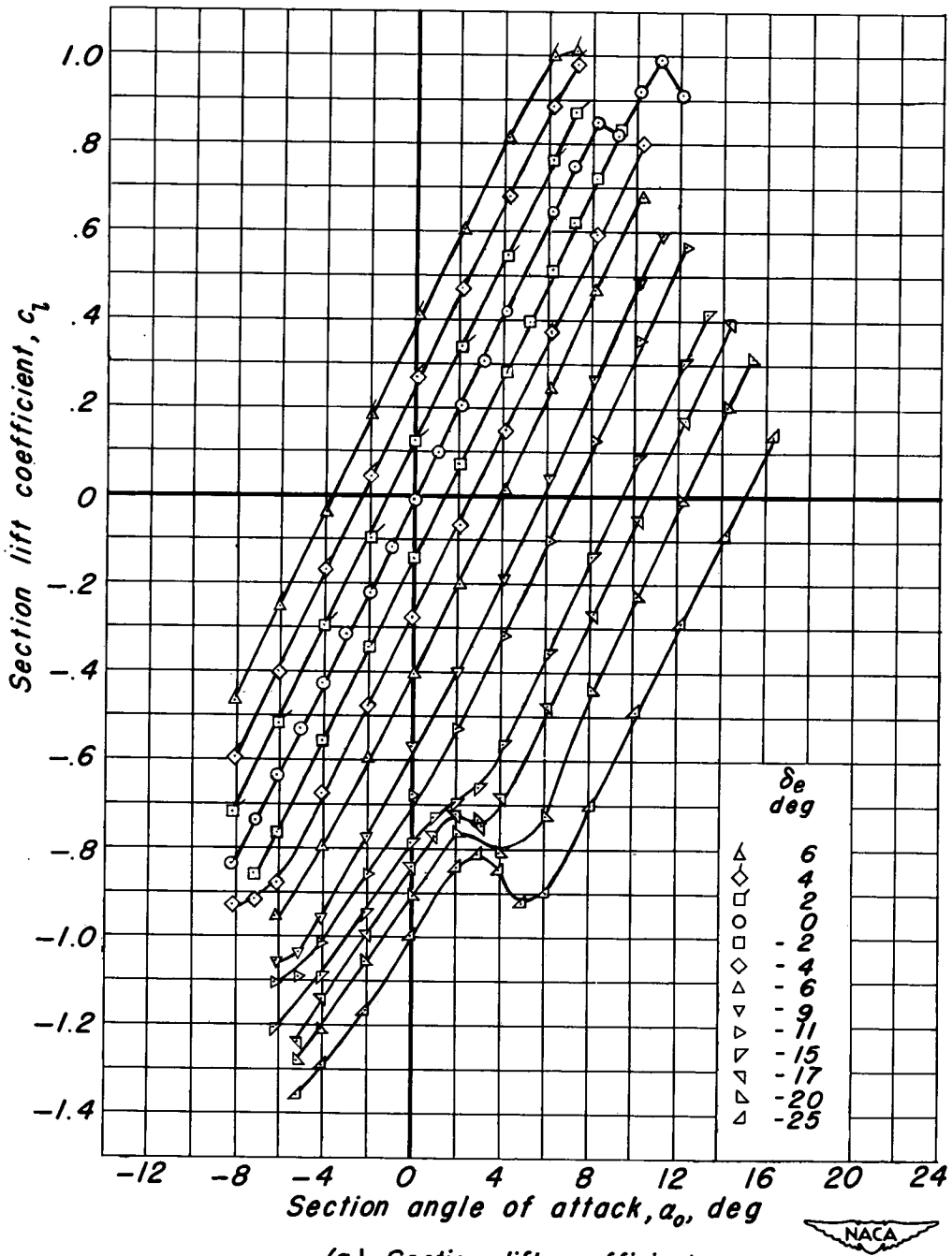

(a) Section lift coefficient.

Figure 3.- Section lift and hinge-moment characteristics of the constant-chord model of the NACA 64A010 airfoil section. R, 3.0×10^6; M, 0.12.

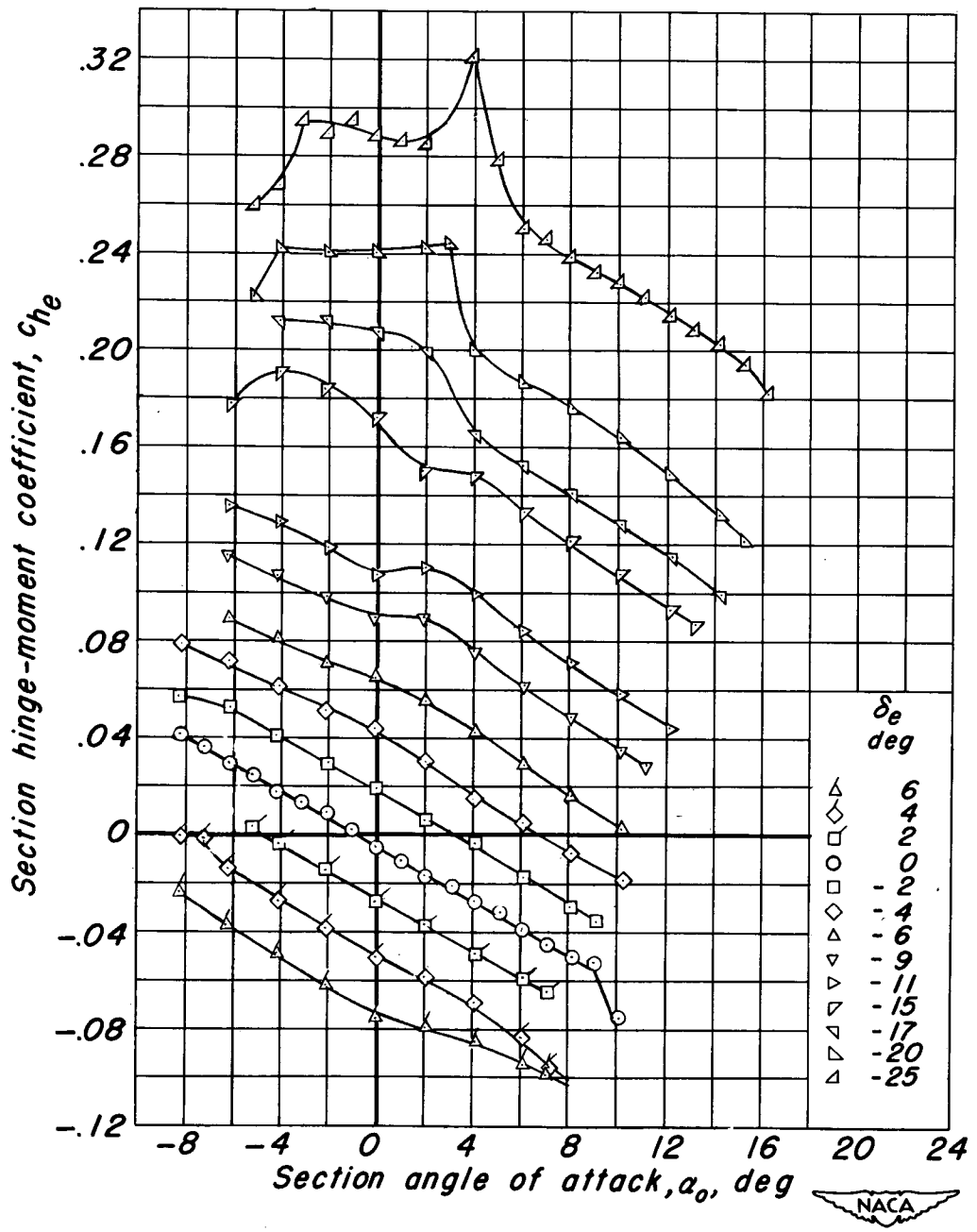

(b) Section hinge-moment coefficient.

Figure 3. -Continued.

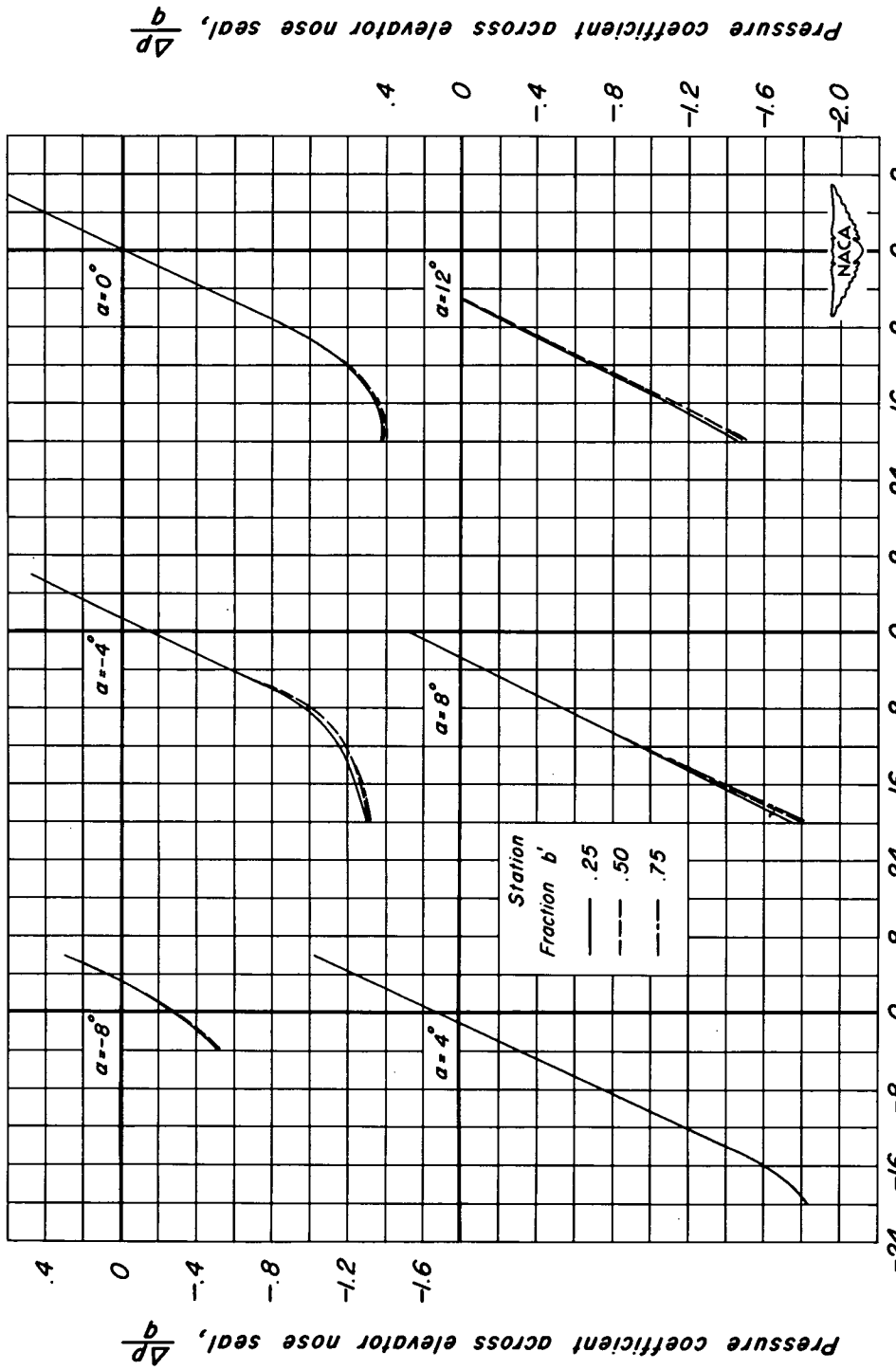

(c) Pressure coefficient.

Figure 3.- Concluded.

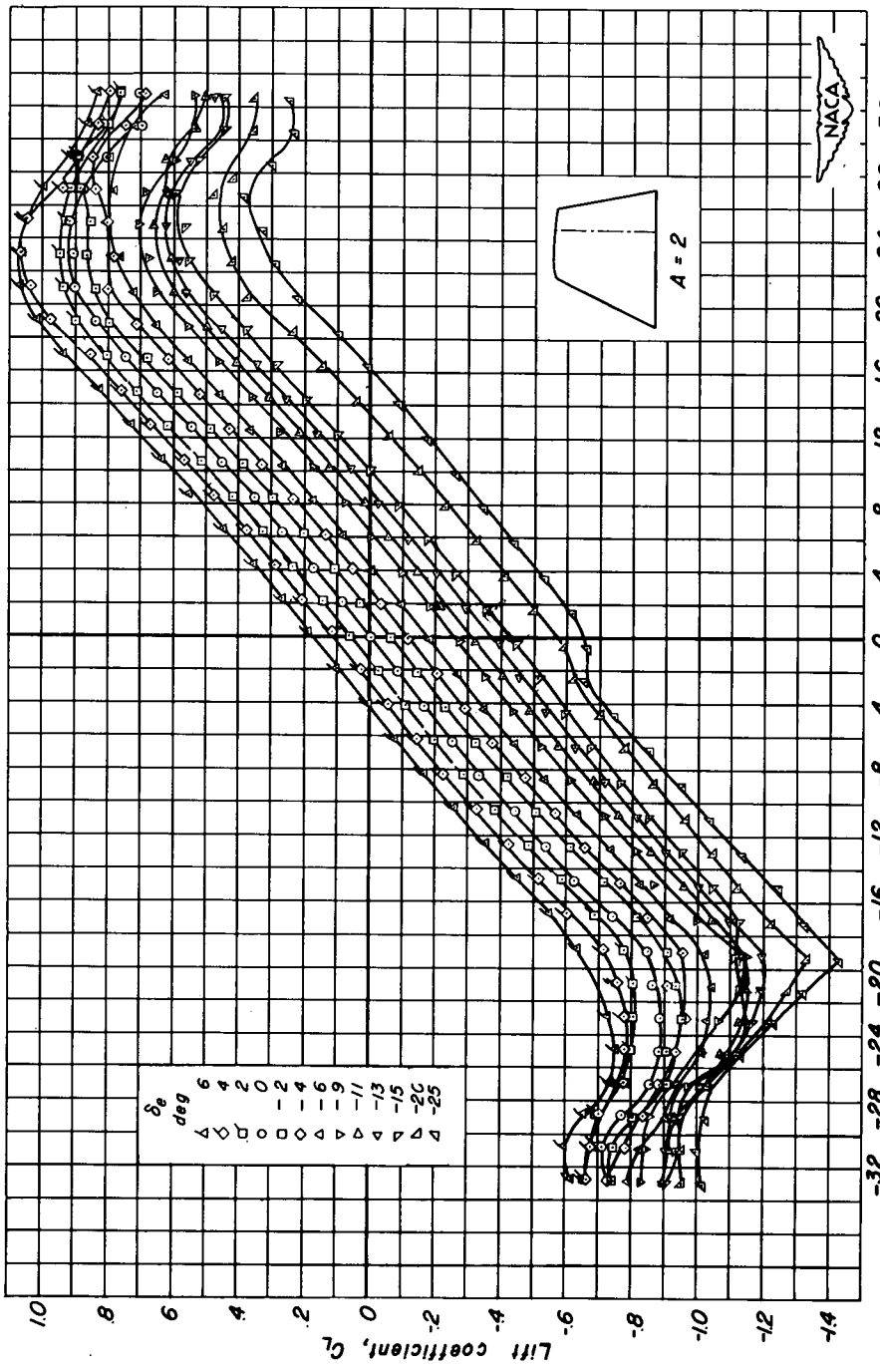

(a) Lift coefficient.

Figure 4.– Lift and hinge-moment characteristics of the unswept model of aspect ratio 2. R, 3.0 x 10⁶; M, 0.14.

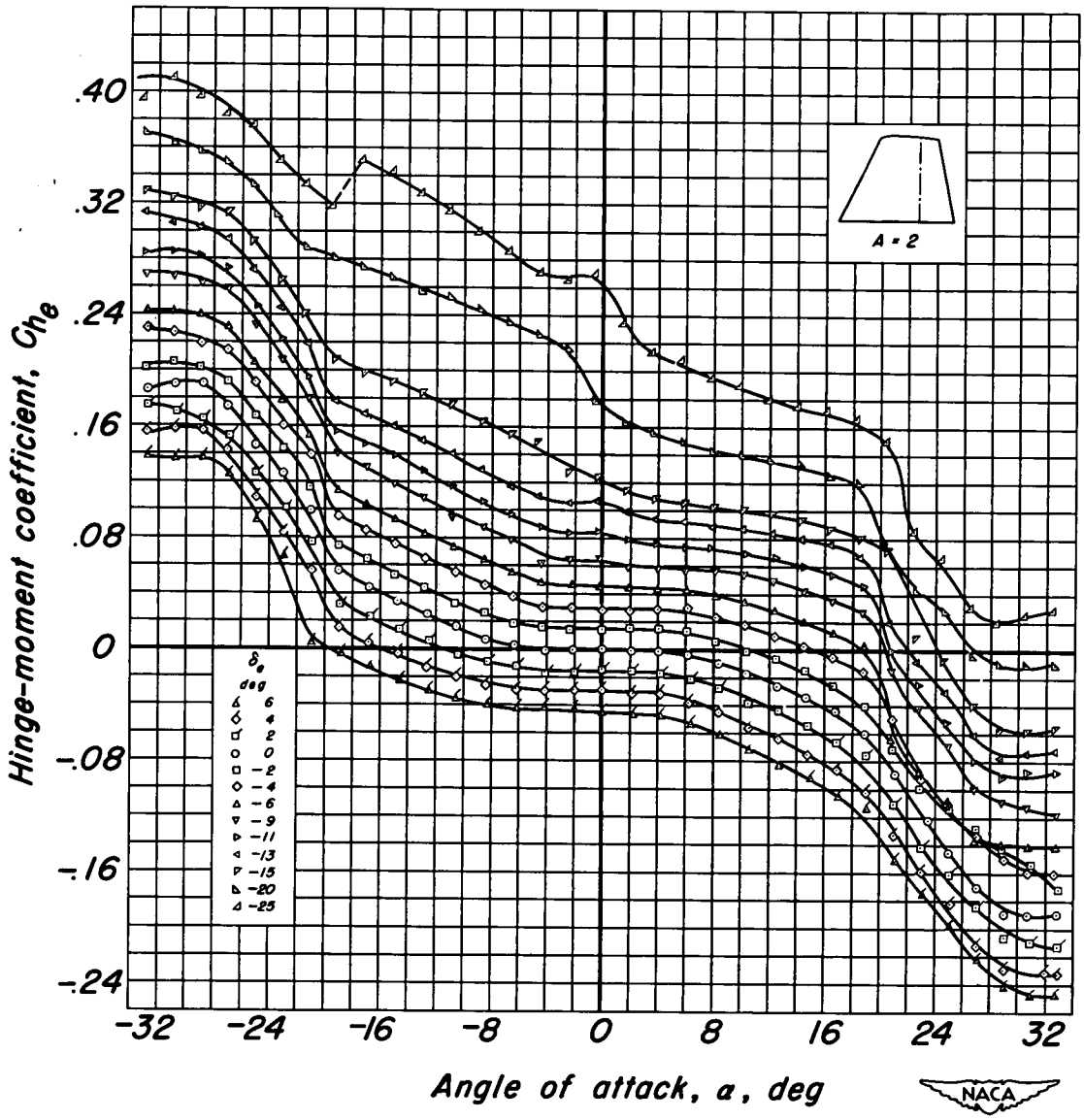

(b) Hinge-moment coefficient.

Figure 4.—Continued .

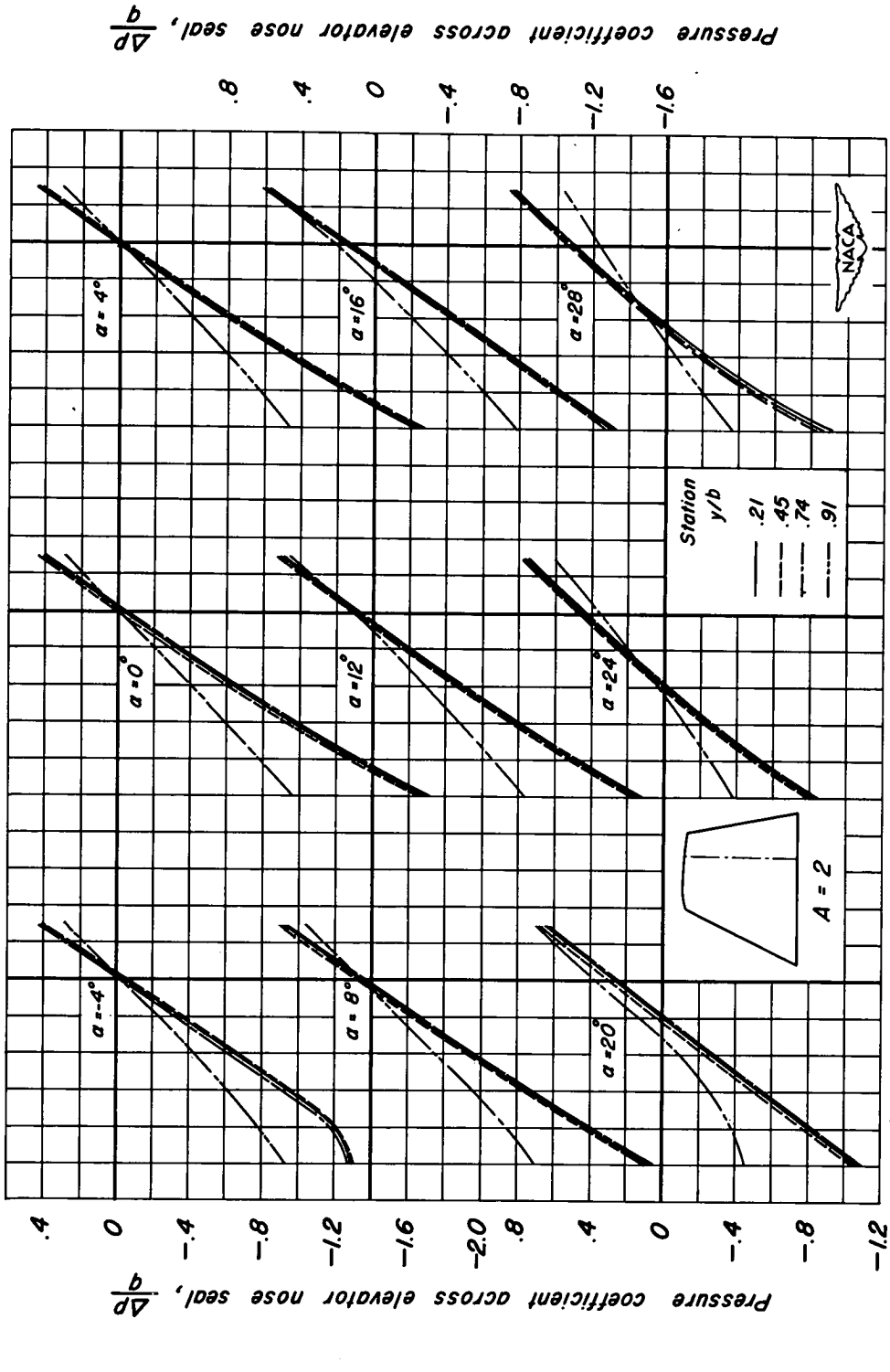

(c) Pressure coefficient.

Figure 4.—Concluded.

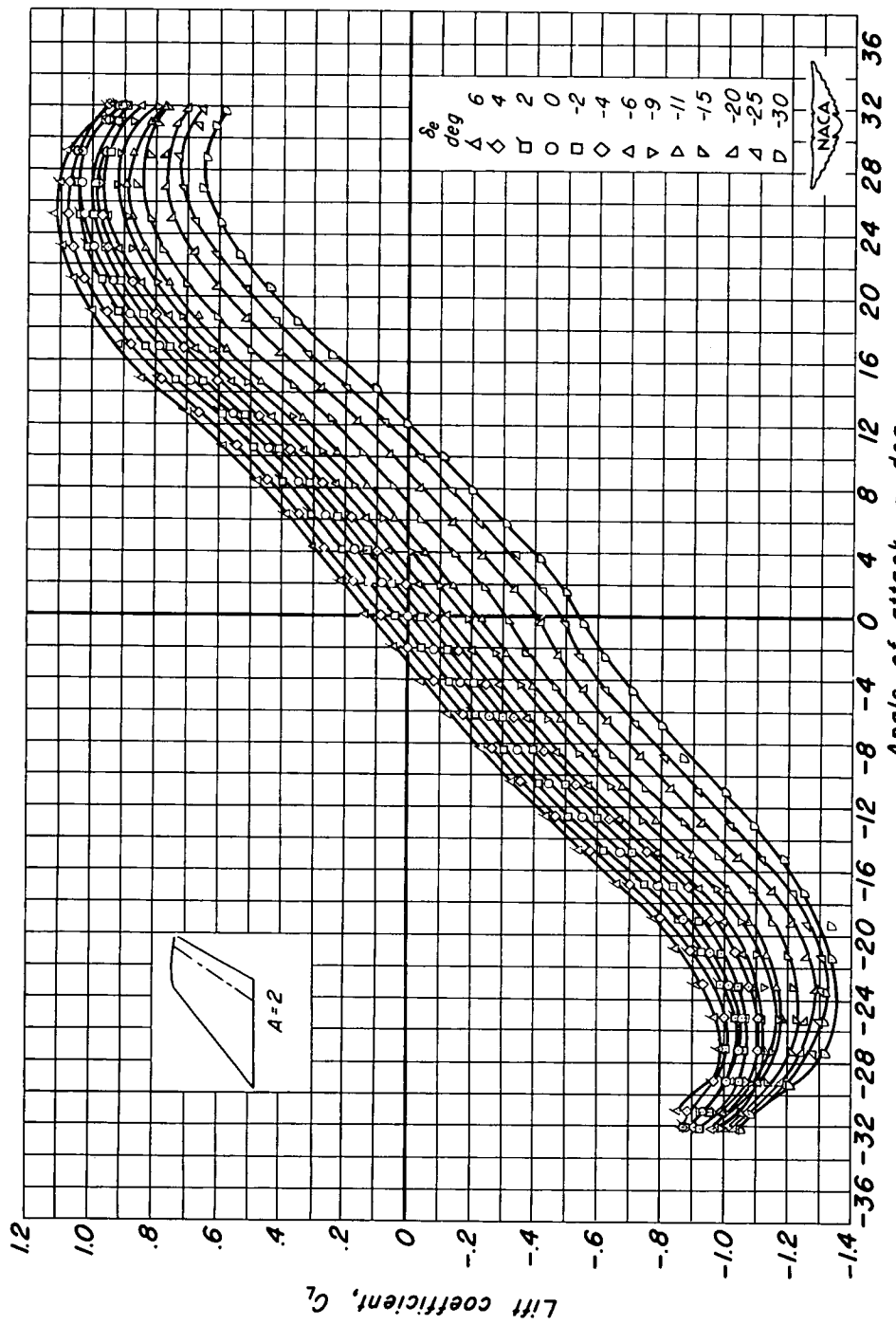

(a) Lift coefficient.

Figure 5.— Lift and hinge-moment characteristics of the 45° swept-back model of aspect ratio 2. R, 3.0×10^6; M, 0.14.

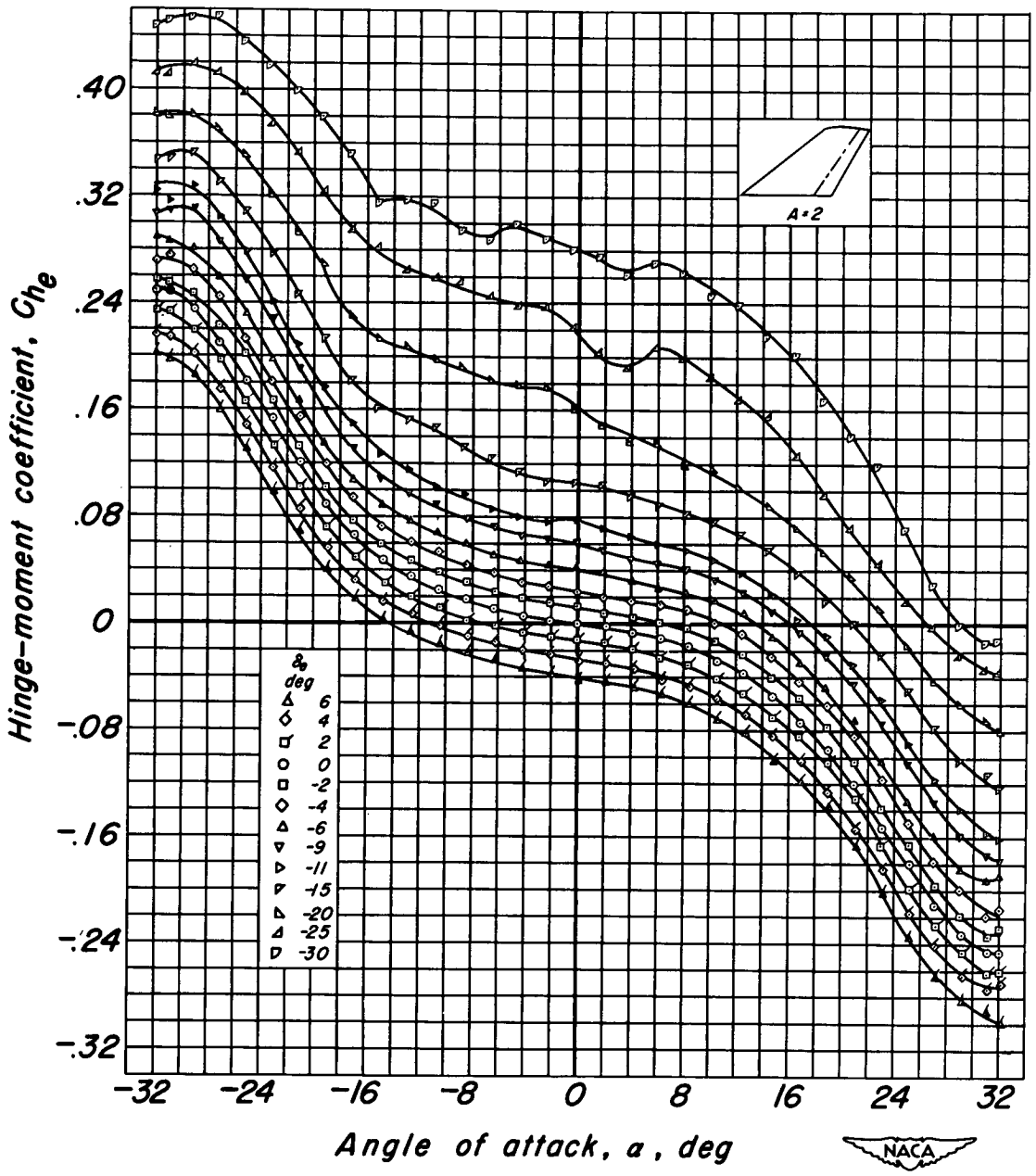

(b) Hinge-moment coefficient.

Figure 5. —Continued .

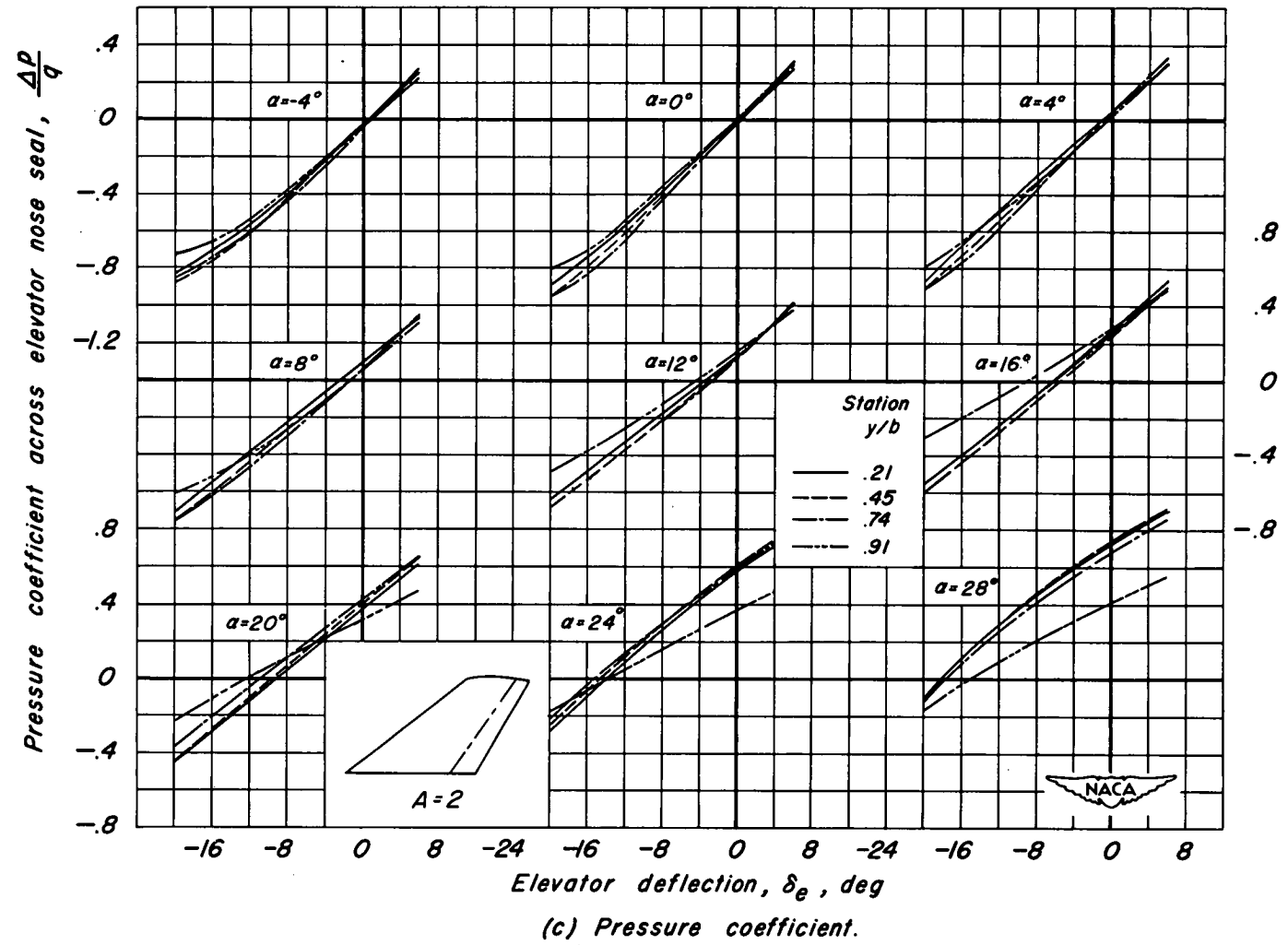

(c) Pressure coefficient.

Figure 5.—Concluded.

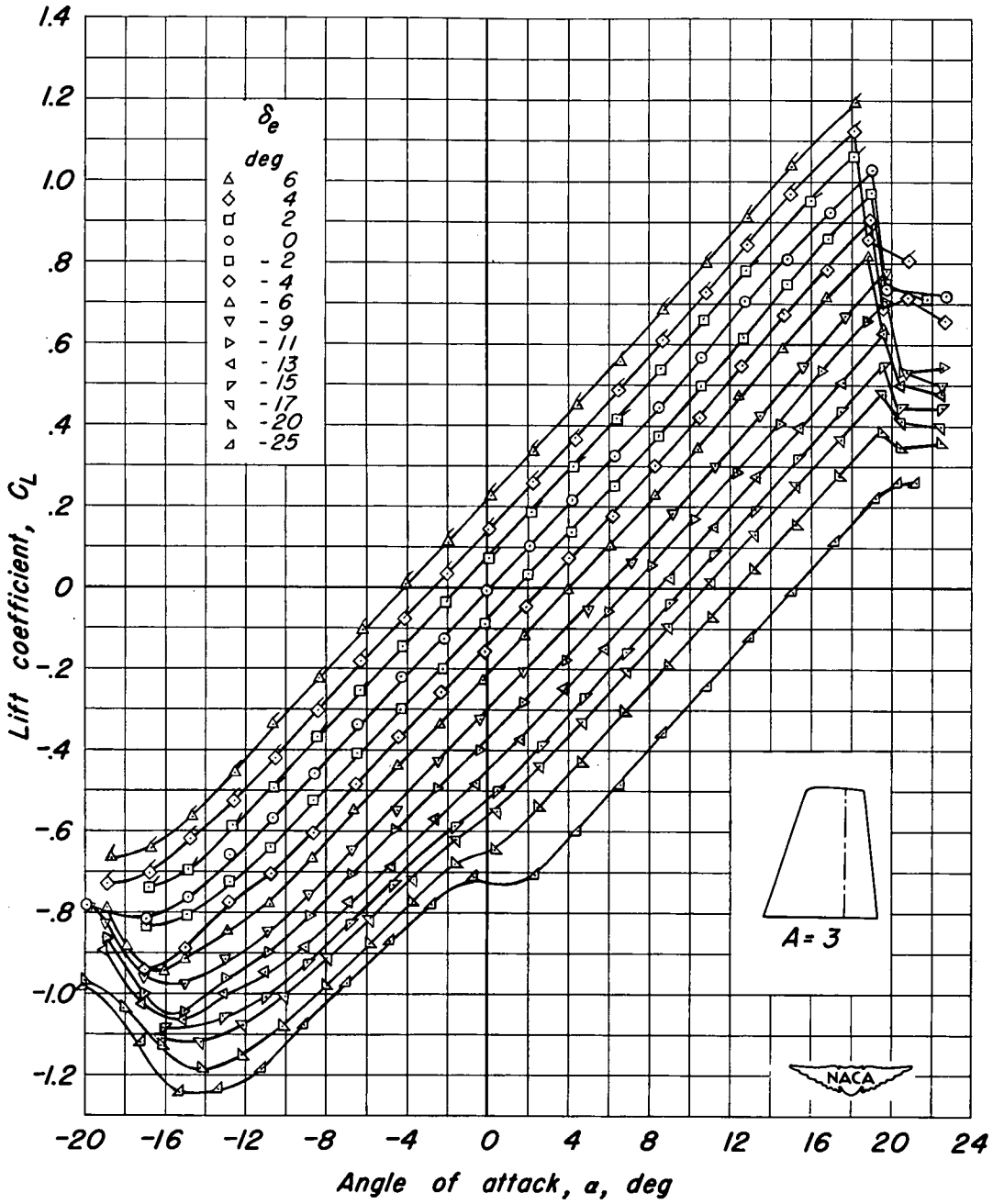

(a) Lift coefficient.

Figure 6.— Lift and hinge-moment characteristics of the unswept model of aspect ratio 3. R, 3.0×10^6; M, 0.17.

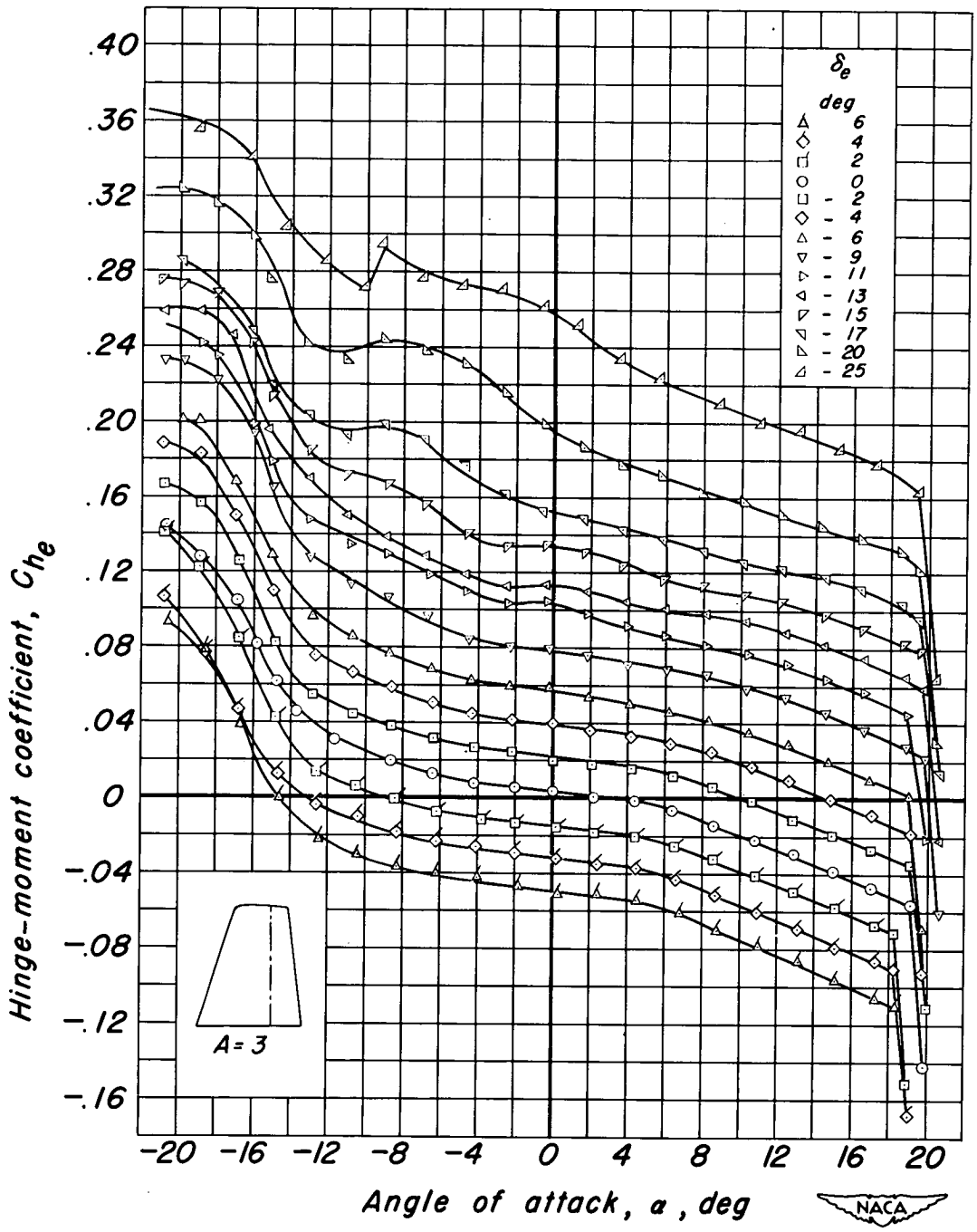

(b) Hinge-moment coefficient.

Figure 6. — Continued.

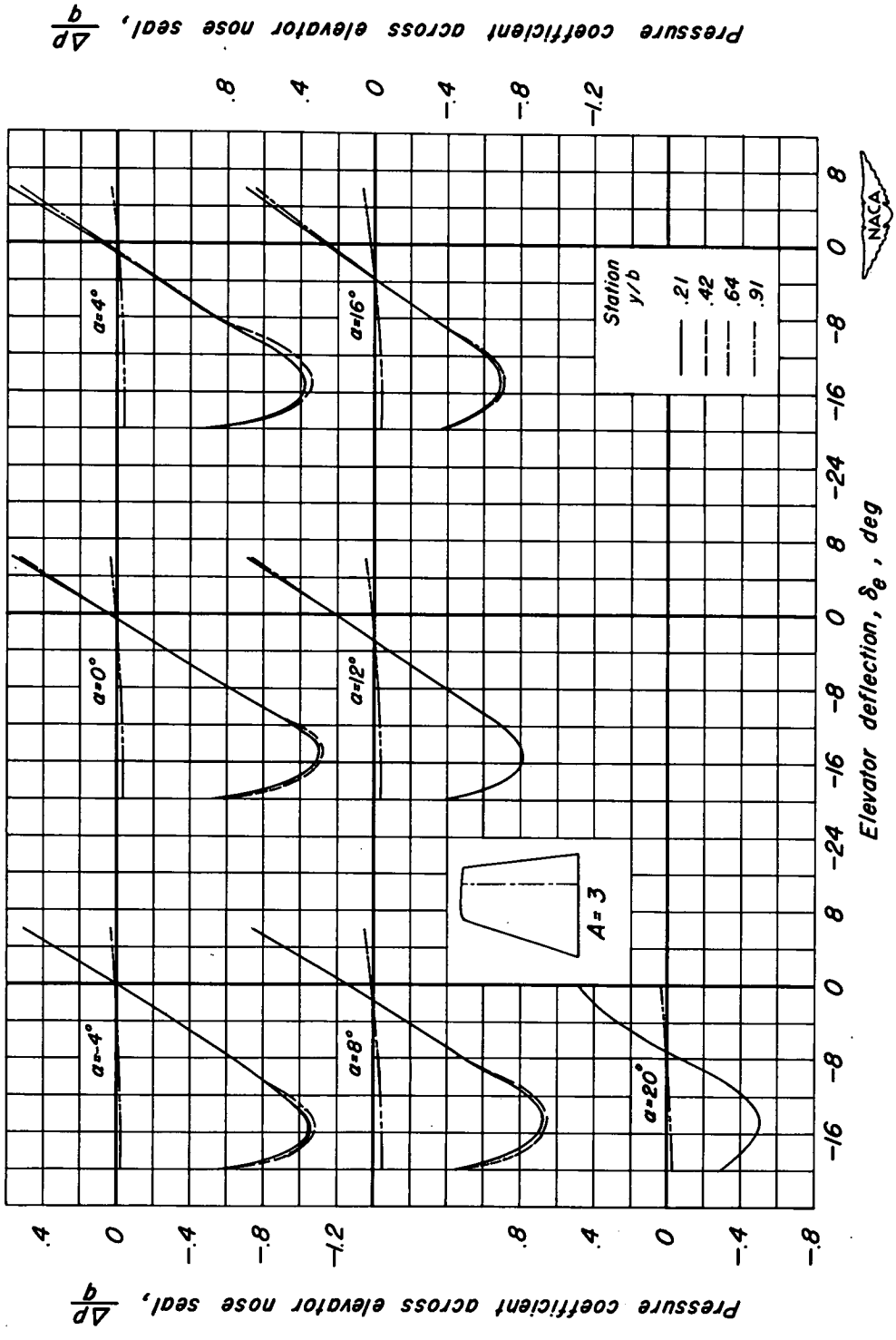

(c) Pressure coefficient.

Figure 6.—Concluded.

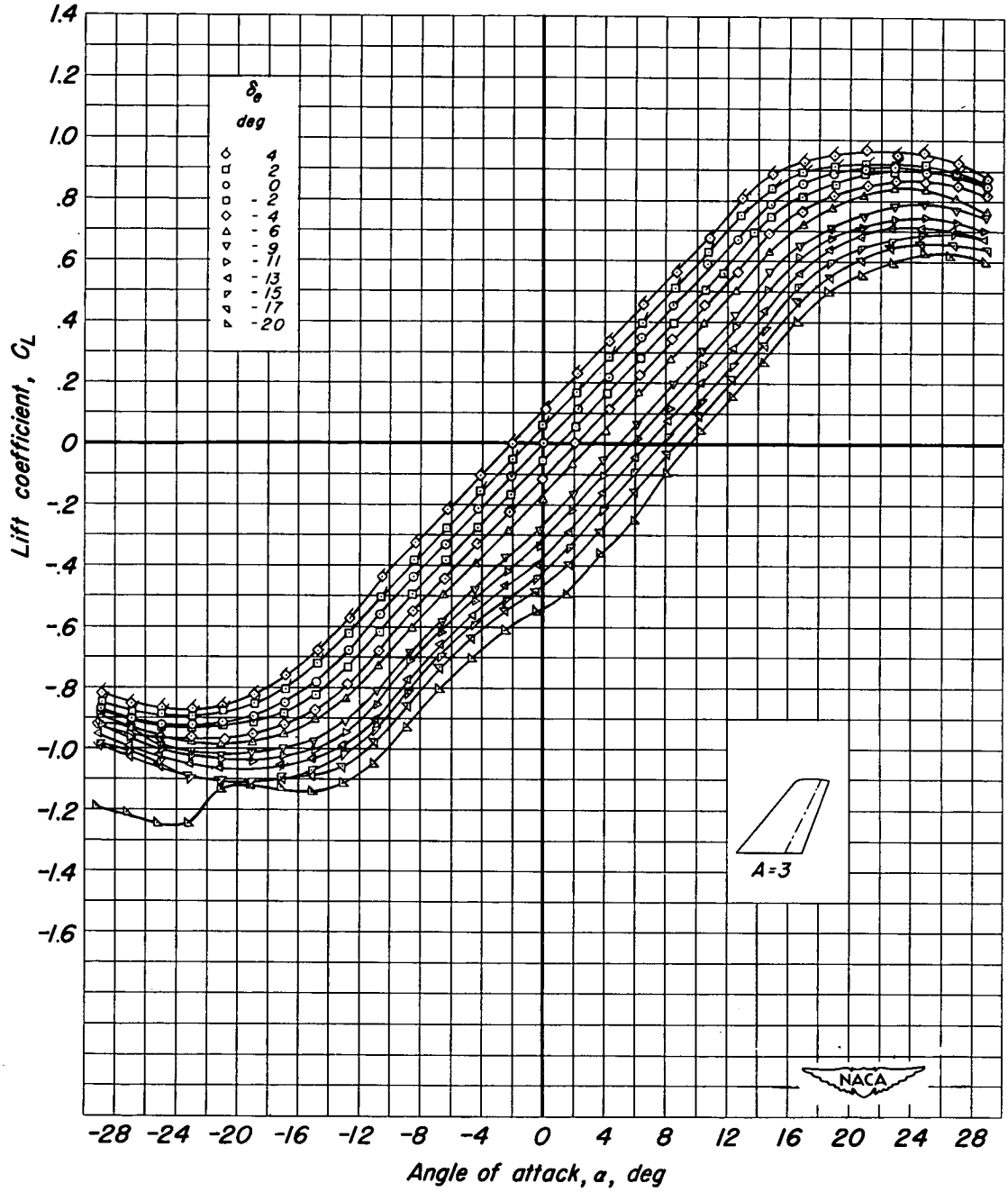

(a) Lift coefficient.

Figure 7.— Lift and hinge-moment characteristics of the 35° swept-back model of aspect ratio 3. R, 3.0×10^6; M, 0.17.

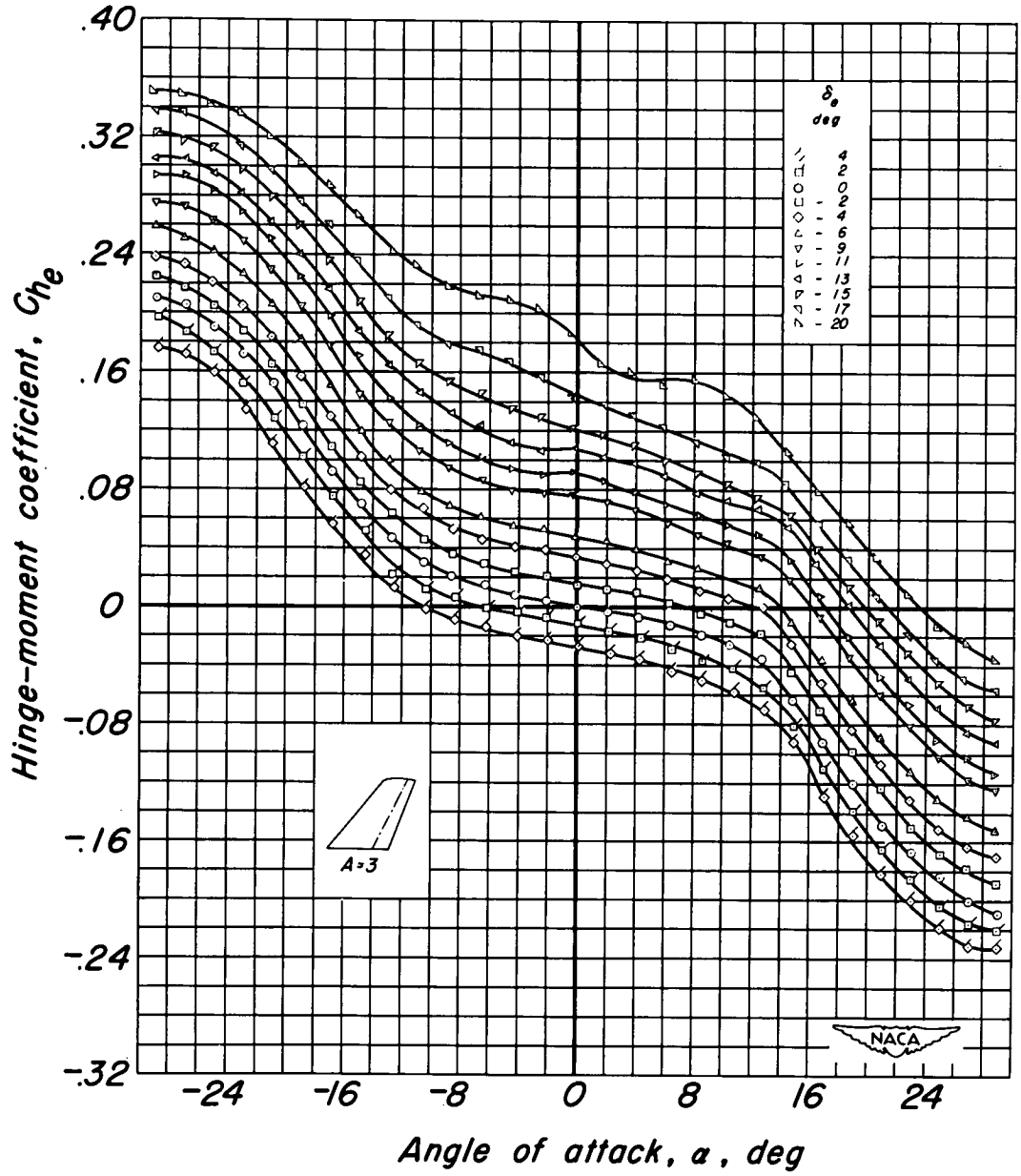

(b) Hinge-moment coefficient.

Figure 7. – Continued.

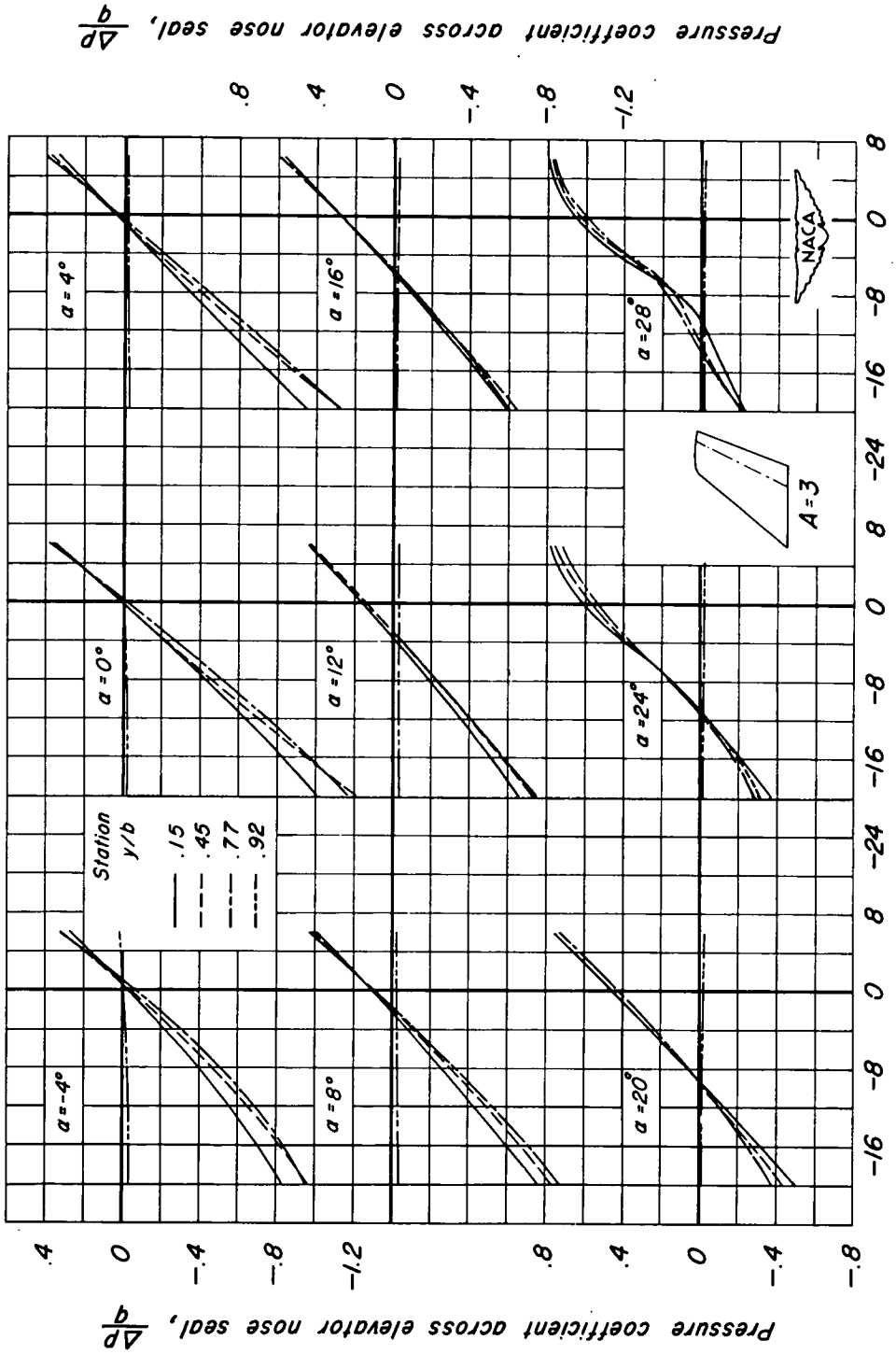

(c) Pressure coefficient.

Figure 7.—Concluded.

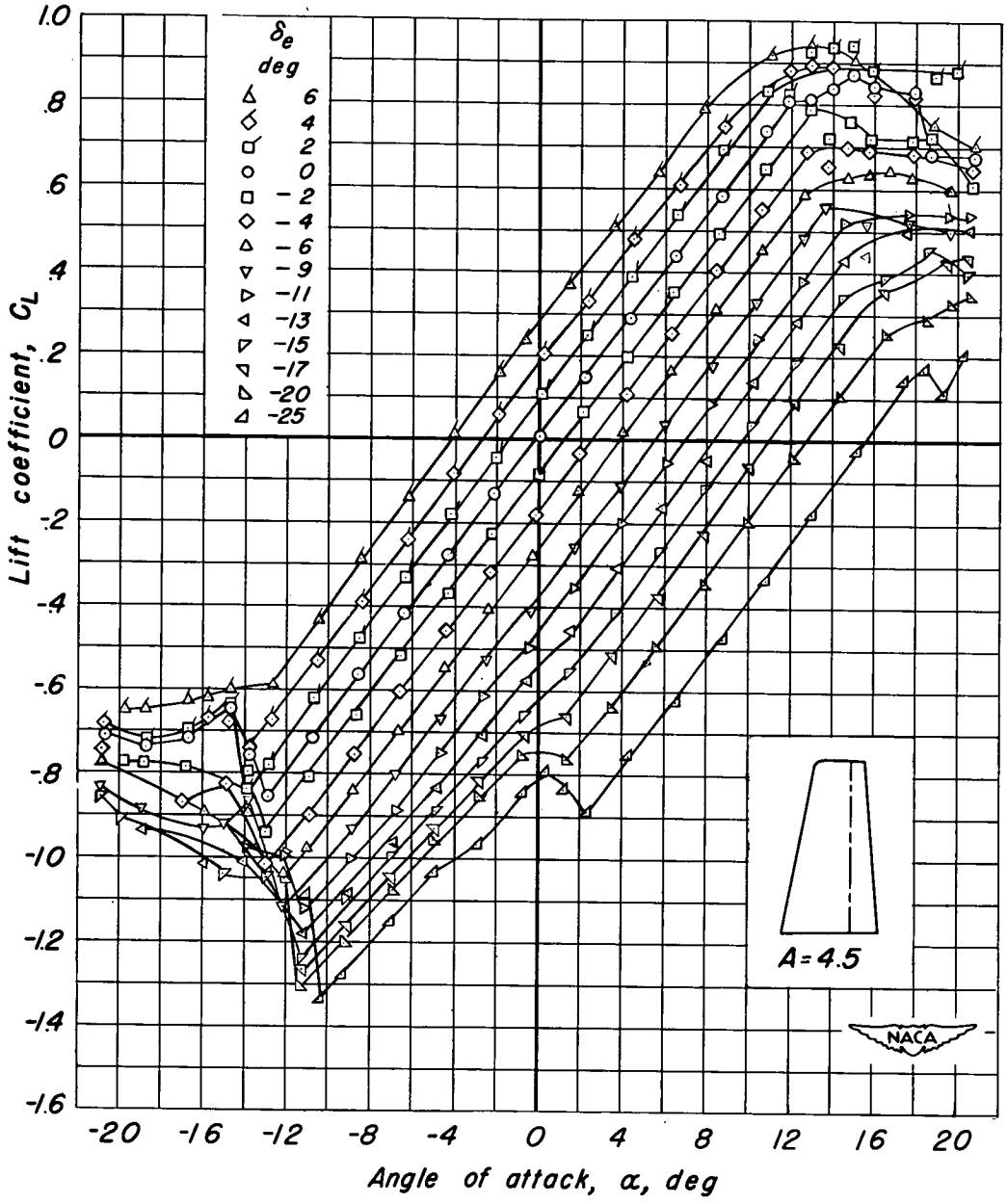

(a) Lift coefficient.

Figure 8.—Lift and hinge-moment characteristics of the unswept model of aspect ratio 4.5. R, 3.0×10^6; M, 0.21.

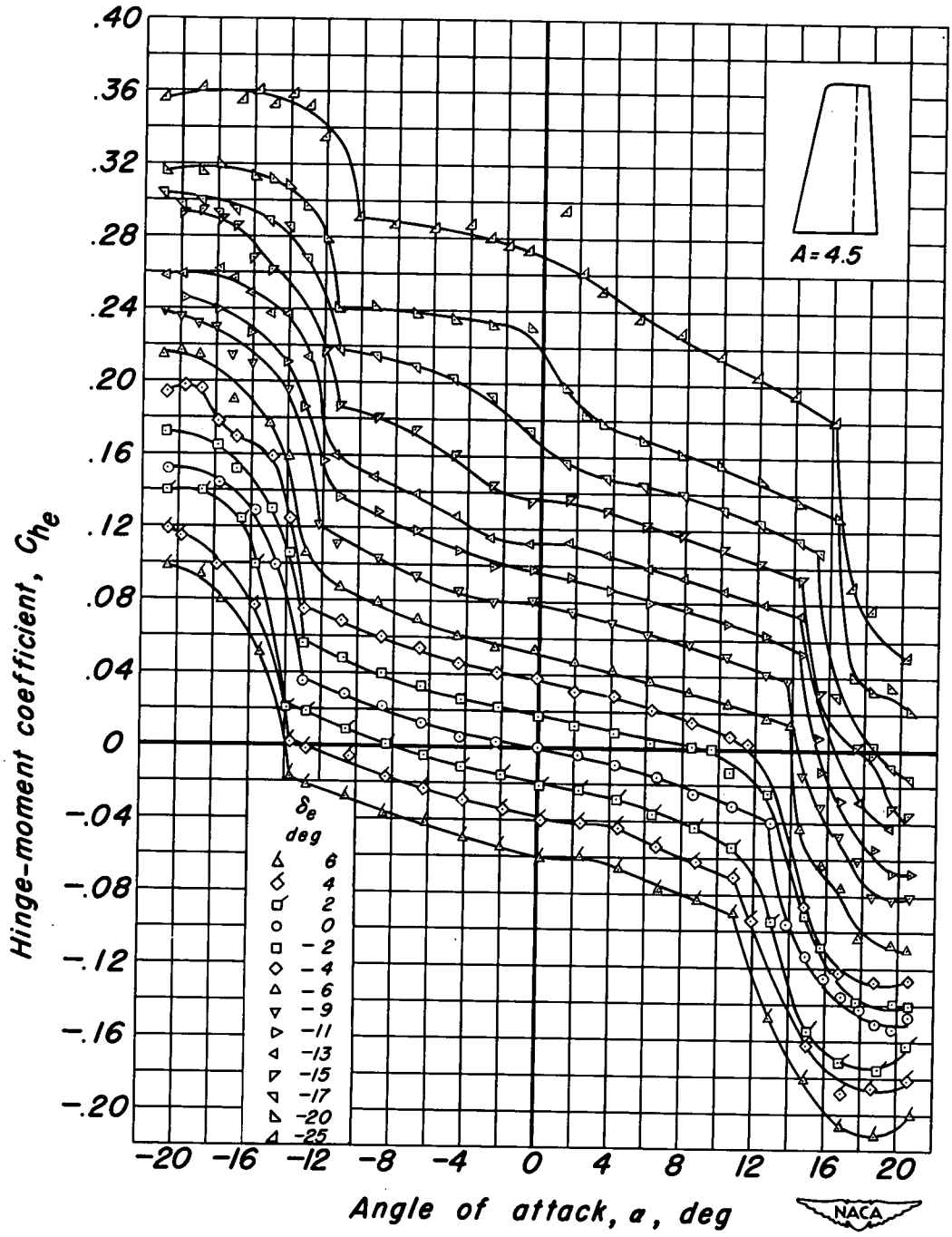

(b) Hinge-moment coefficient.

Figure 8. – Continued.

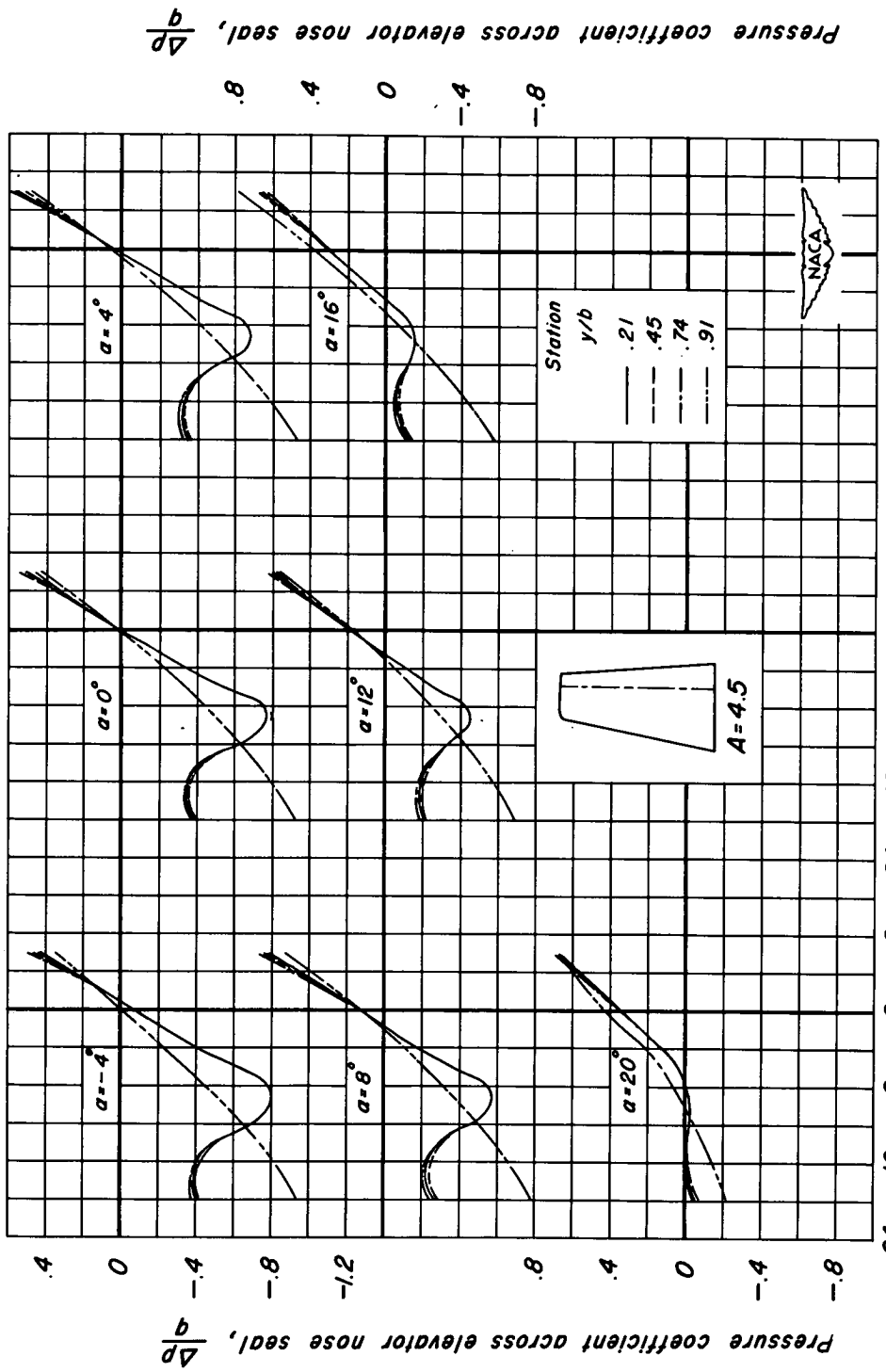

(c) Pressure coefficient.

Figure 8.- Concluded.

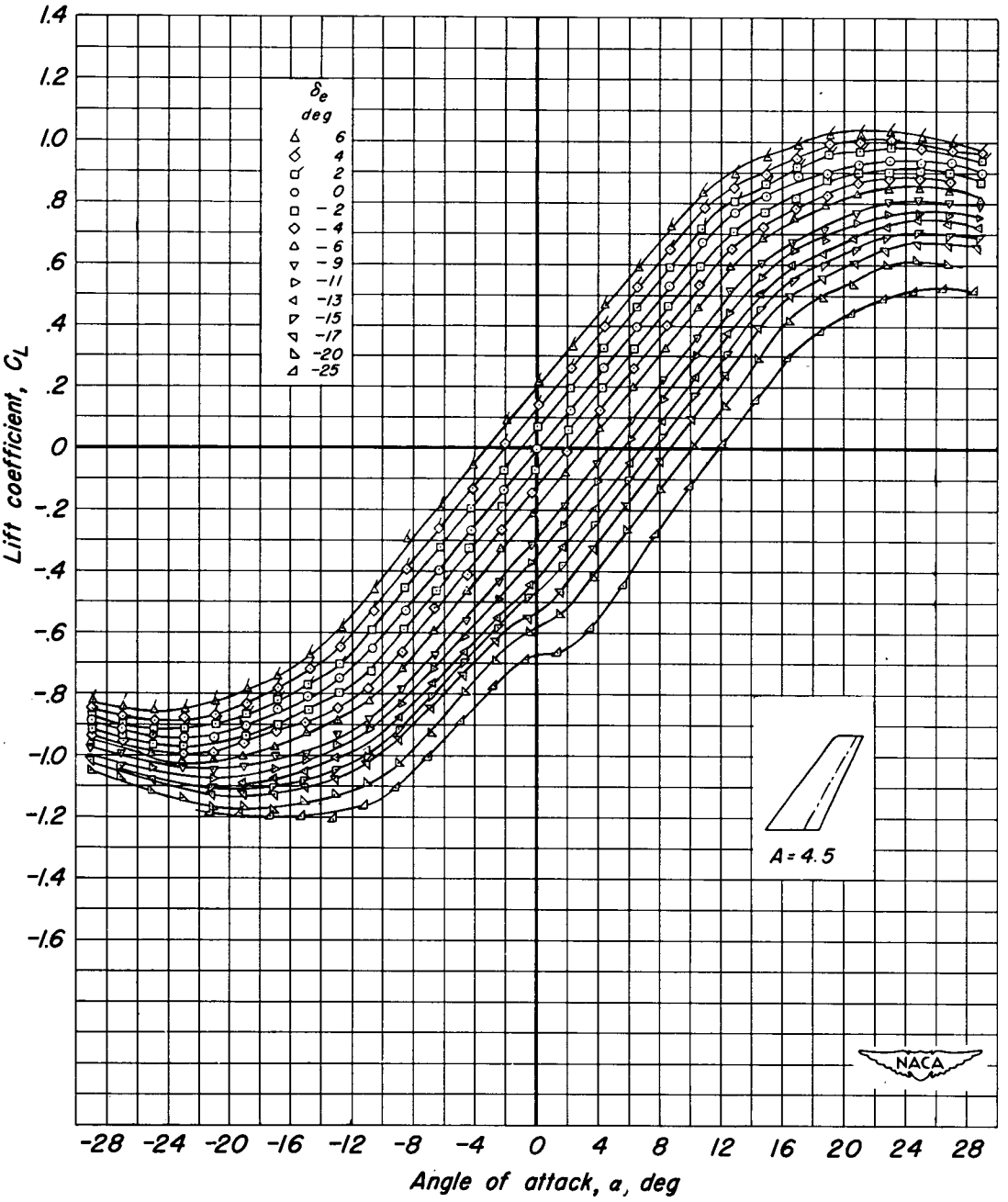

(a) Lift coefficient.

Figure 9.— Lift and hinge-moment characteristics of the 35° swept-back model of aspect ratio 4.5. R, 3.0×10^6; M, 0.21.

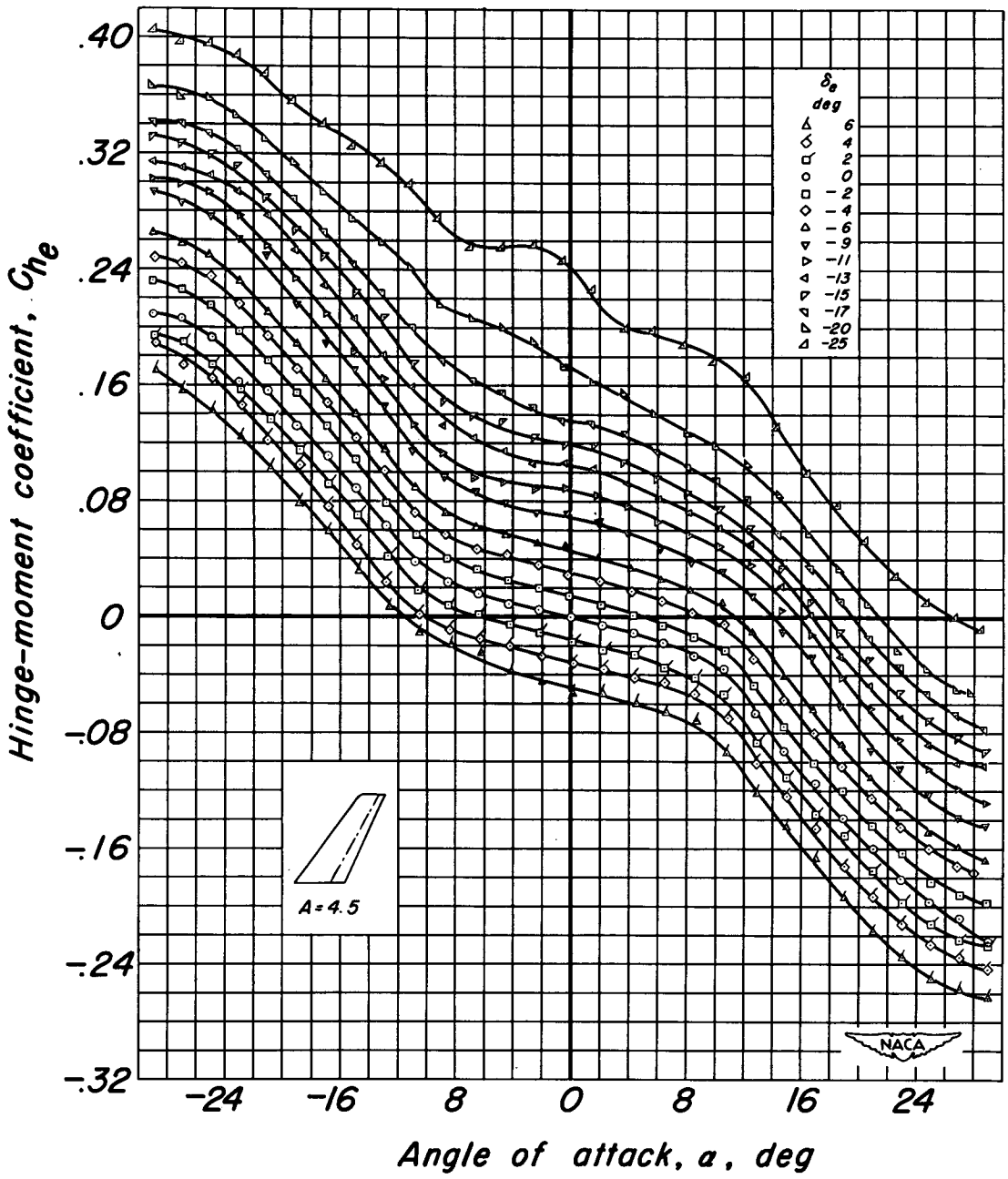

(b) Hinge-moment coefficient.

Figure 9.— Continued.

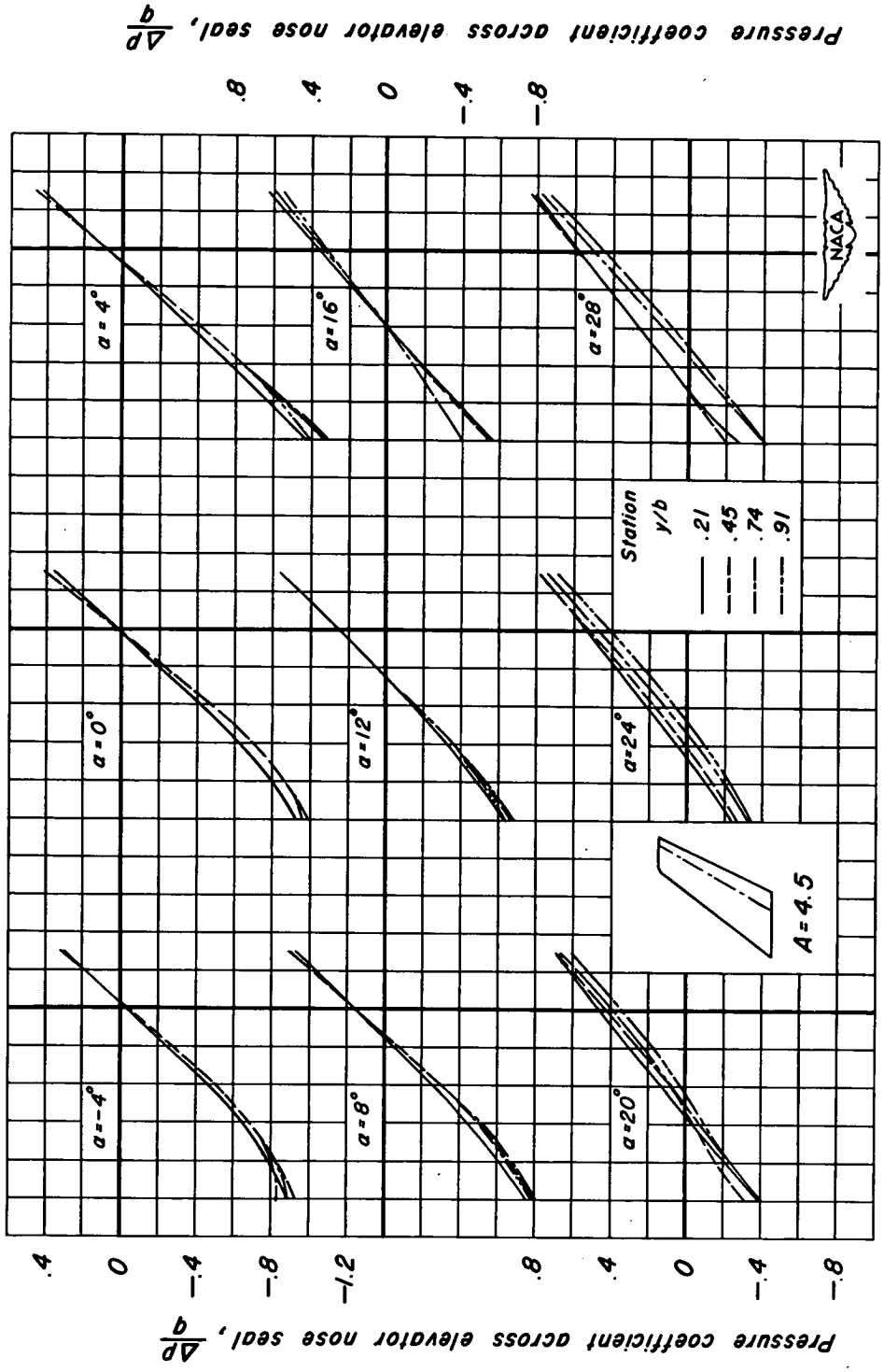

(c) Pressure coefficient.

Figure 9.- Concluded.

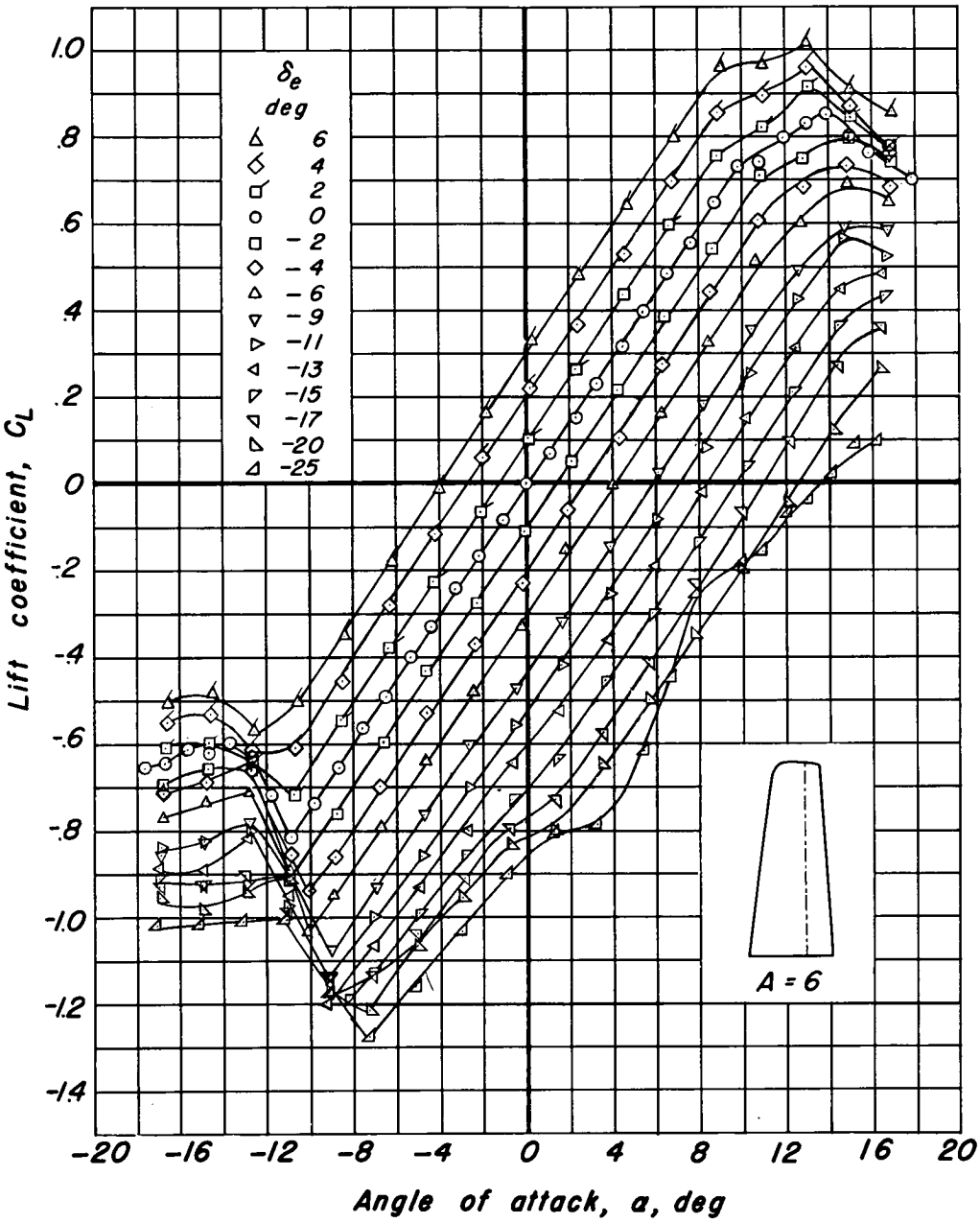

(a) Lift coefficient.

Figure 10.—Lift and hinge-moment characteristics of the unswept model of aspect ratio 6. R, 3.0×10^6; M, 0.23.

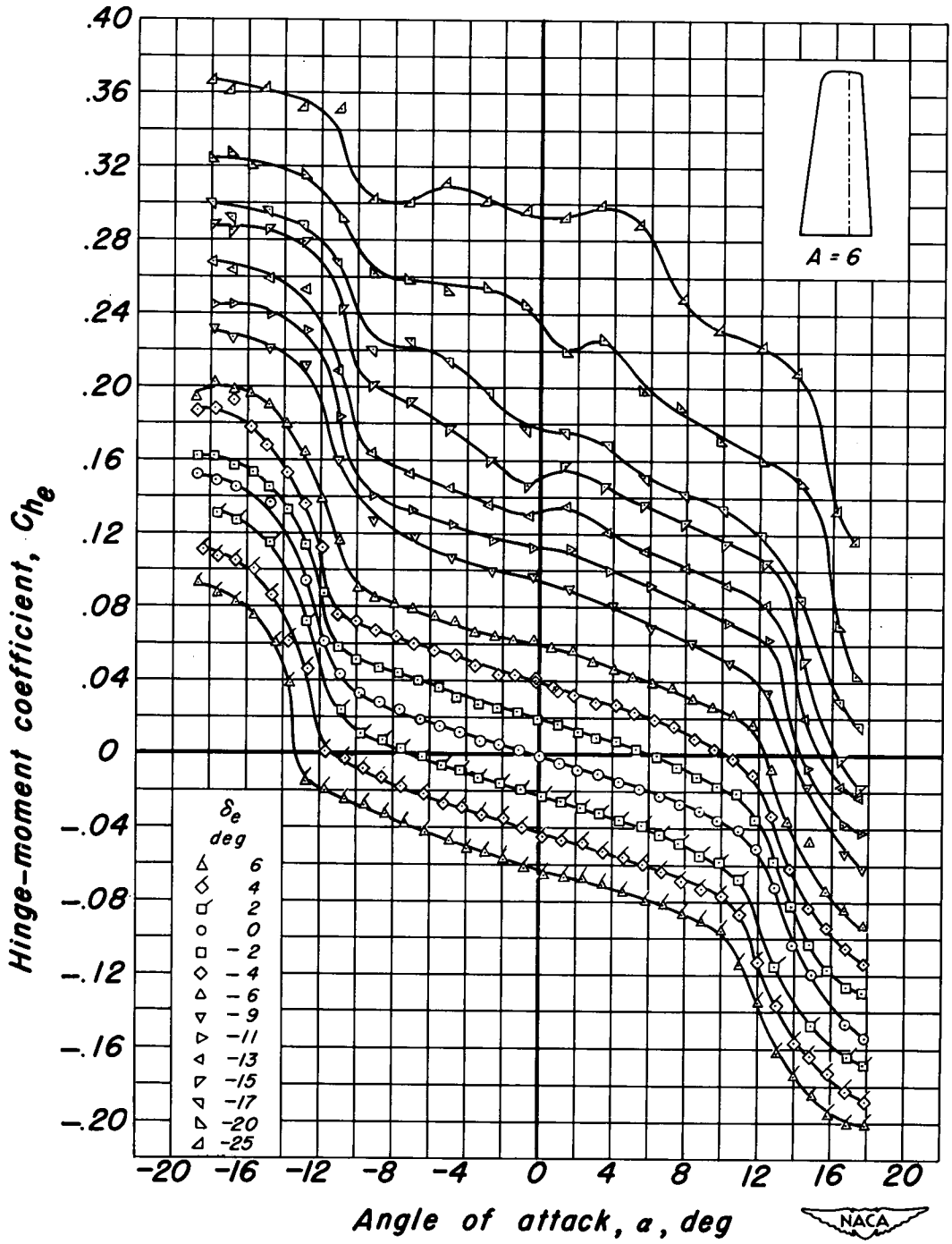

(b) Hinge-moment coefficient.

Figure 10. — Continued.

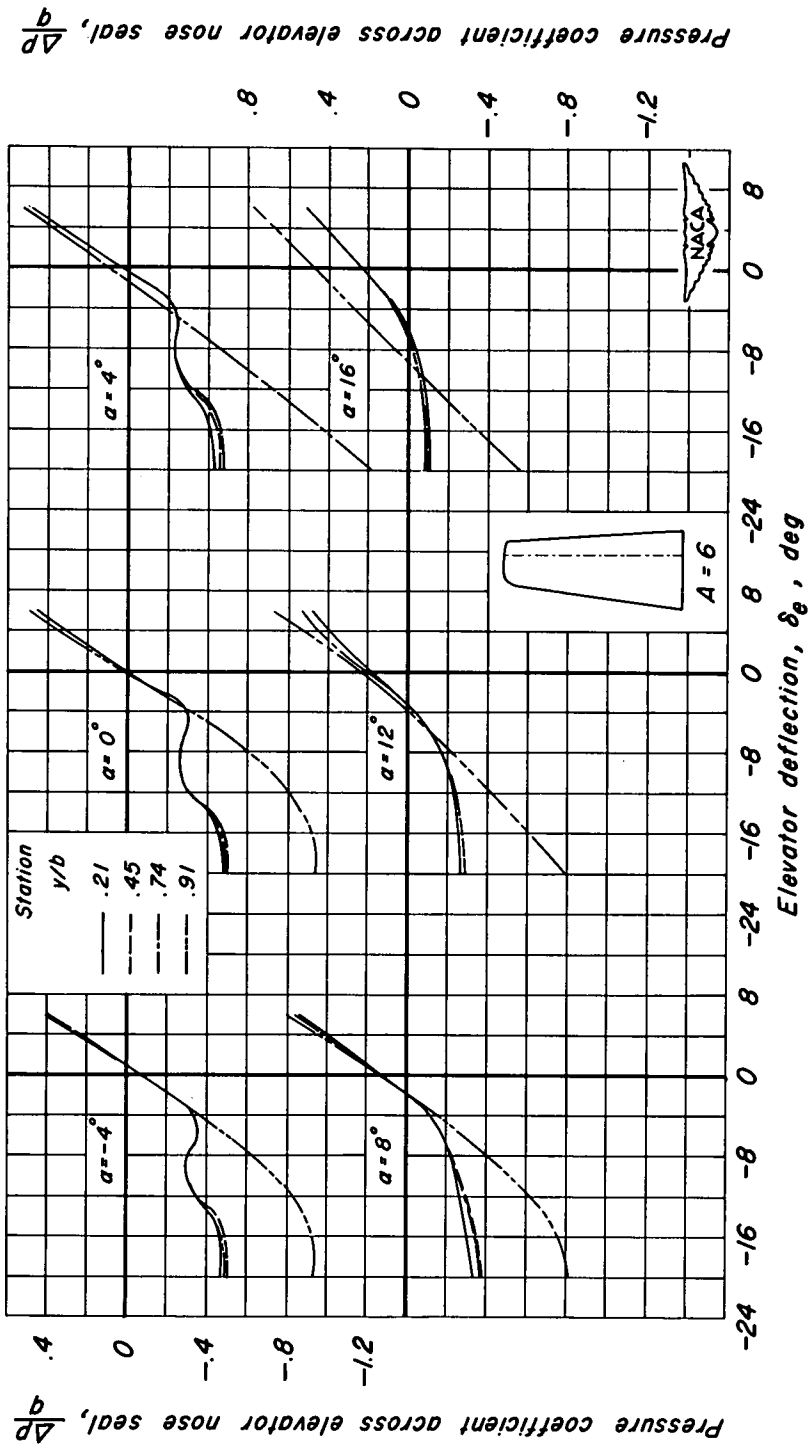

(c) Pressure coefficient.

Figure 10.—Concluded.

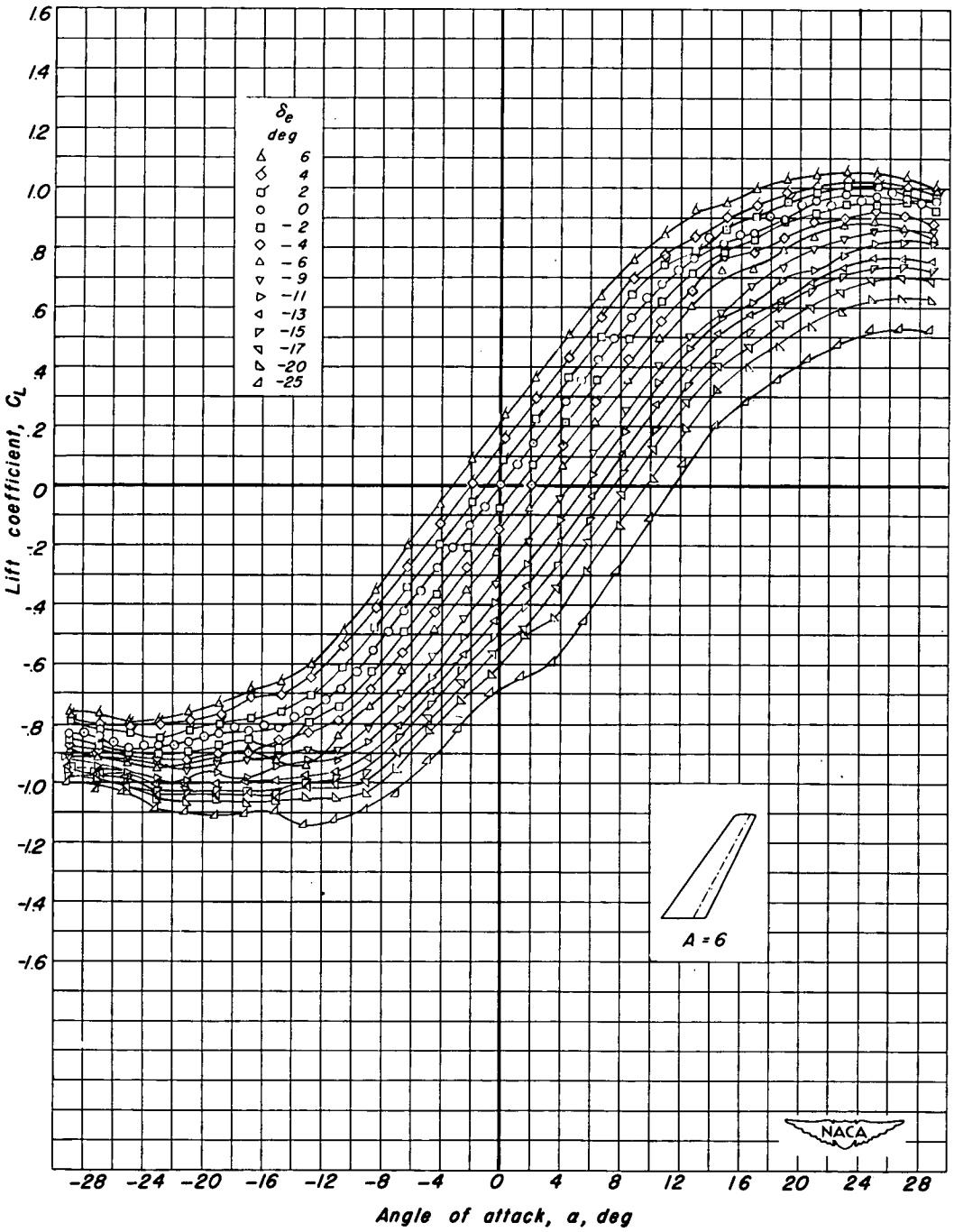

(a) Lift coefficient.

Figure 11.— Lift and hinge-moment characteristics of the 35° swept-back model of aspect ratio 6. R, 3.0 x 10^6; M, 0.23.

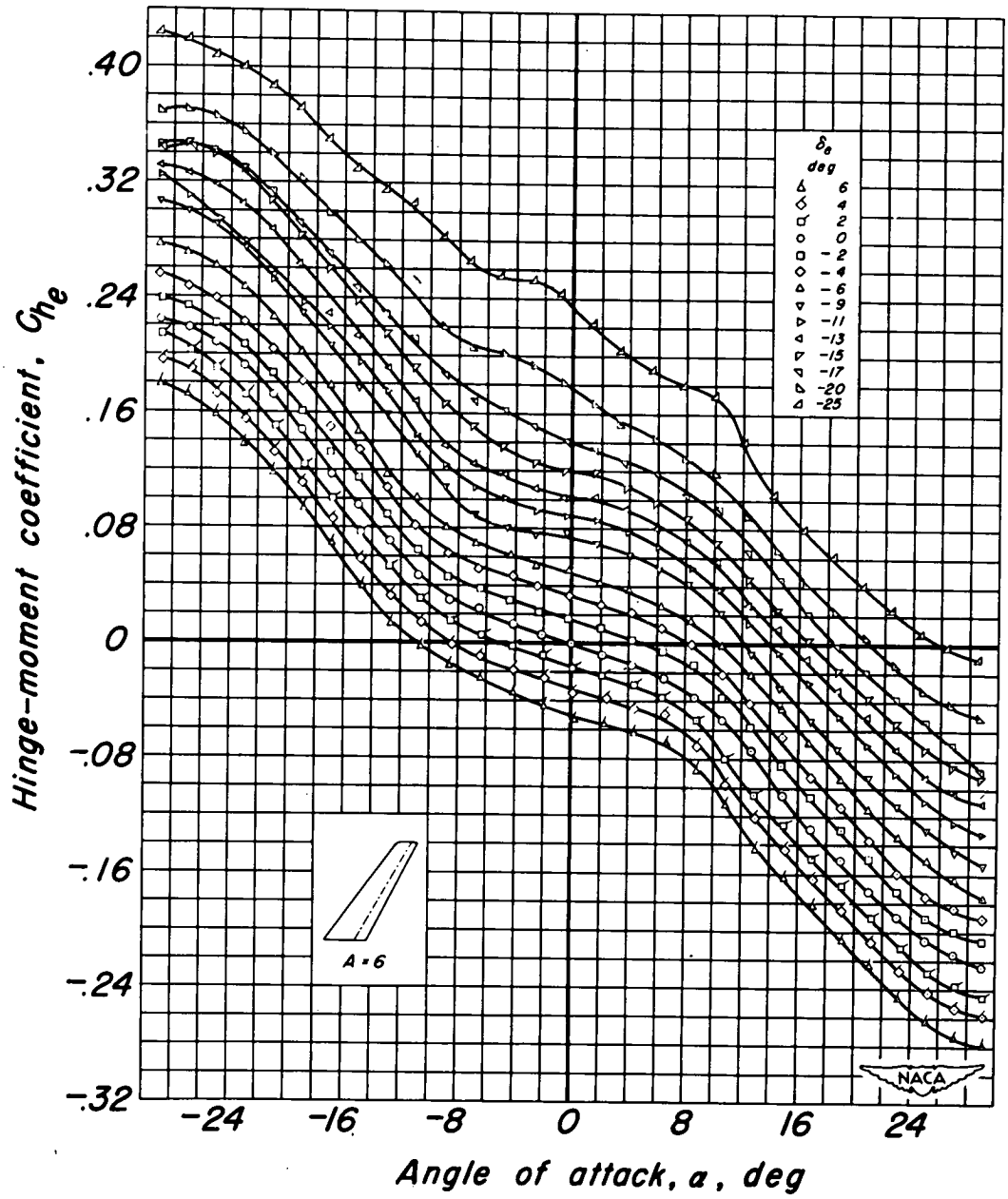

(b) Hinge-moment coefficient.

Figure 11.— Continued.

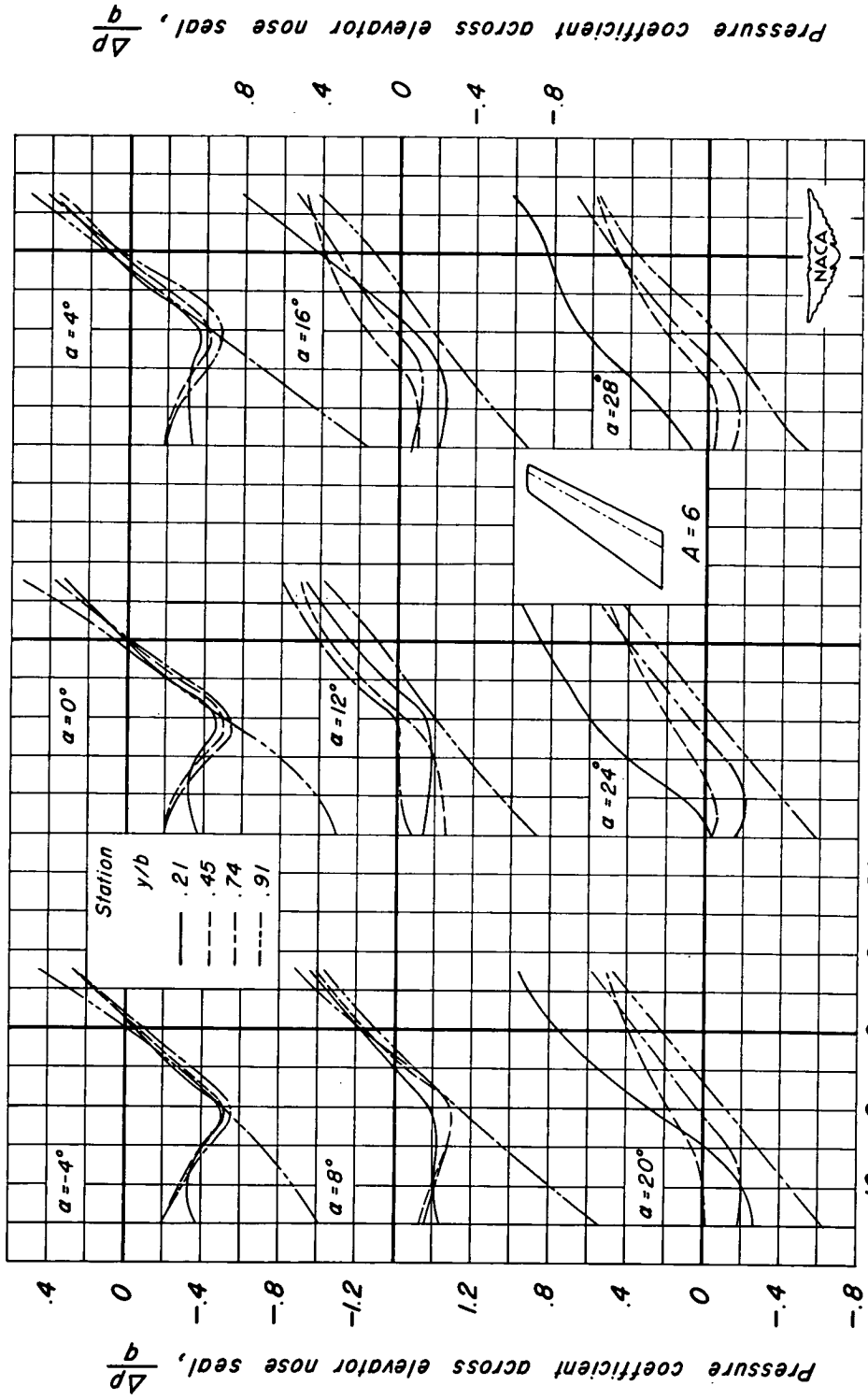

(c) Pressure coefficient.

Figure 11.—Concluded.

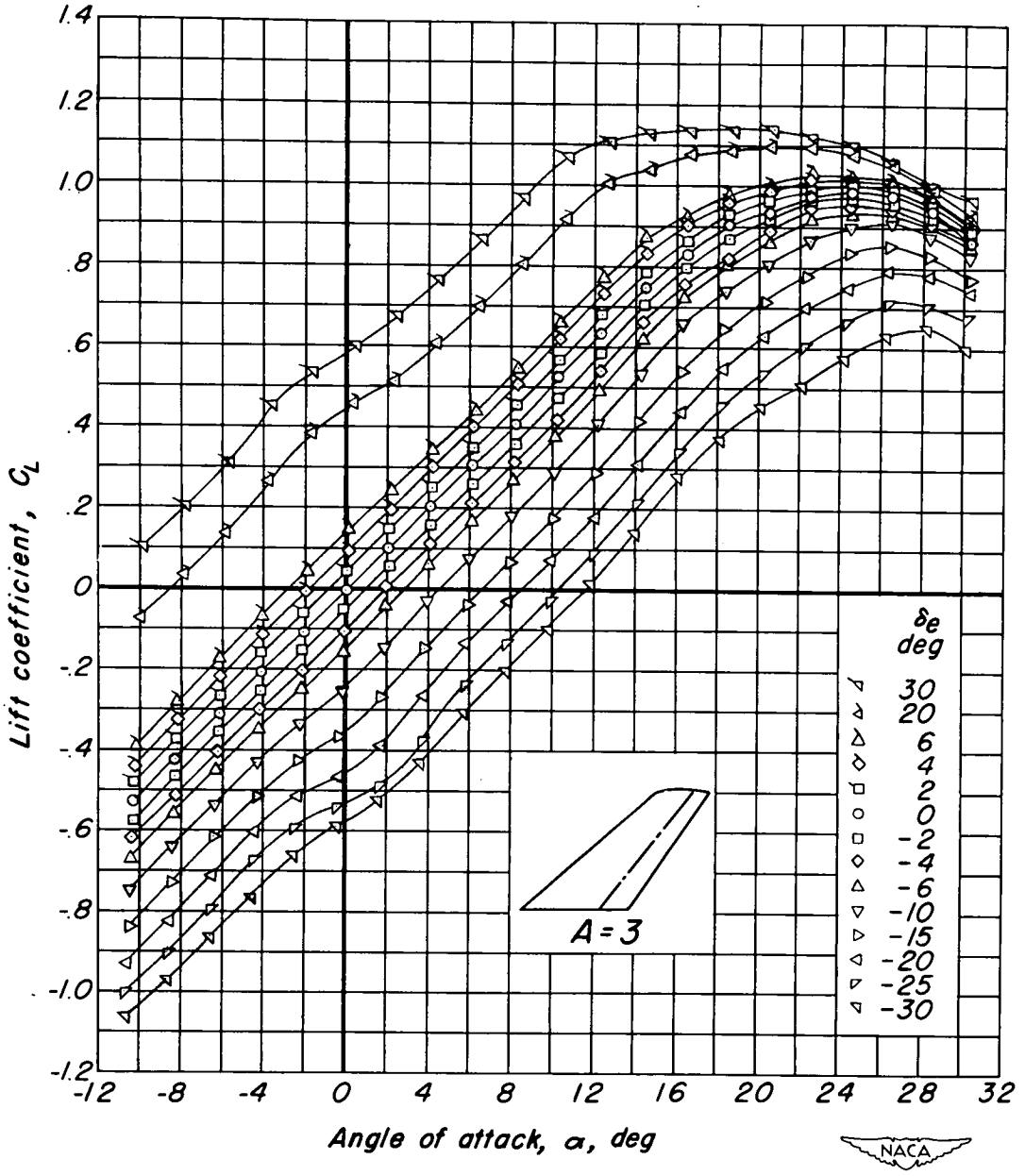

(a) M, 0.25.

Figure 12.- The variation of lift coefficient with angle of attack for the 45° swept-back model of aspect ratio 3. R, 4.0×10^6.

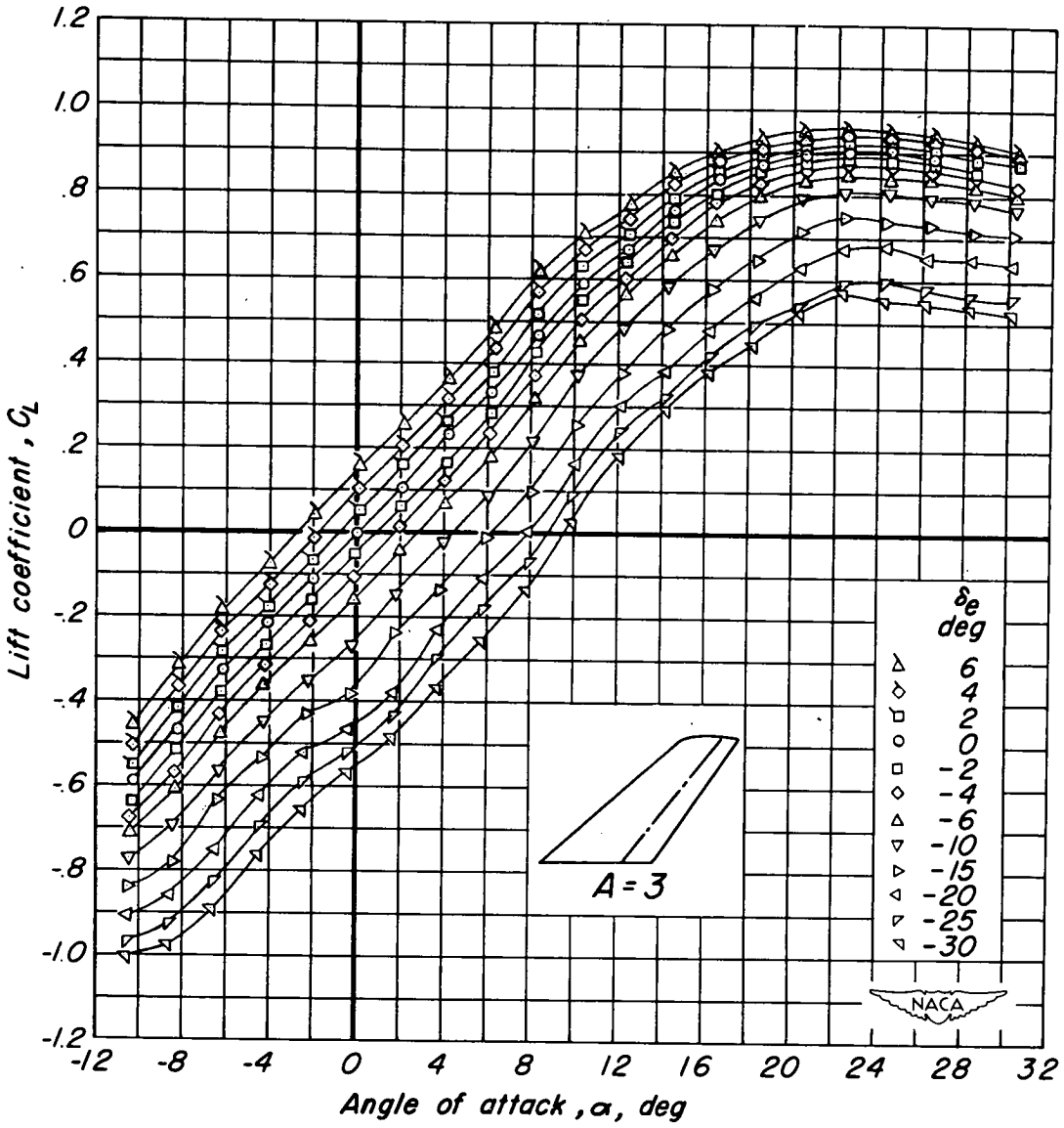

(b) M, 0.60.

Figure 12.—Continued.

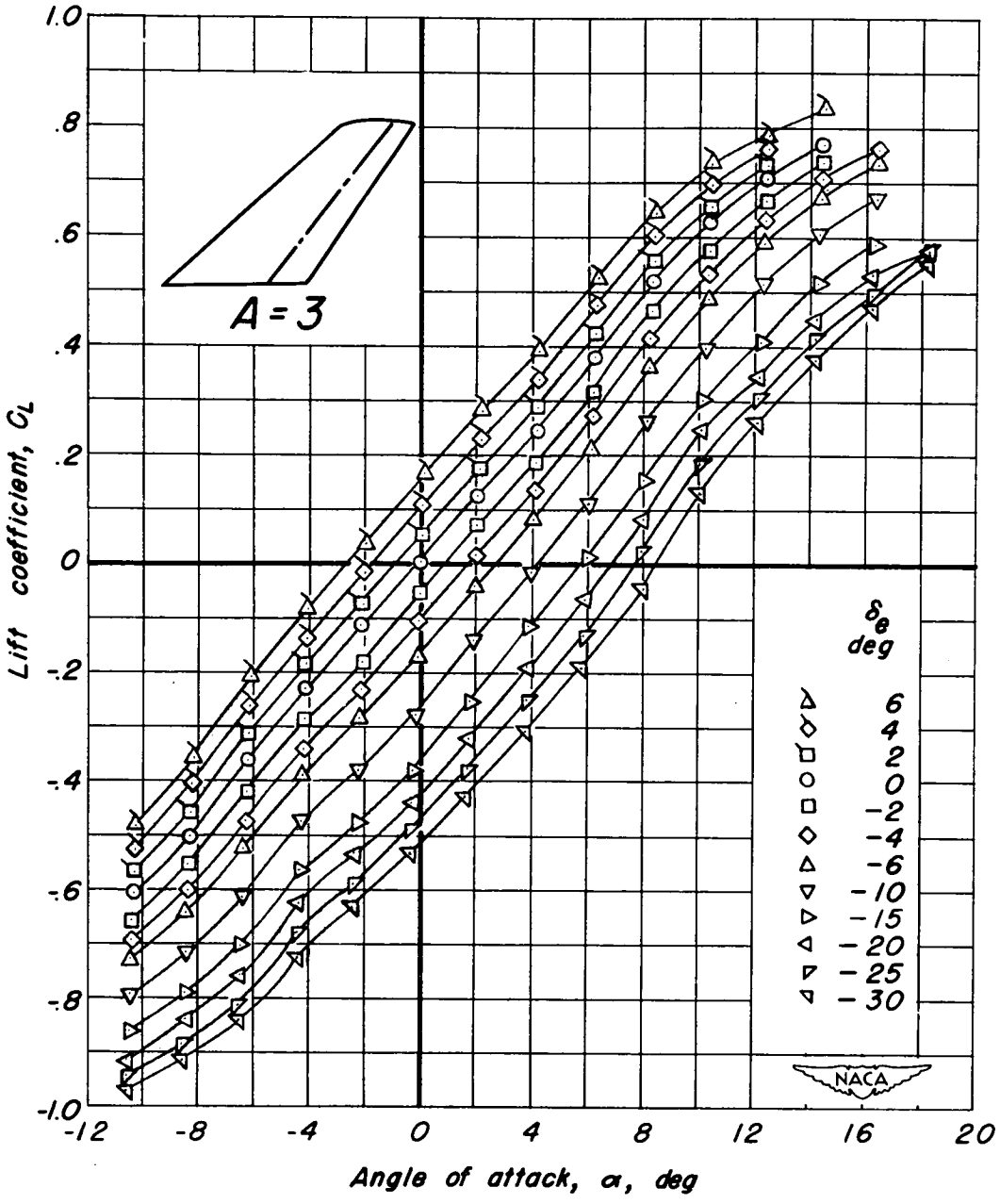

(c) M, 0.80.

Figure 12.–Continued.

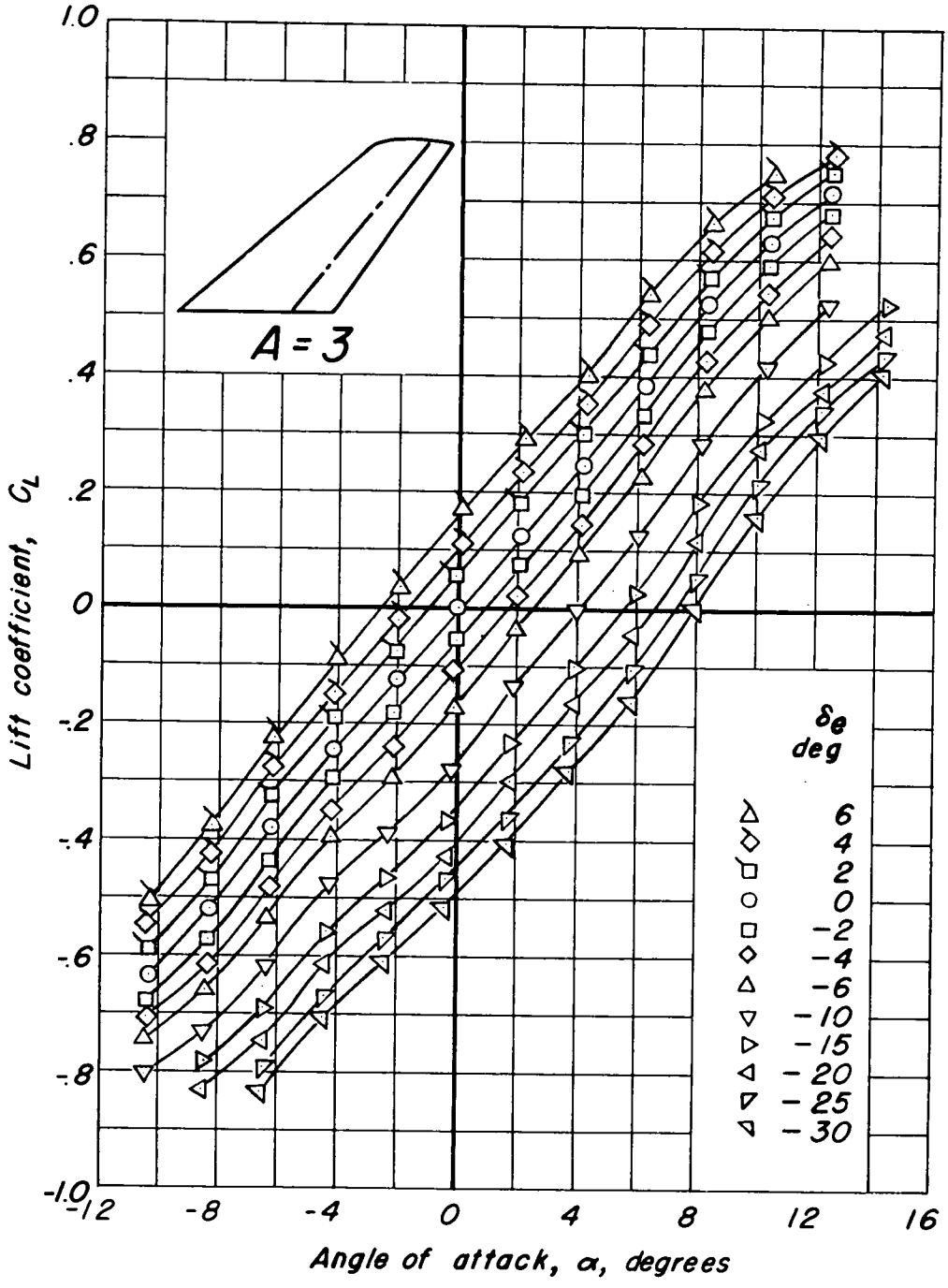

(d) M, 0.85.

Figure 12.—Continued.

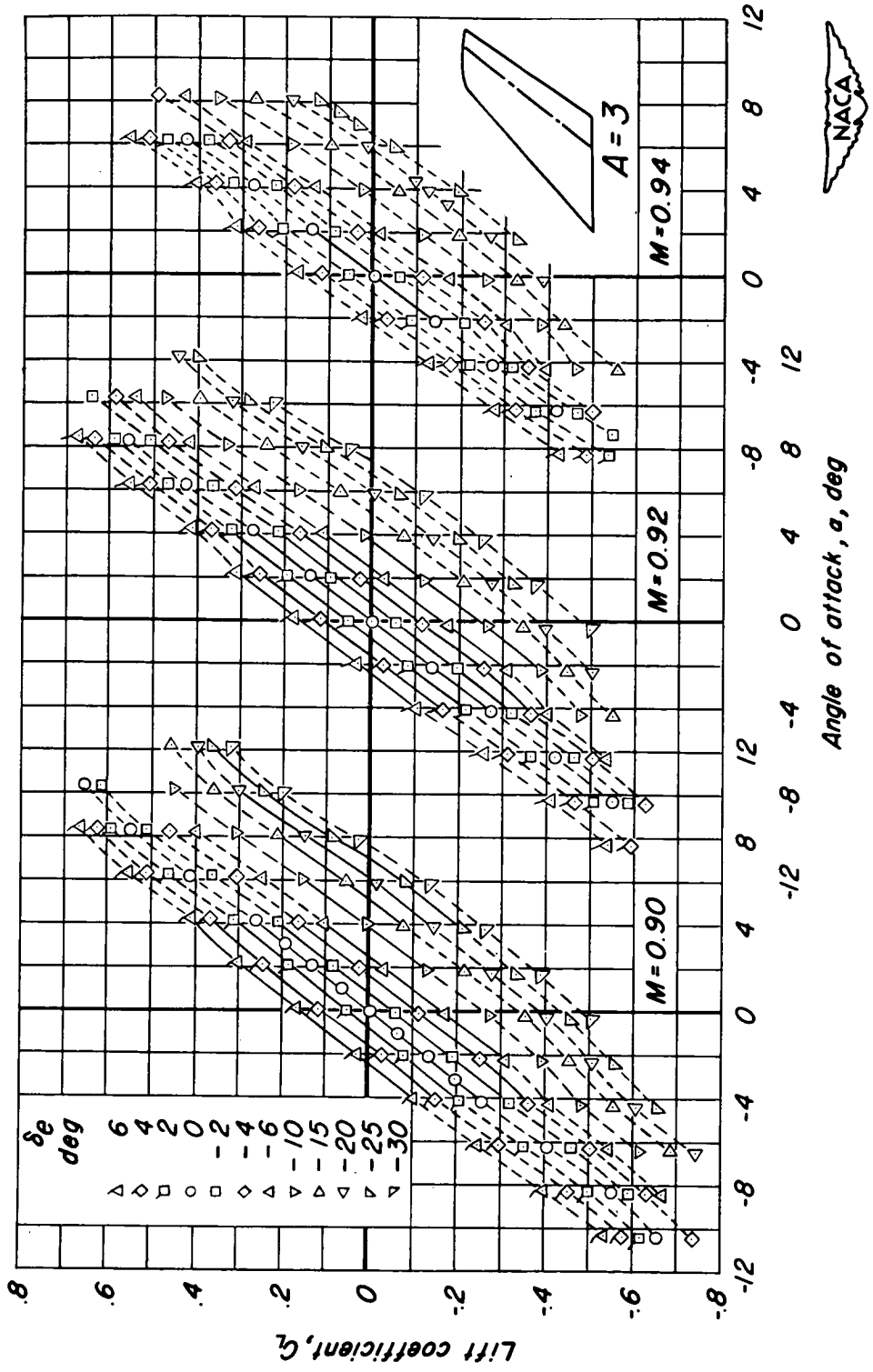

Figure 12.—Concluded.

(e) M, 0.90; M, 0.92; M, 0.94.

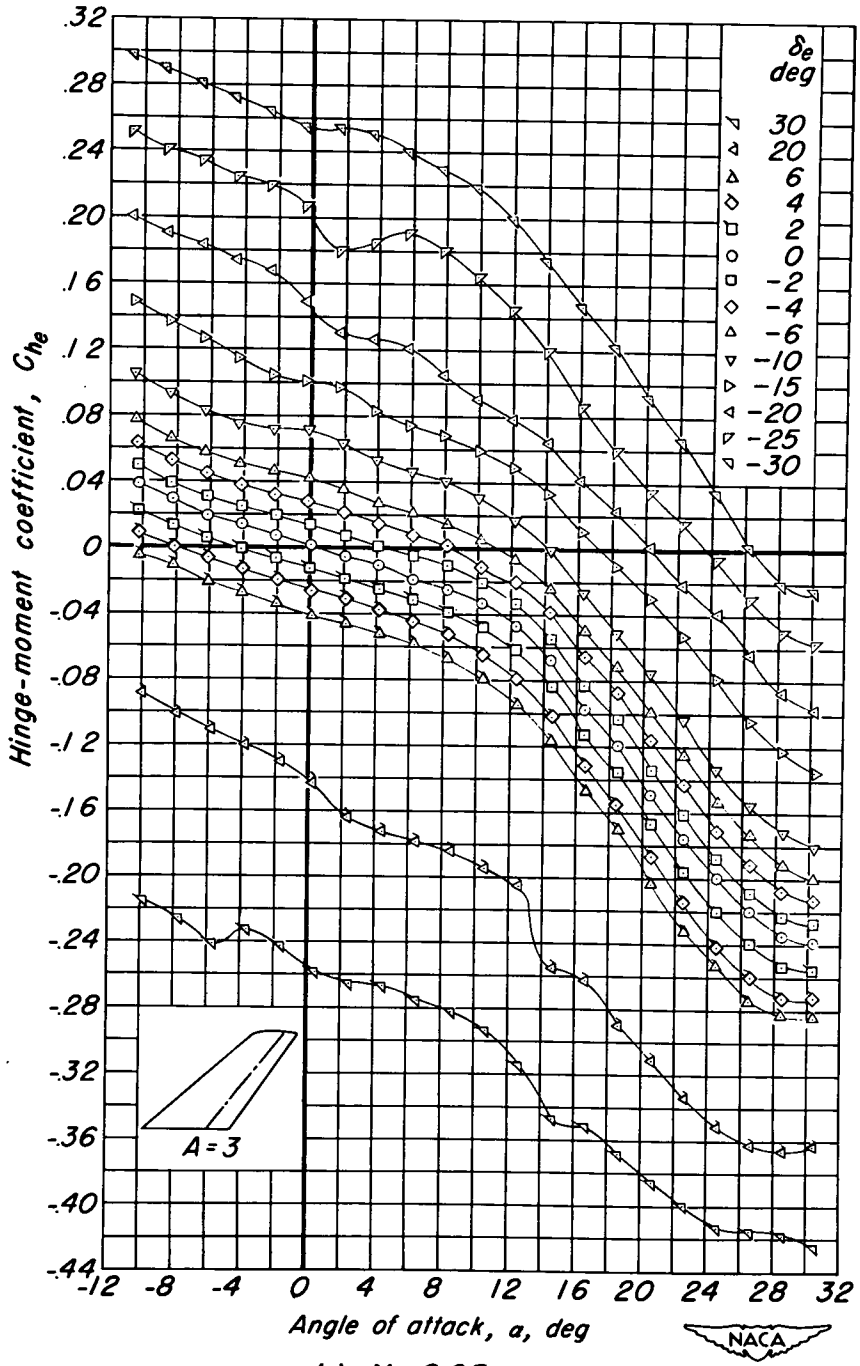

(a) M, 0.25.

Figure 13.—The variation of elevator hinge-moment coefficient with angle of attack for the 45° swept-back model of aspect ratio 3. R, 4.0 x 10^6.

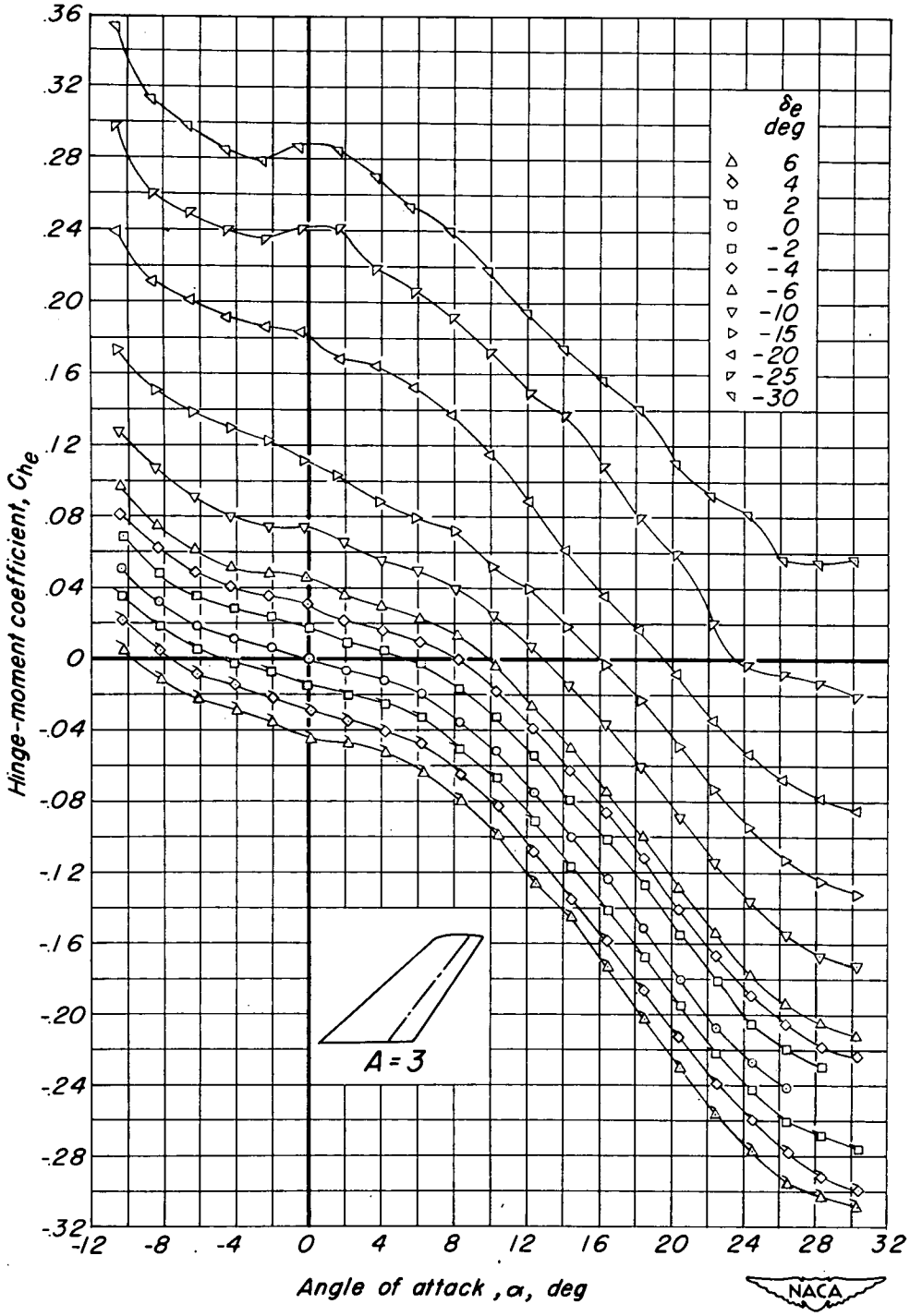

(b) M, 0.60.

Figure 13.–Continued.

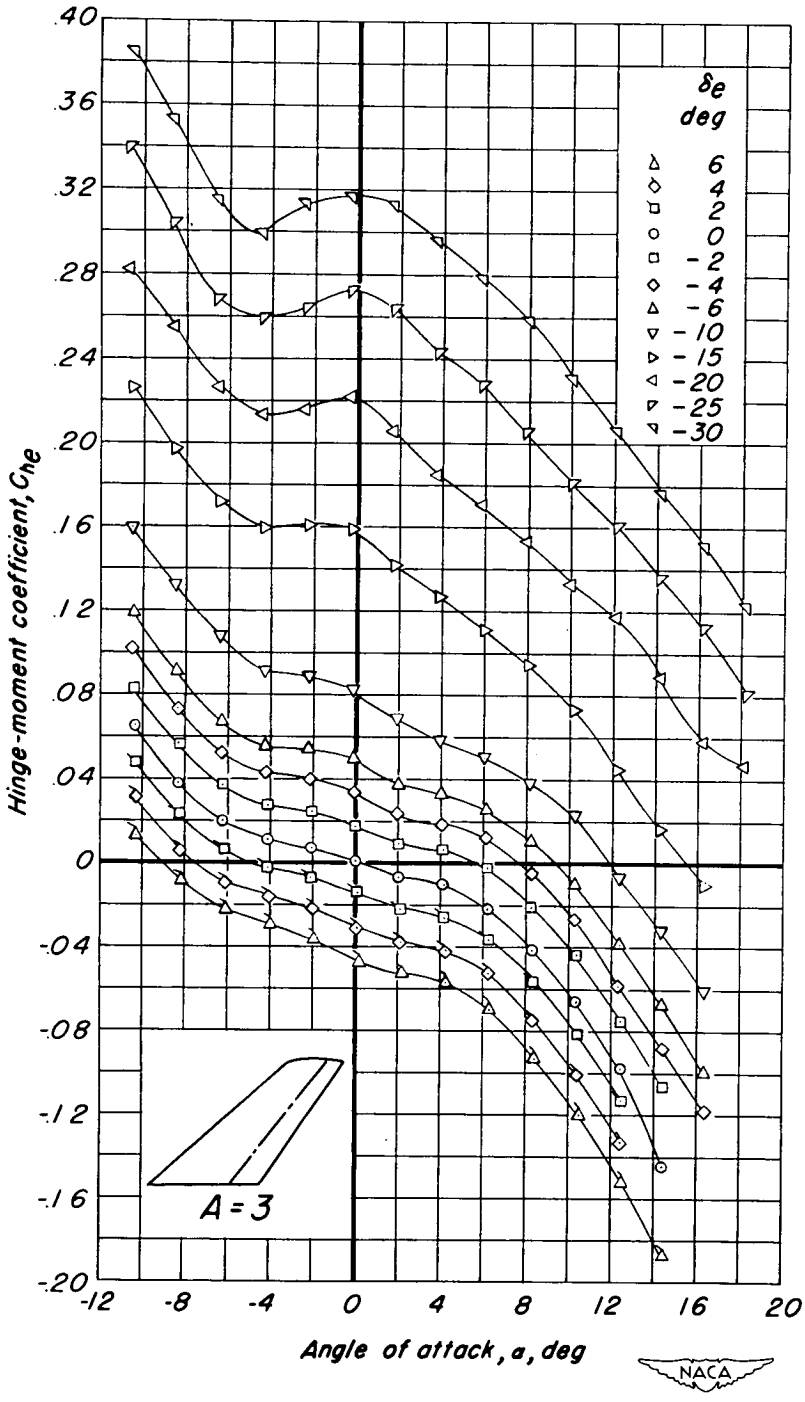

(c) M, 0.80.

Figure 13.–Continued.

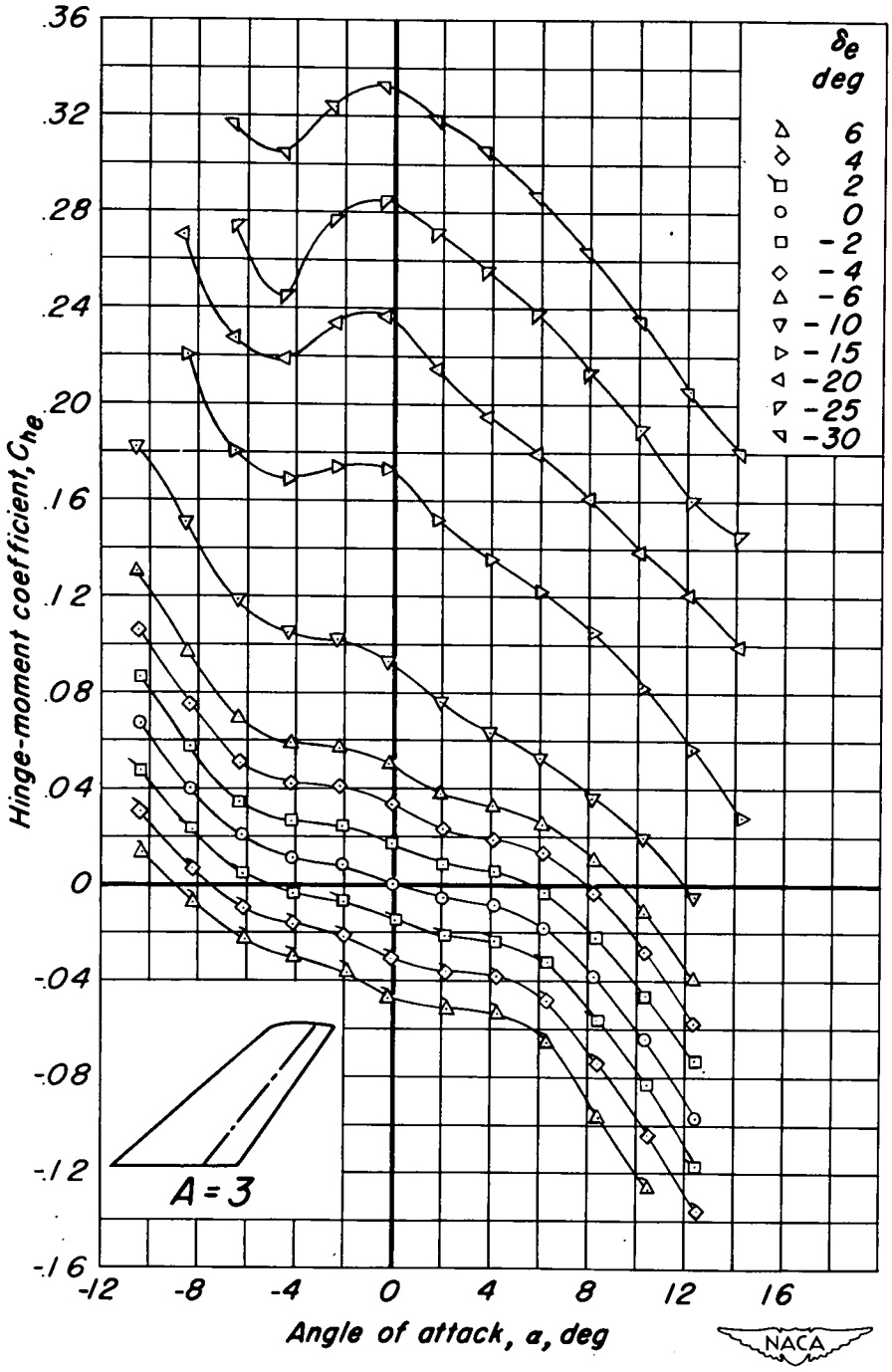

(d) M, 0.85.

Figure 13.—Continued.

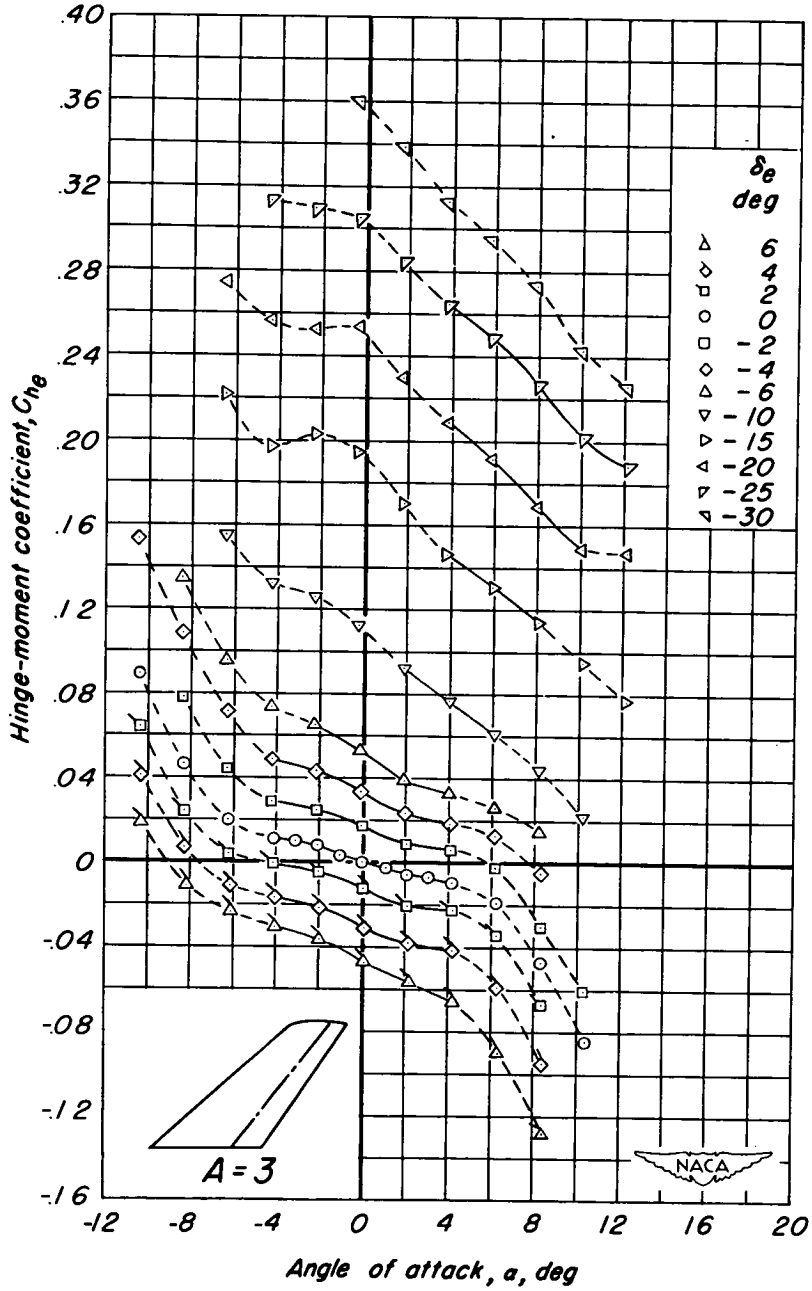

(e) M, 0.90.

Figure 13.- Continued.

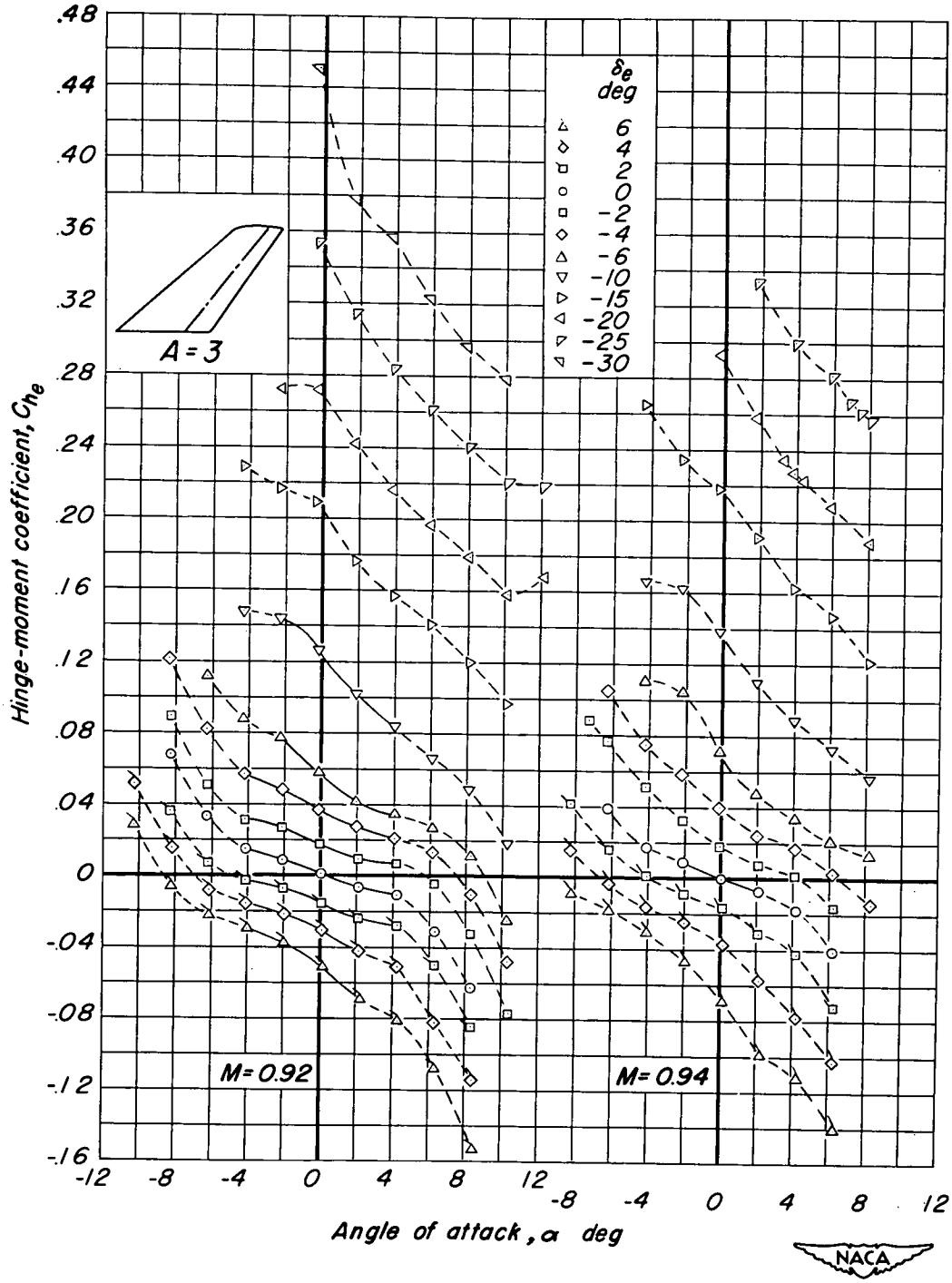

(f) M,0.92 ; M,0.94.

Figure 13.–Concluded.

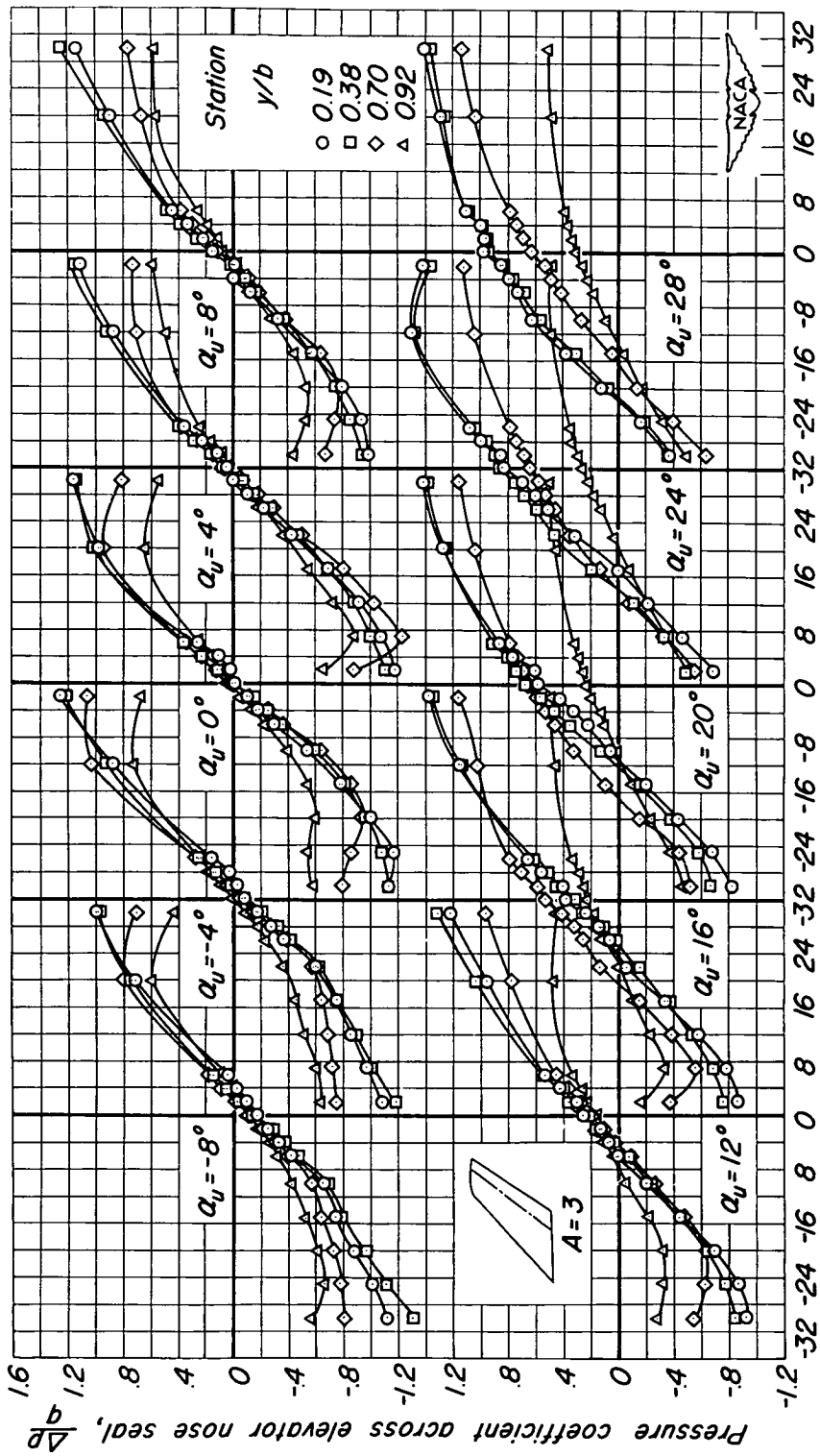

(a) M, 0.25.

Figure 14.—The variation of pressure coefficient across the elevator nose seal with elevator deflection for the 45° swept-back model of aspect ratio 3. R, 4.0 x 10^6.

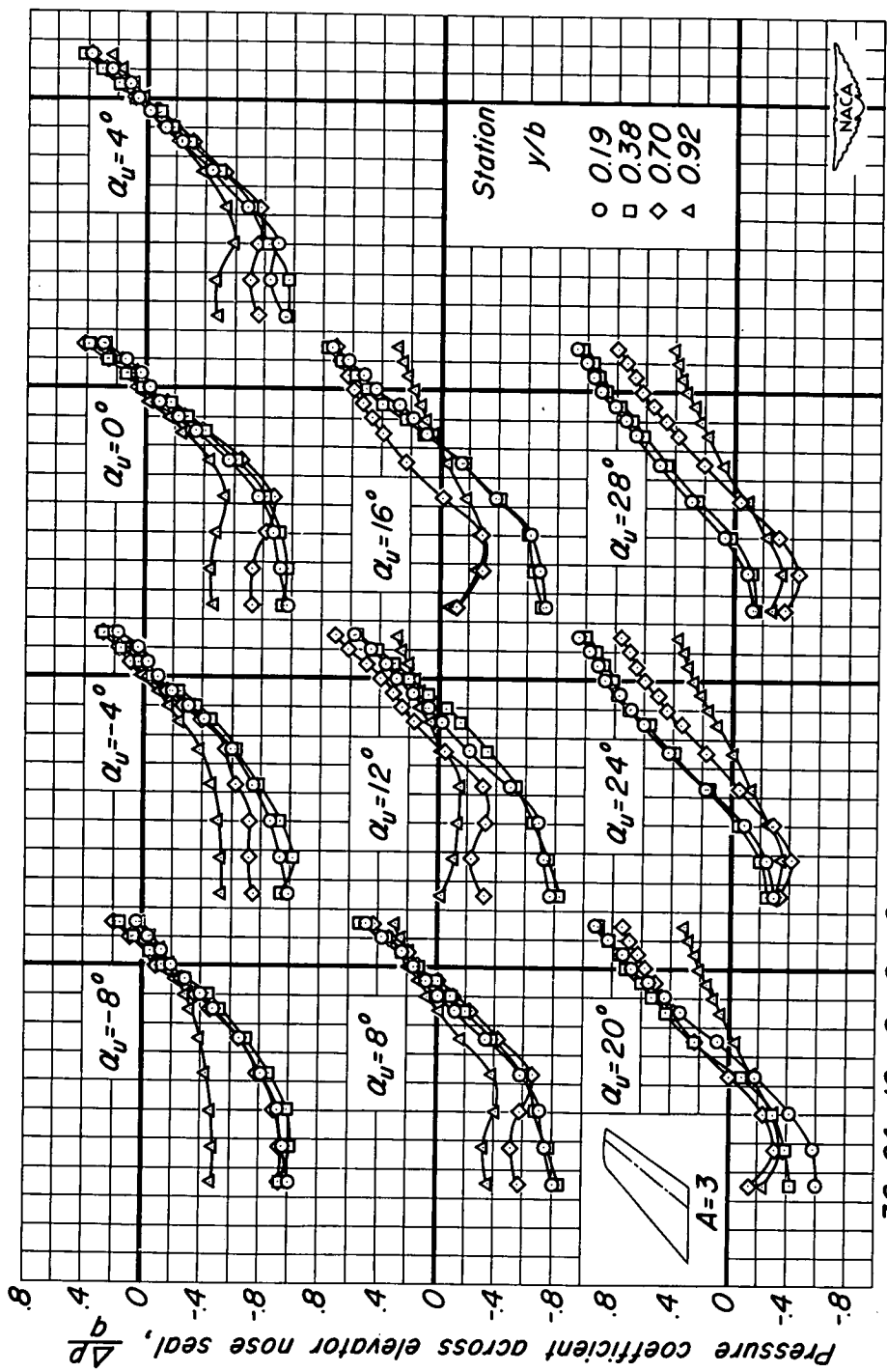

Figure 14.–Continued.

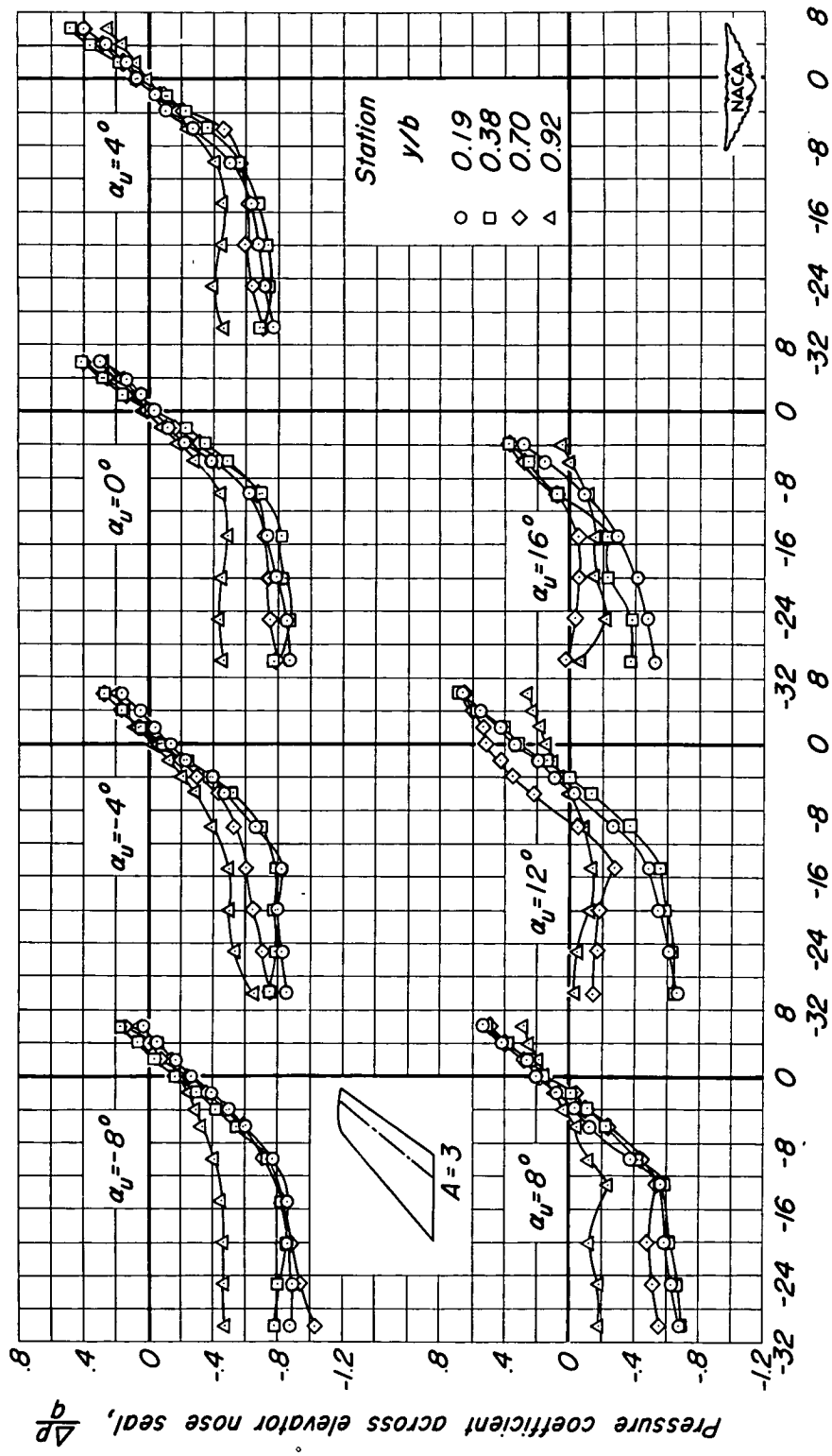

(c) M,0.80.

Figure 14-Continued.

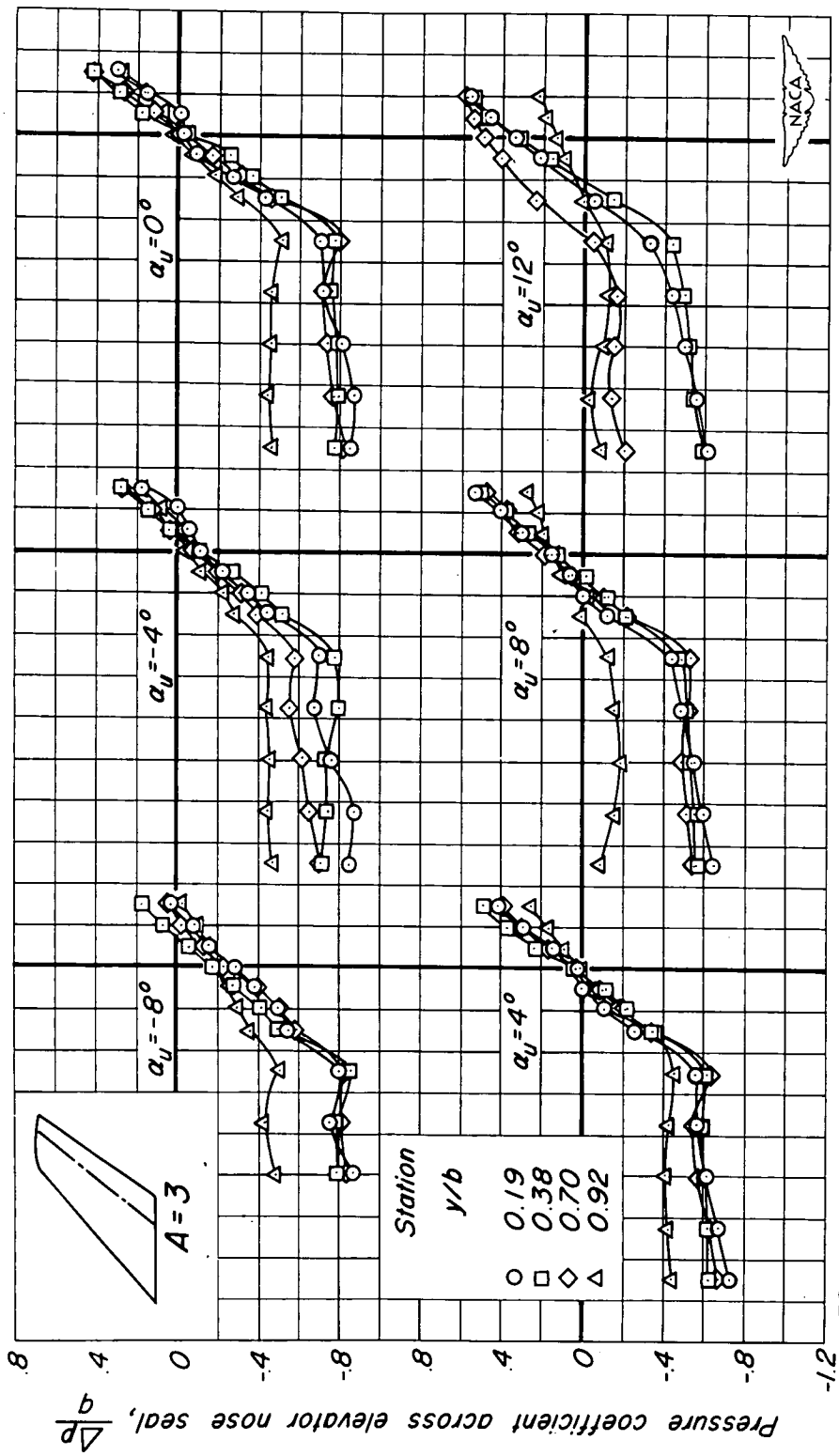

Figure 14.-Continued.

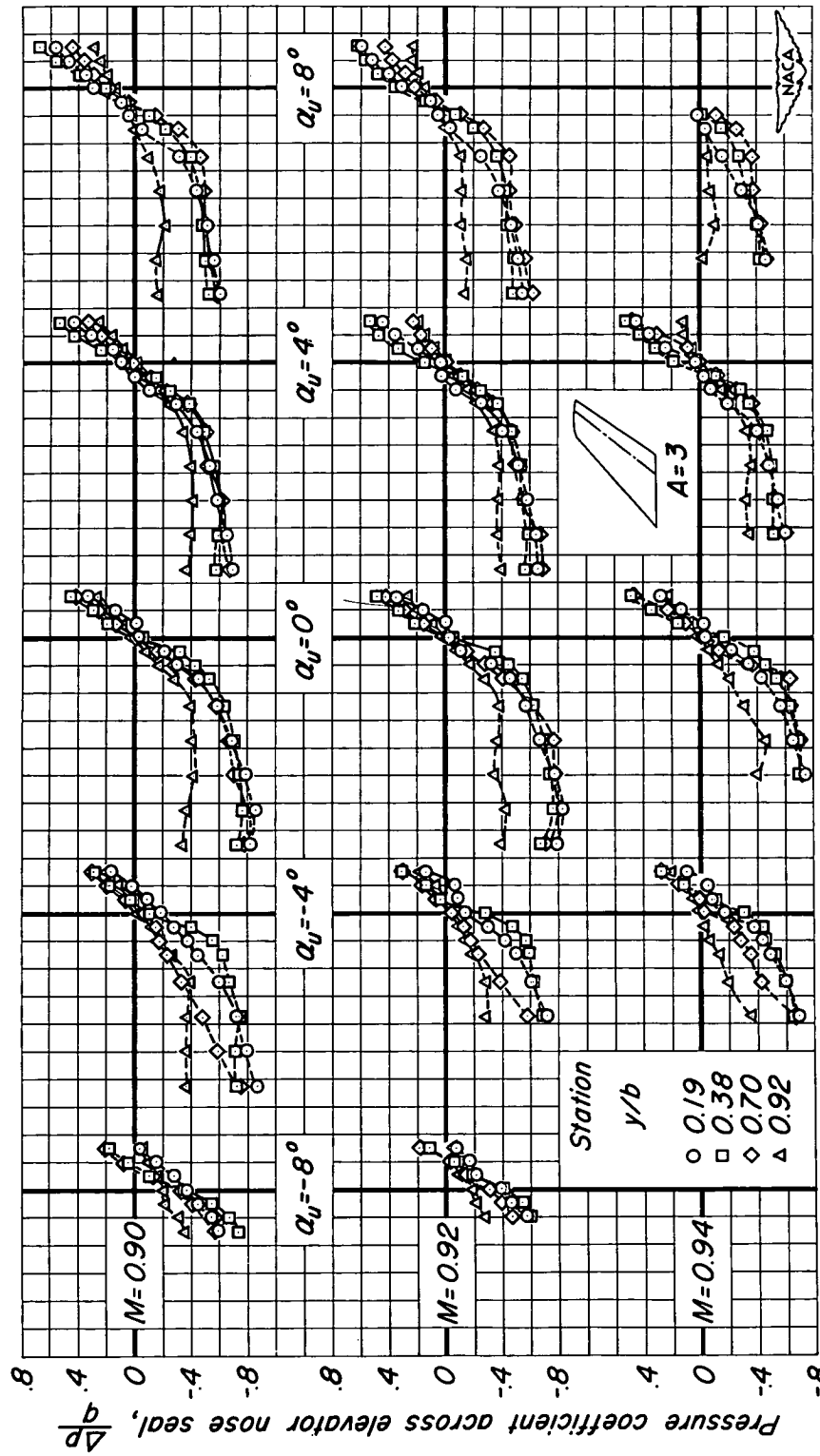

(e) M,0.90; M,0.92; M,0.94.

Figure 14-Concluded.

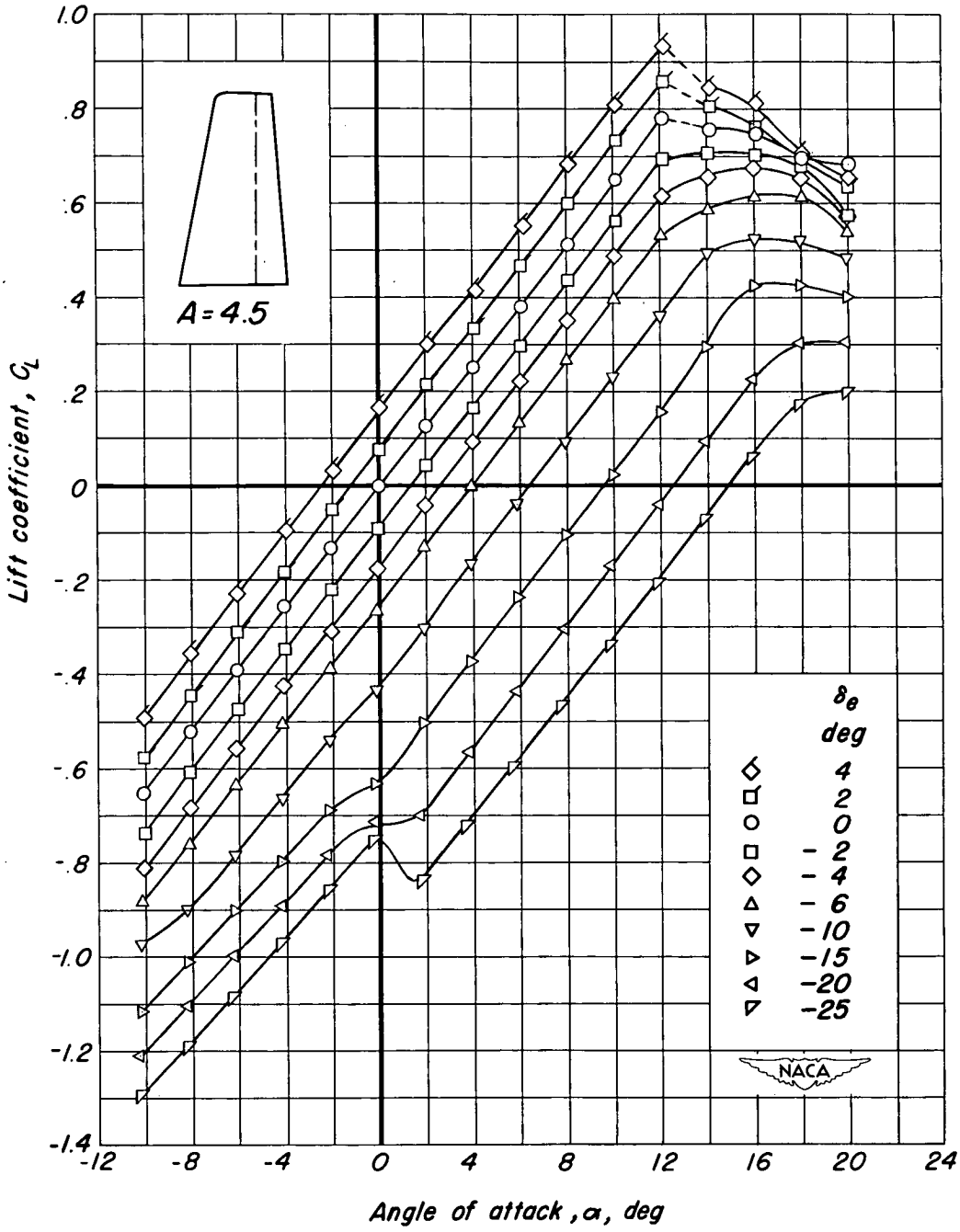

(a) M, 0.21.

Figure 15.– The variation of lift coefficient with angle of attack for the unswept model of aspect ratio 4.5. R, 2.0×10^6; $\delta_t = 0°$.

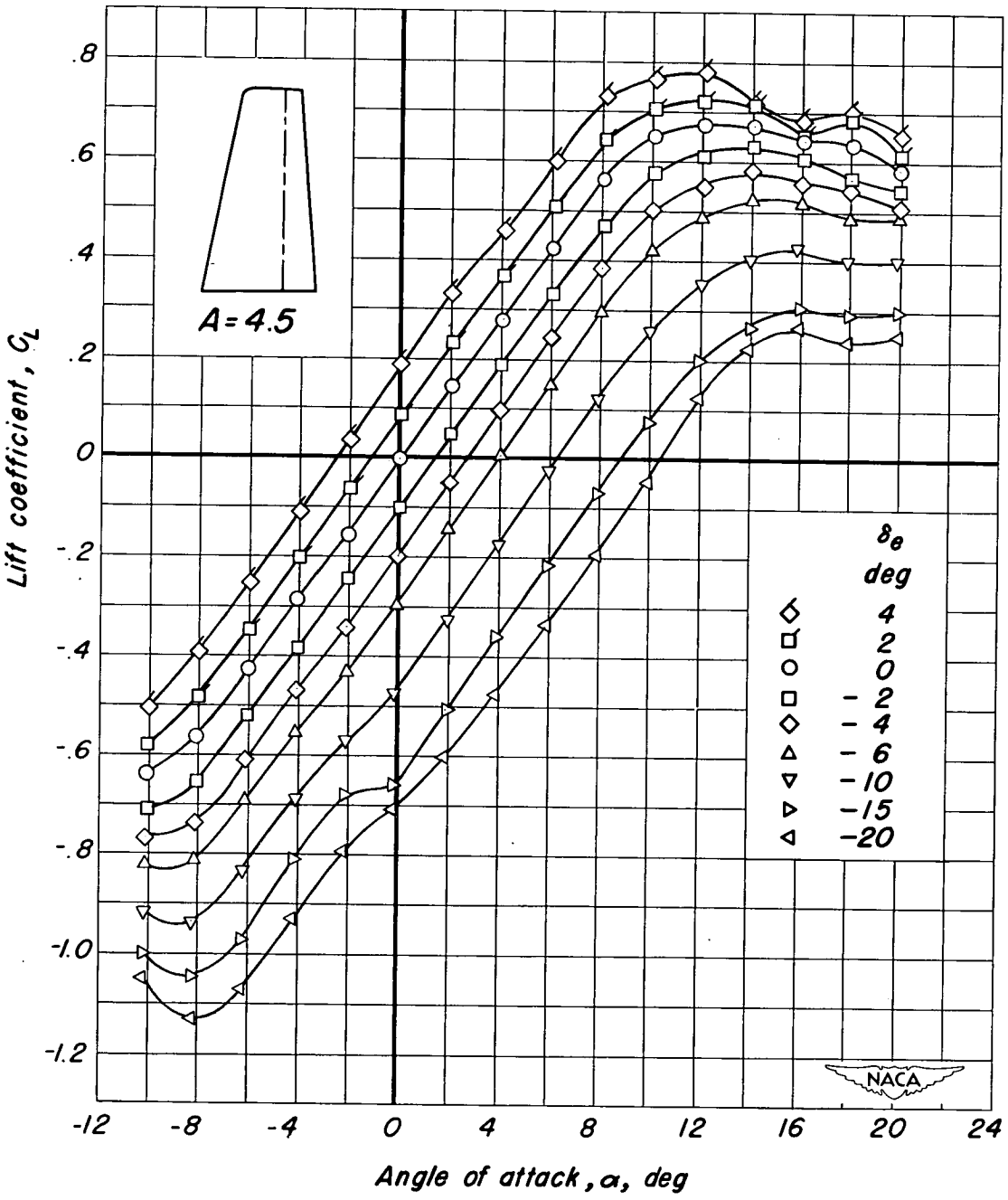

(b) M, 0.60.

Figure 15.— Continued.

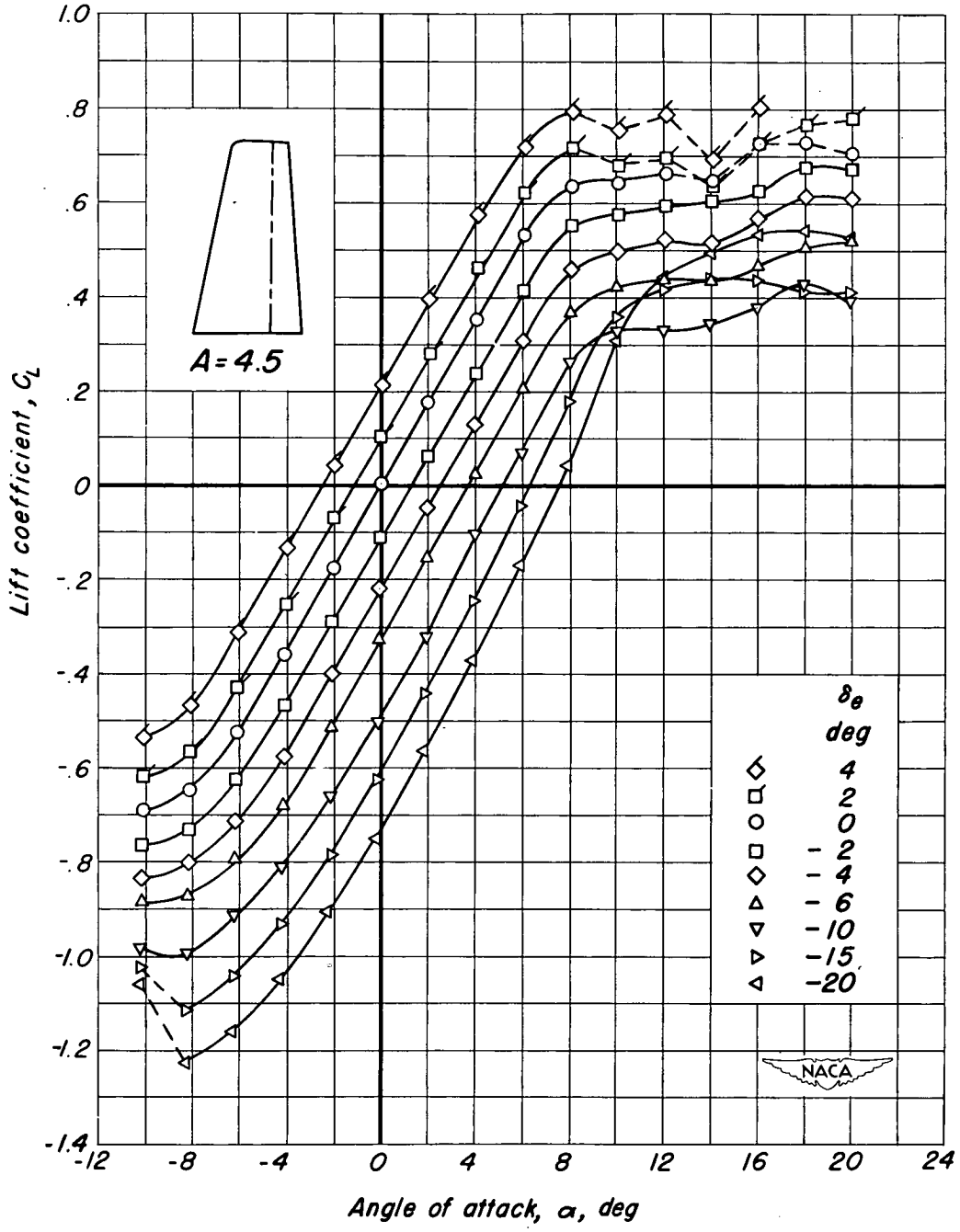

(c) M, 0.80.

Figure 15.— Continued.

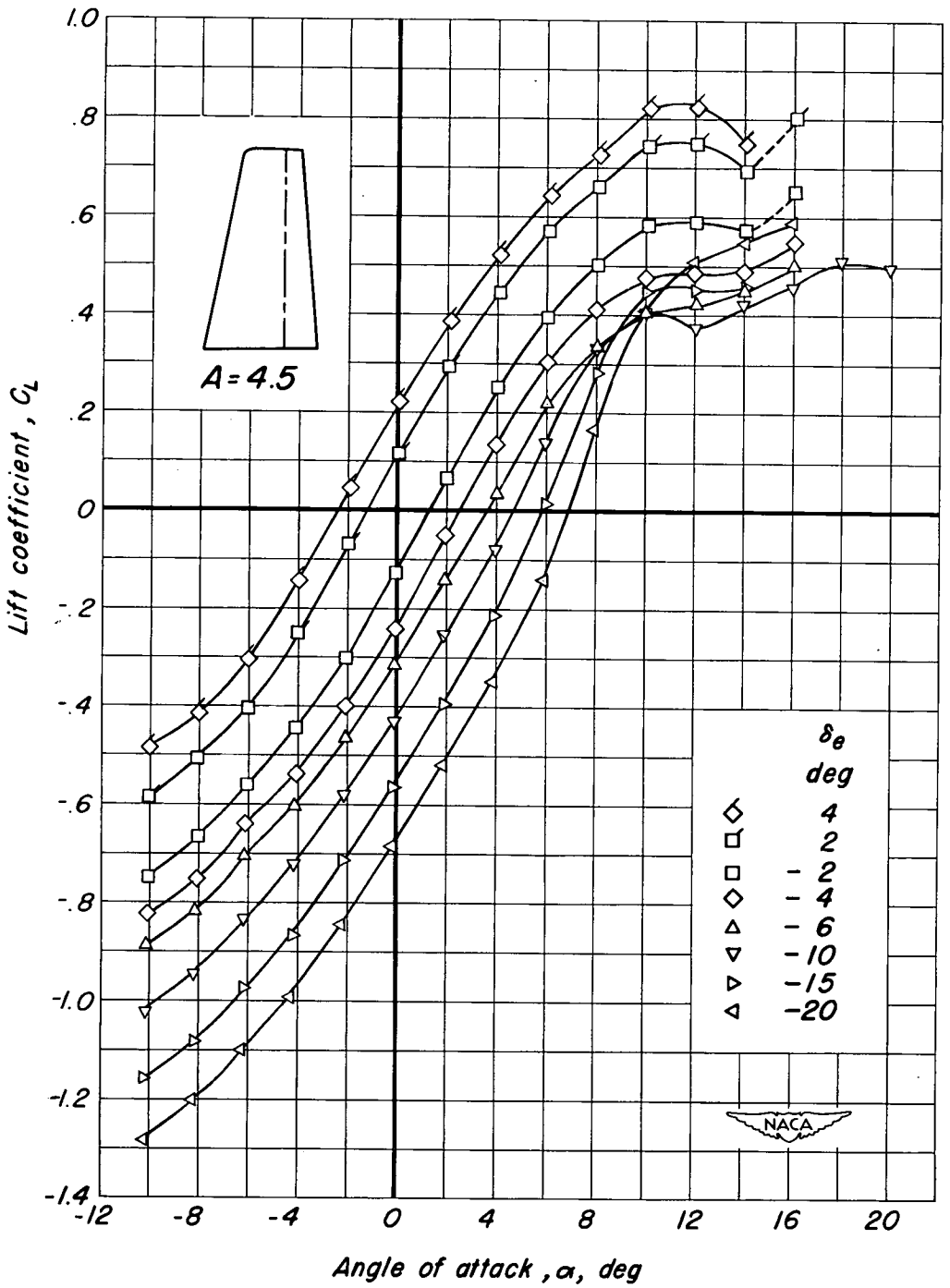

(d) M, 0.85.

Figure 15.— Continued.

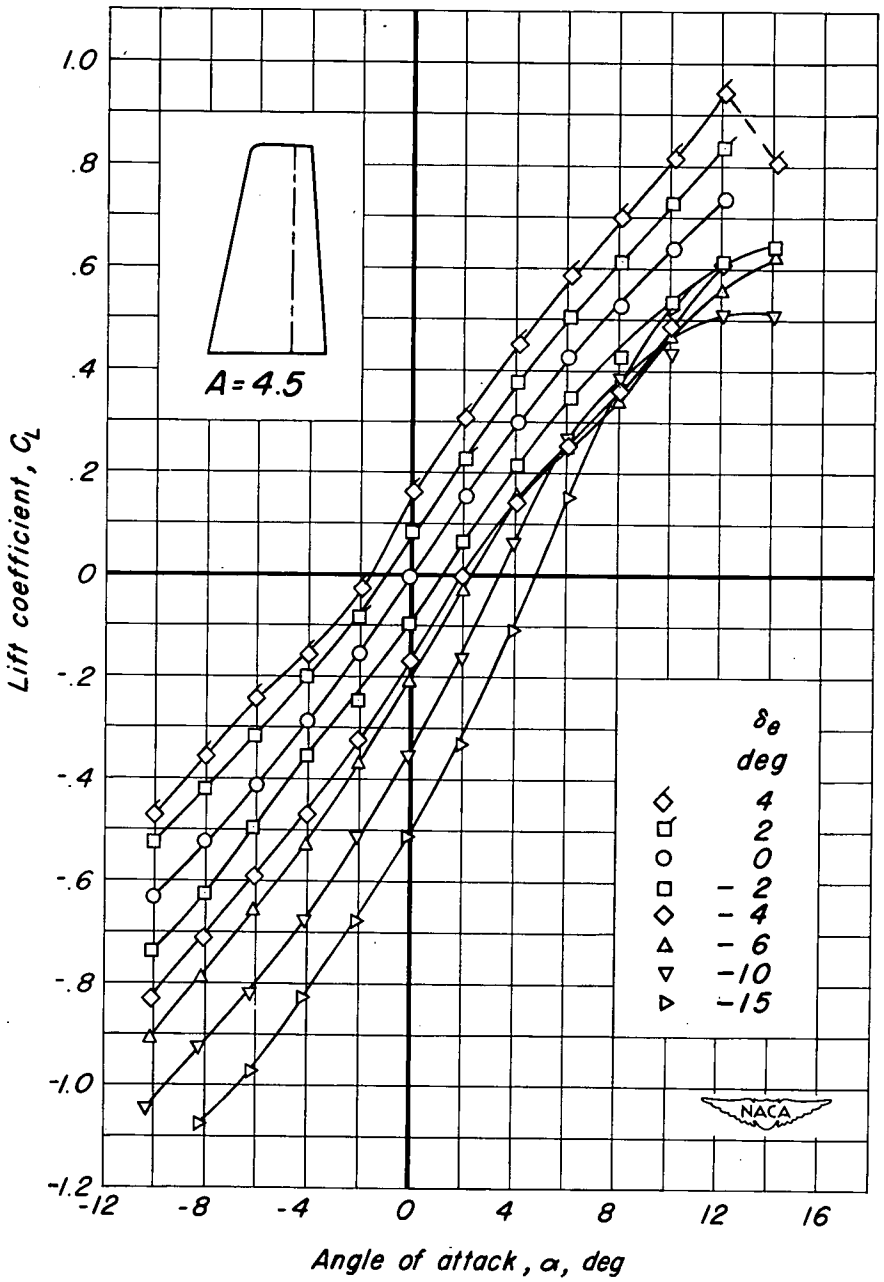

(e) M, 0.88.

Figure 15.— Concluded.

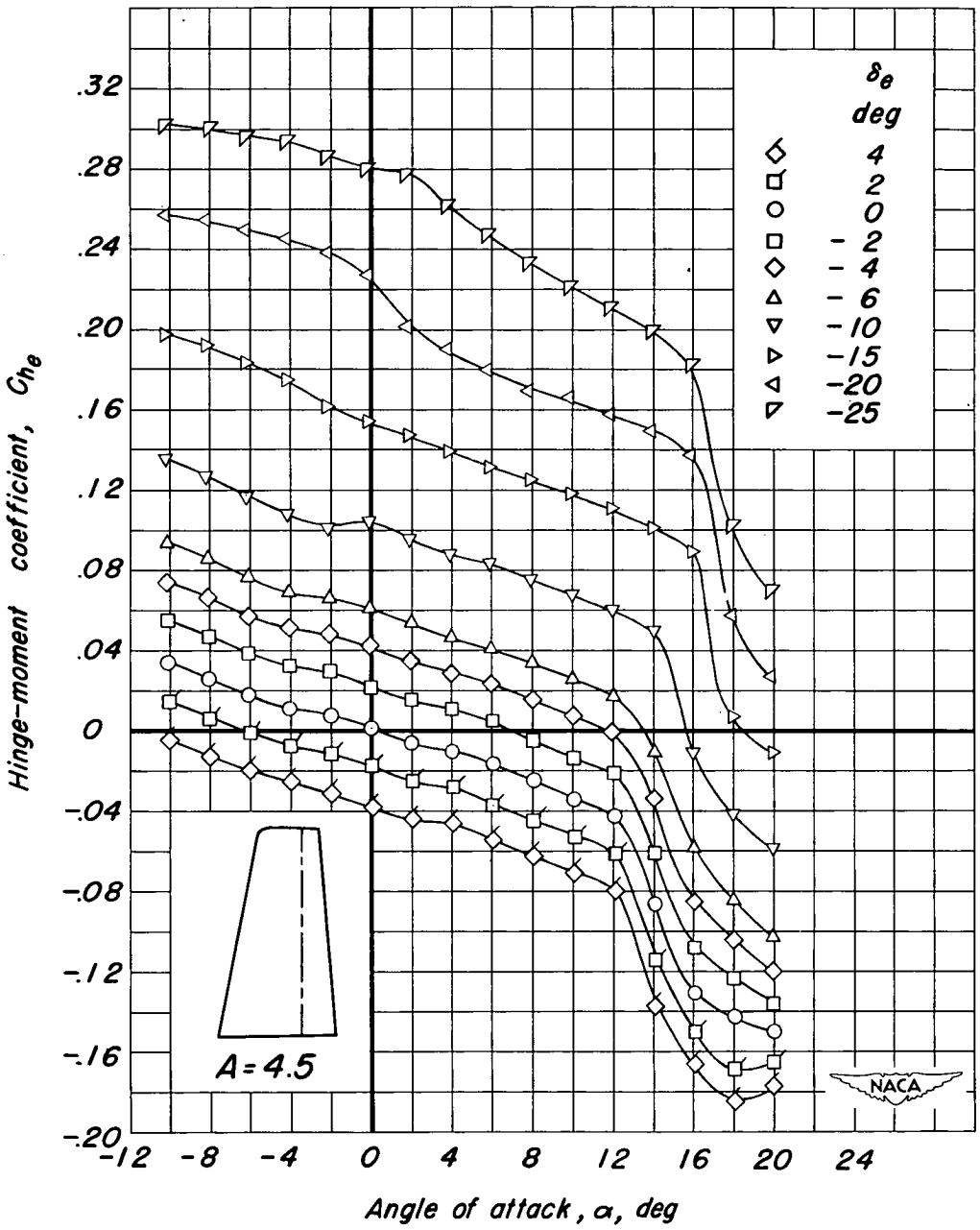

(a) M, 0.21.

Figure 16.– The variation of elevator hinge-moment coefficient with angle of attack for the unswept model of aspect ratio 4.5. R, 2.0×10^6; $\delta_t = 0°$.

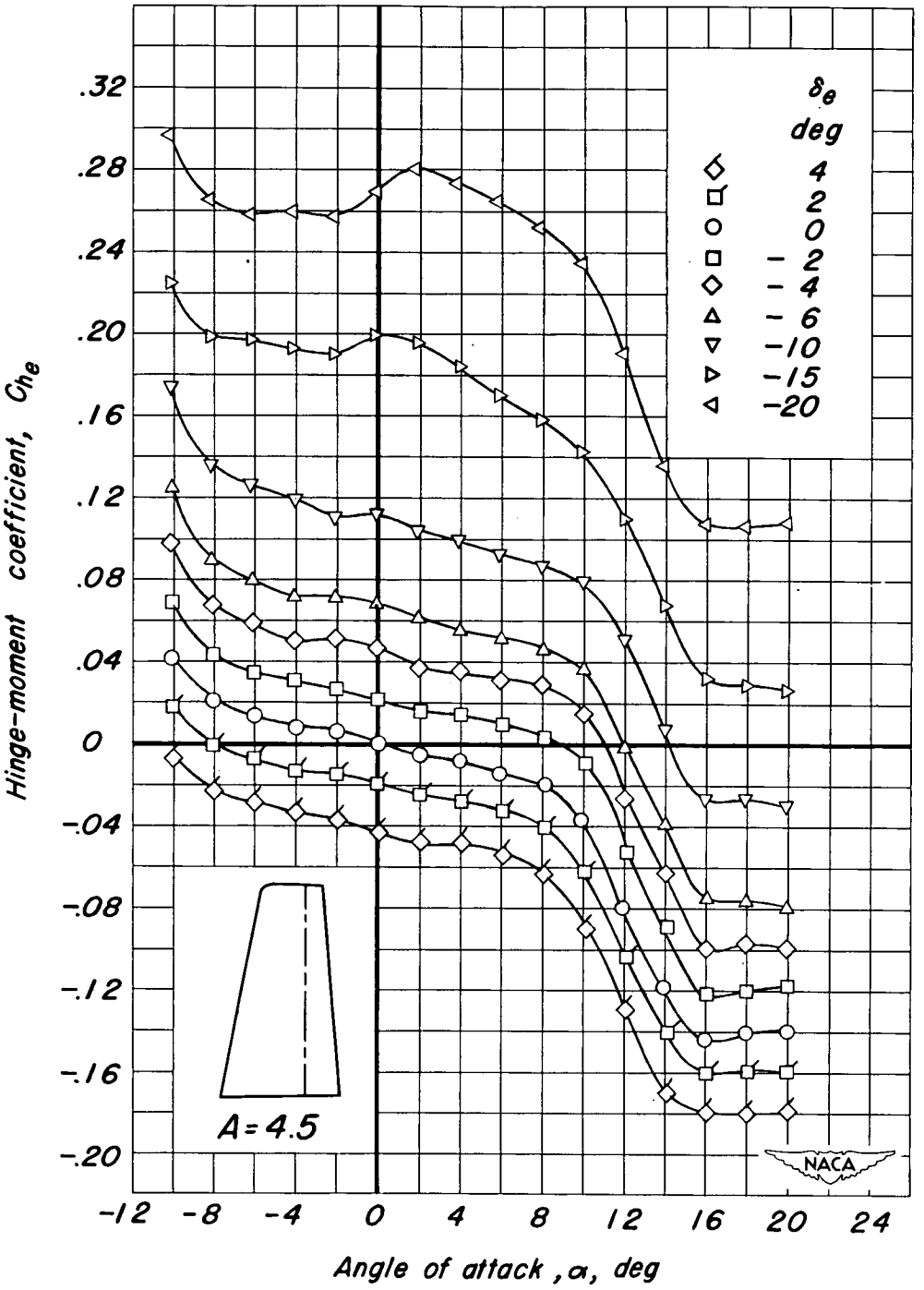

(b) M, 0.60.

Figure 16.— Continued.

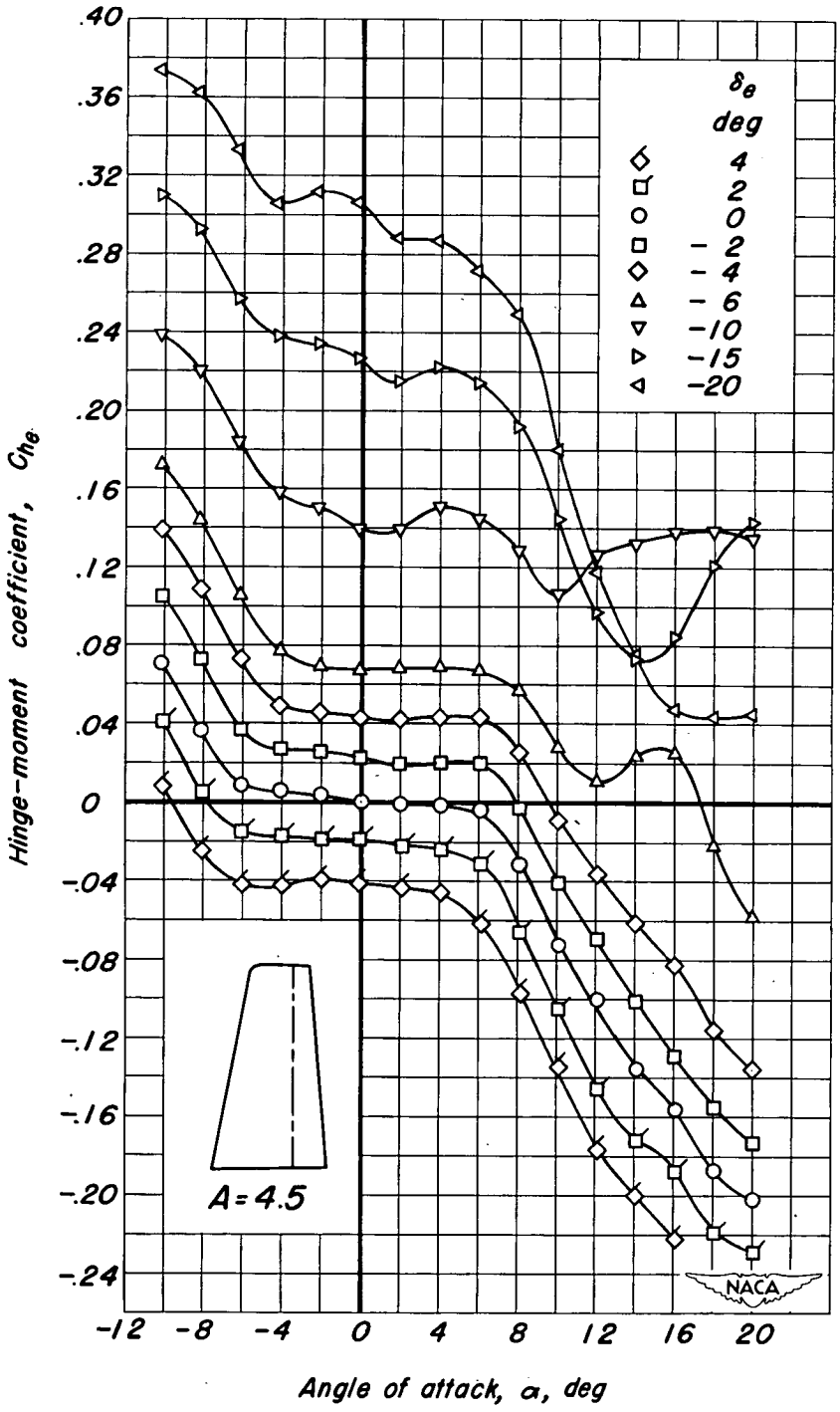

(c) M, 0.80.

Figure 16. — Continued.

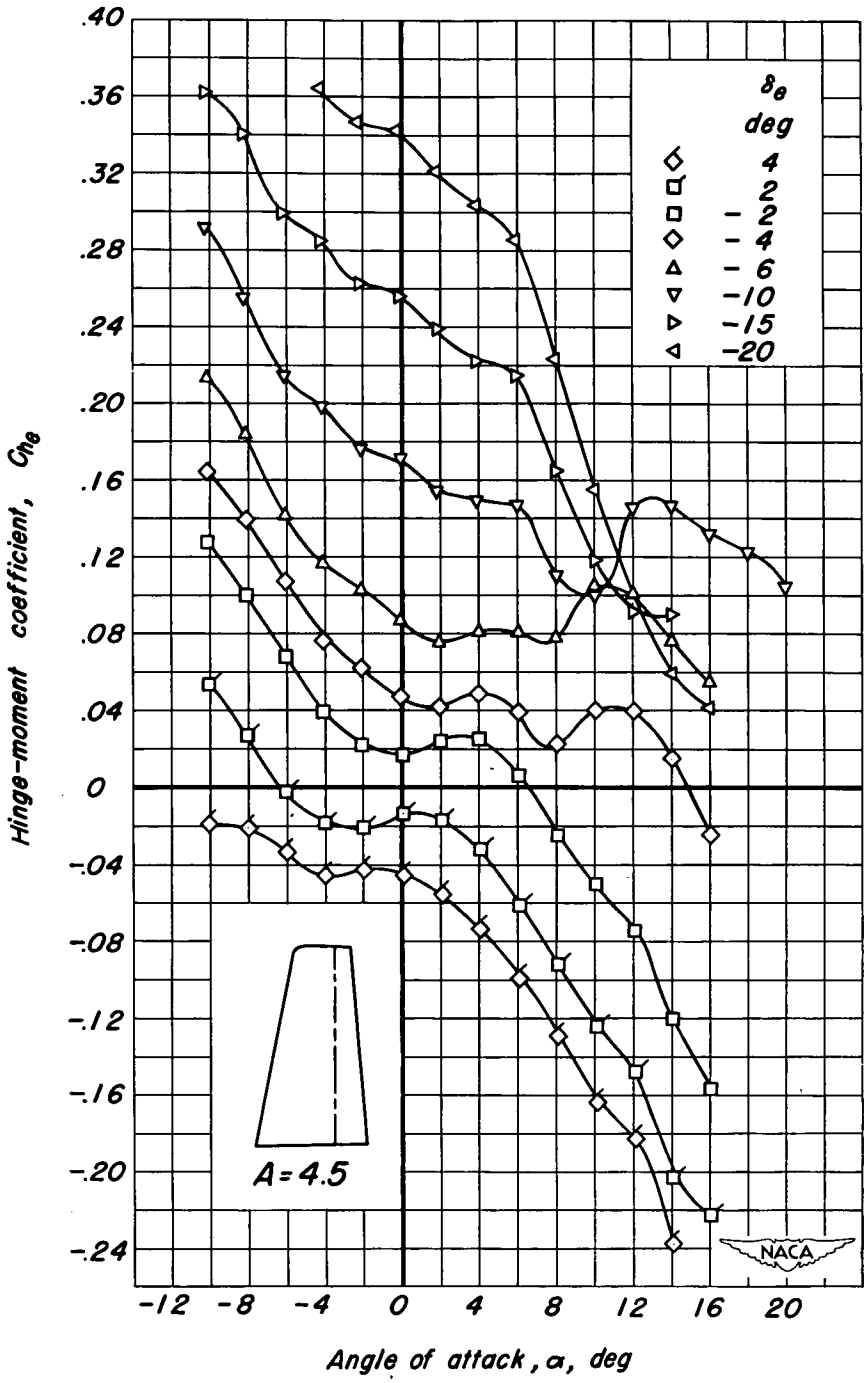

(d) M, 0.85.

Figure 16. — Continued.

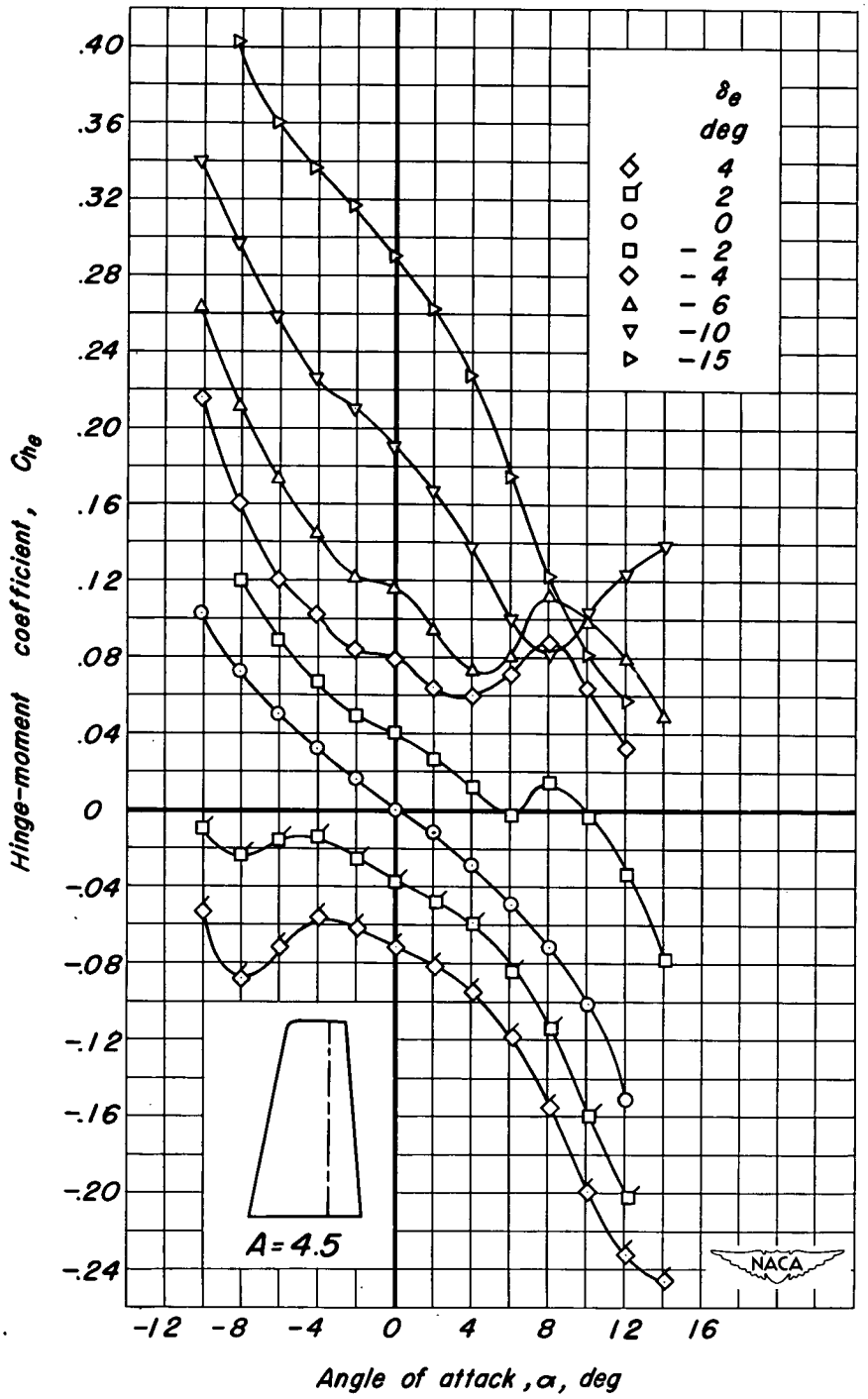

(e) M, 0.88.

Figure 16. — Concluded.

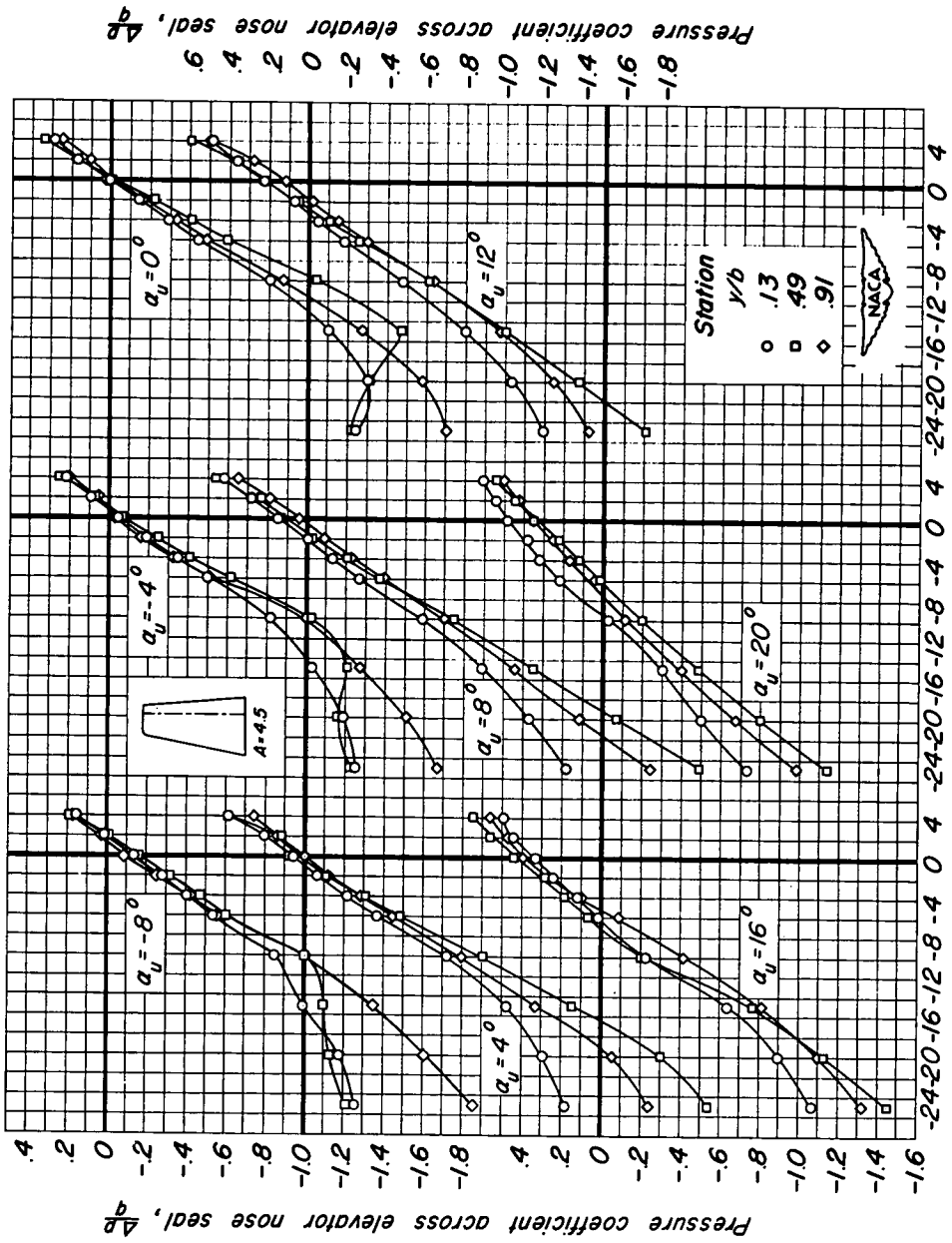

(a) M, 0.21.

Figure 17.- The variation of pressure coefficient across the elevator nose seal with elevator deflection for the unswept model of aspect ratio 4.5. R, 2.0 x 10^6; δ_t=0°.

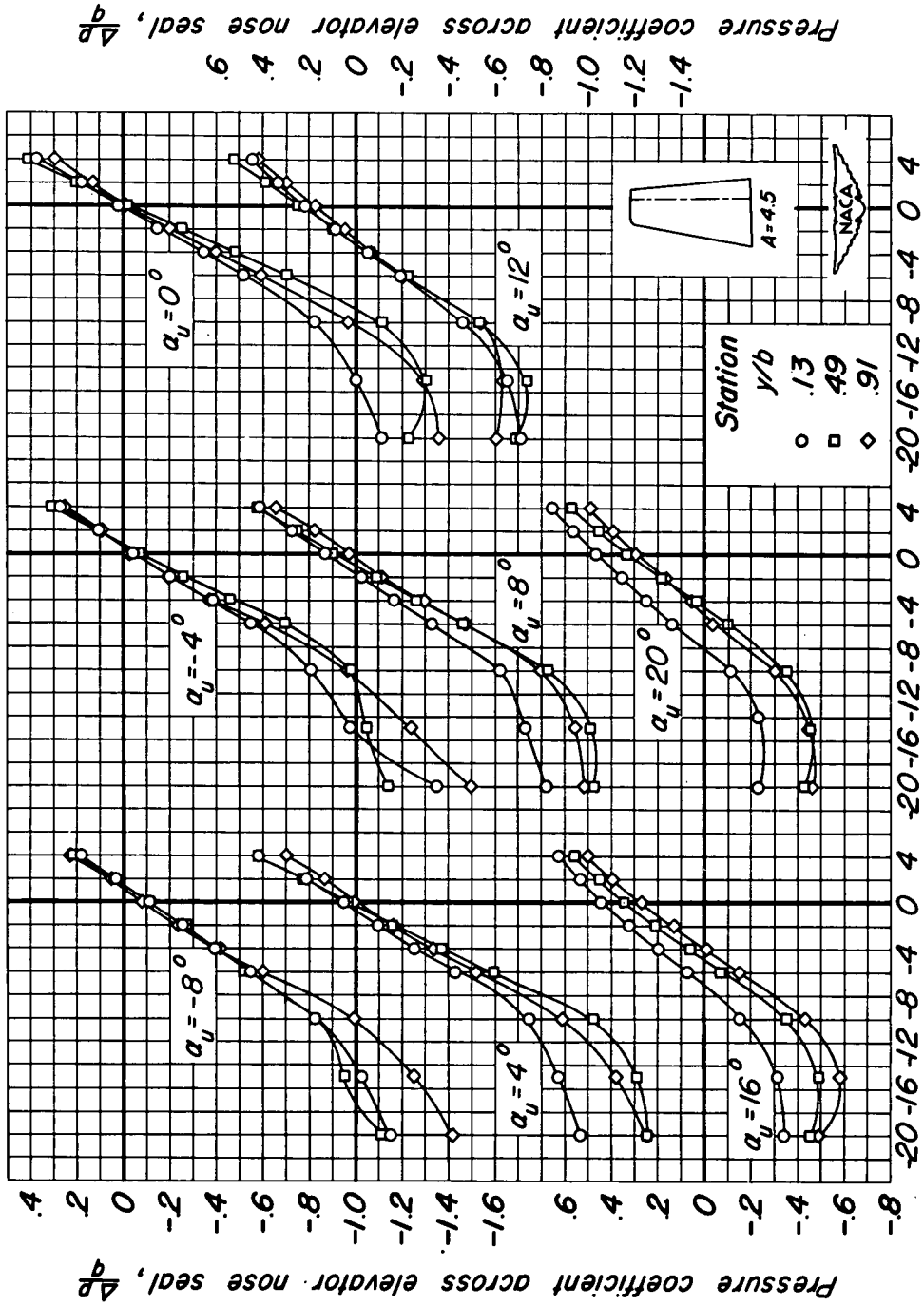

(b) M, 0.60.

Figure 17.— Continued.

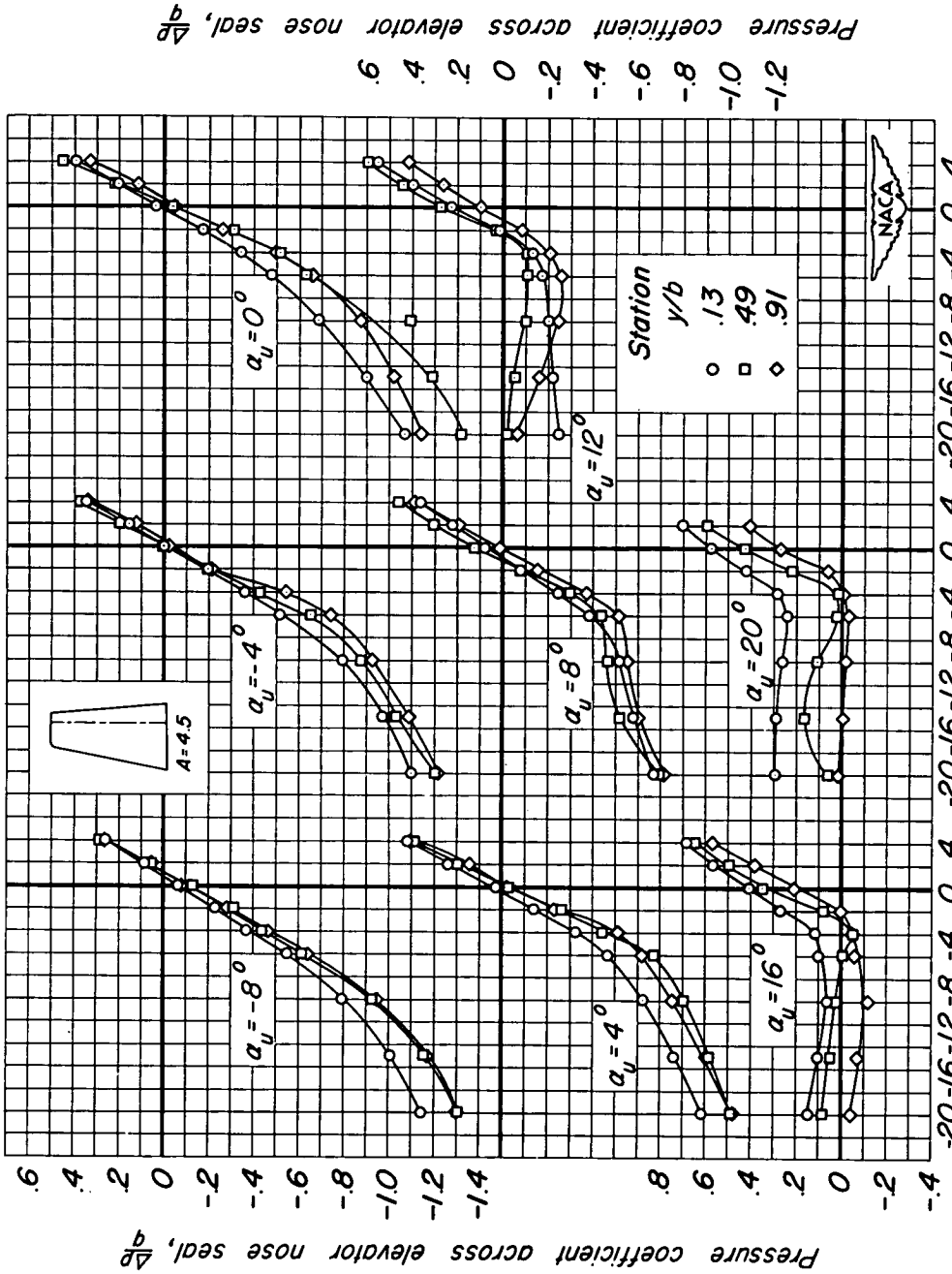

(c) M, 0.80.

Figure 17.— Continued.

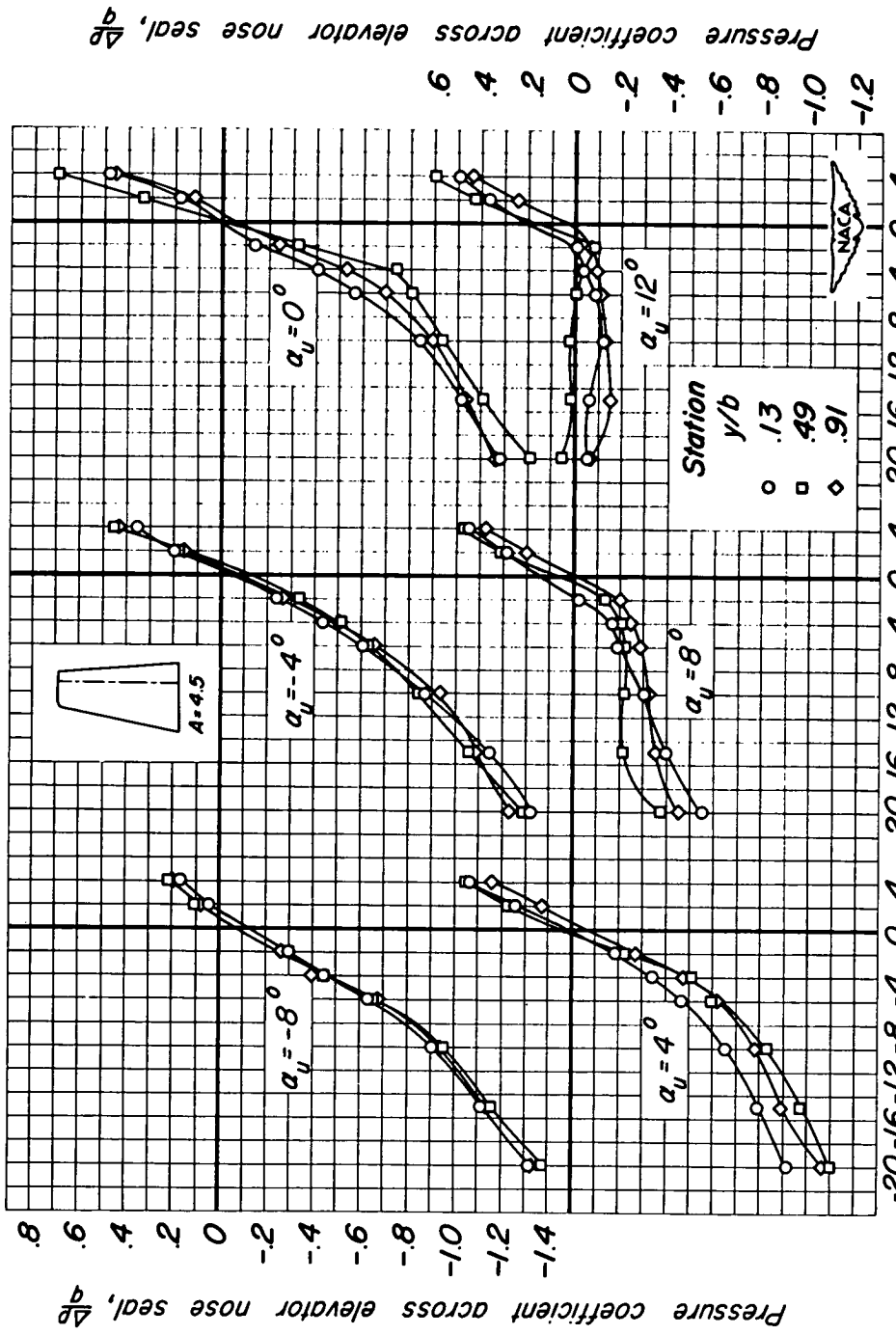

(d) M, 0.85.

Figure 17.— Continued.

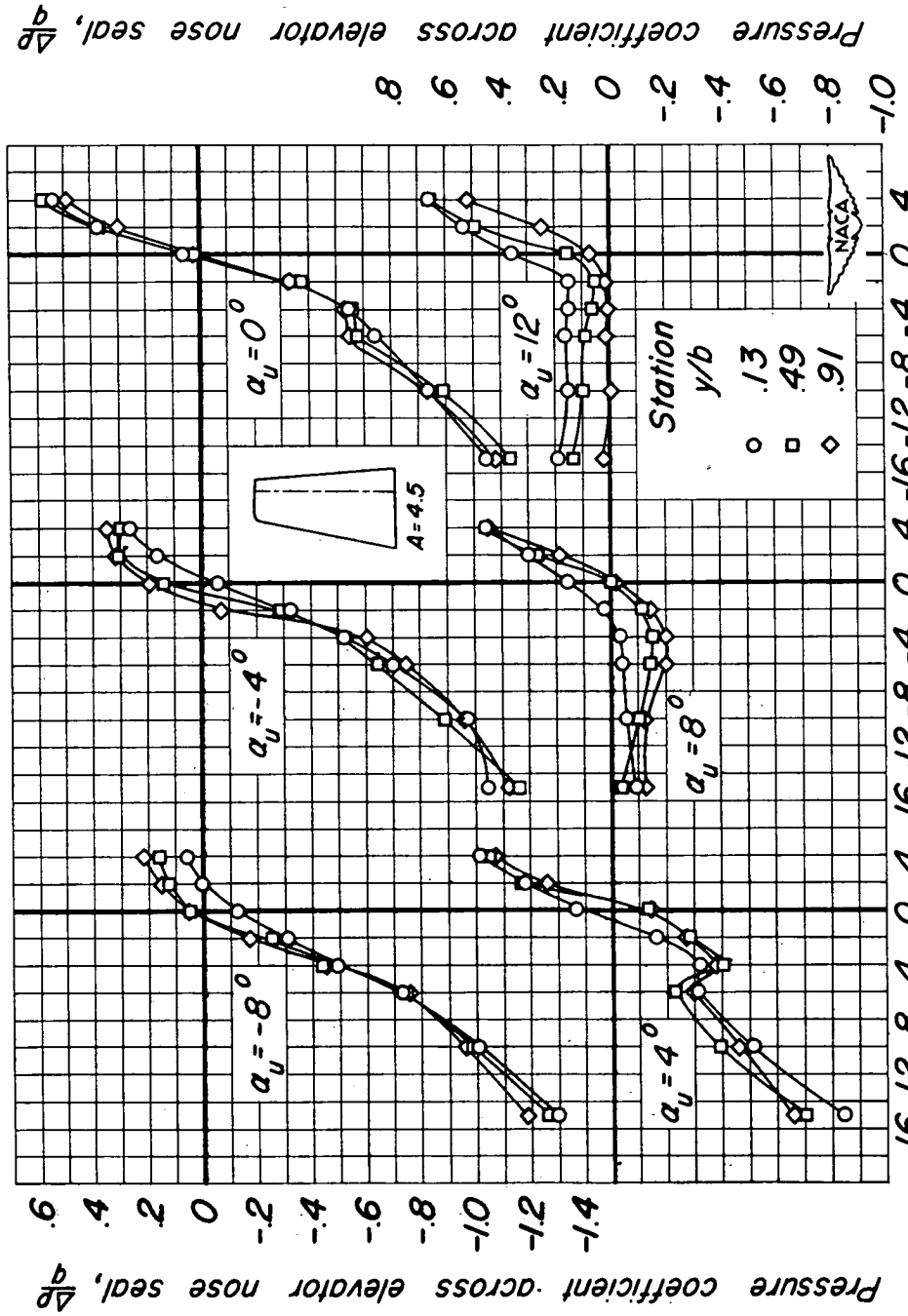

Figure 17.— Concluded.

(e) M, 0.88.

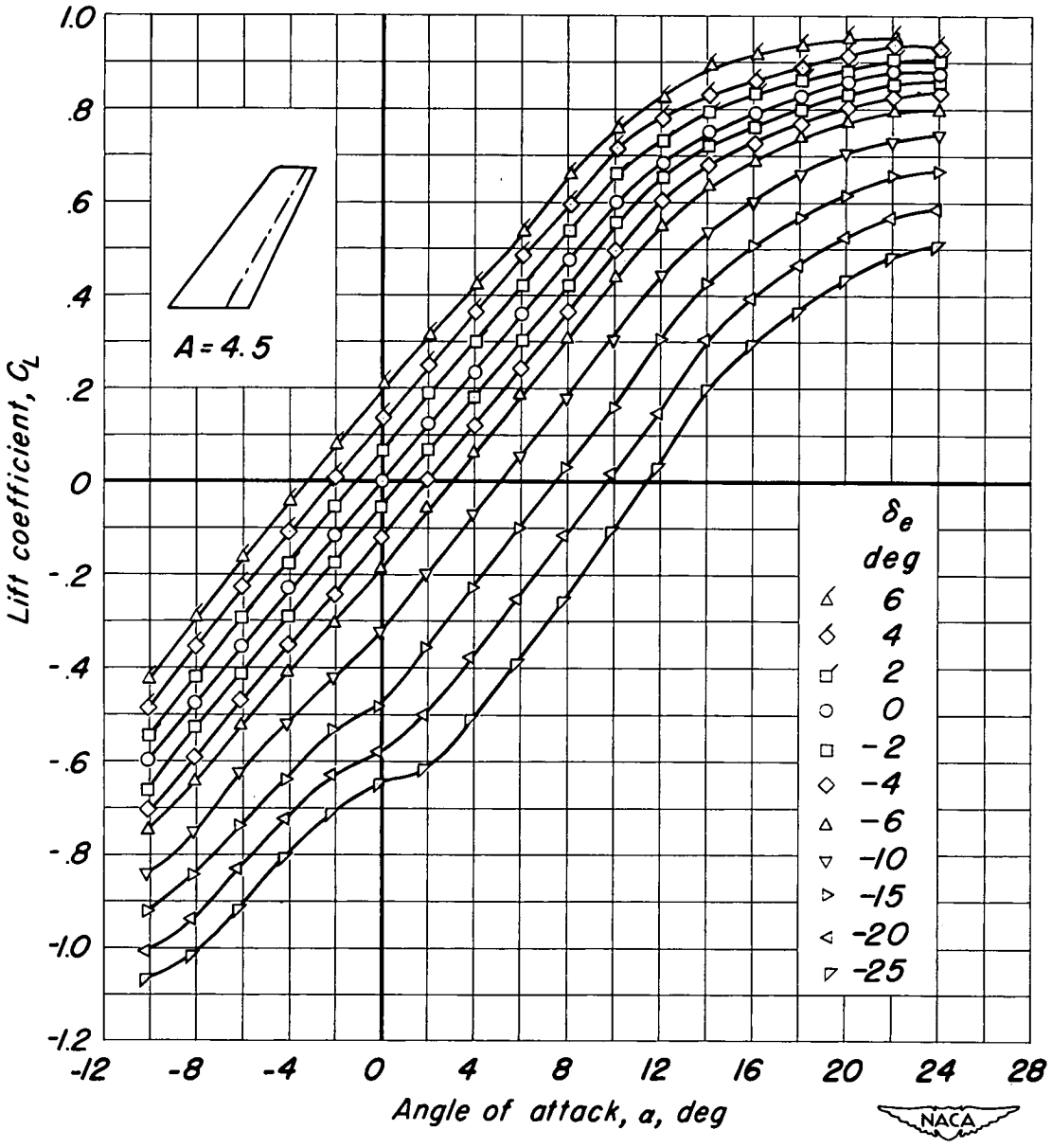

(a) M, 0.21.

Figure 18.— The variation of lift coefficient with angle of attack for the 35° swept-back model of aspect ratio 4.5. R, 2.0 x 10^6; δ_t=0°.

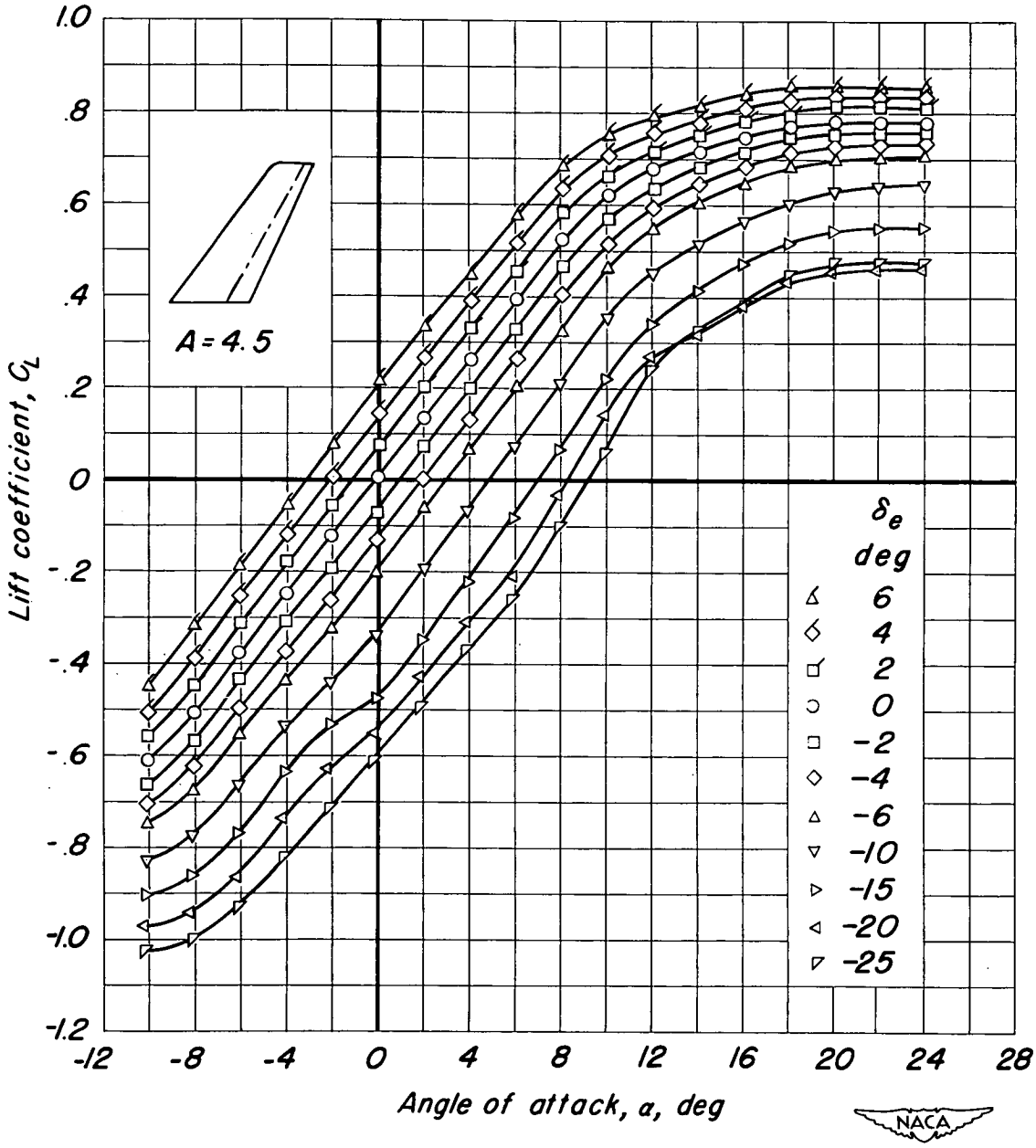

(b) M, 0.60.

Figure 18-Continued.

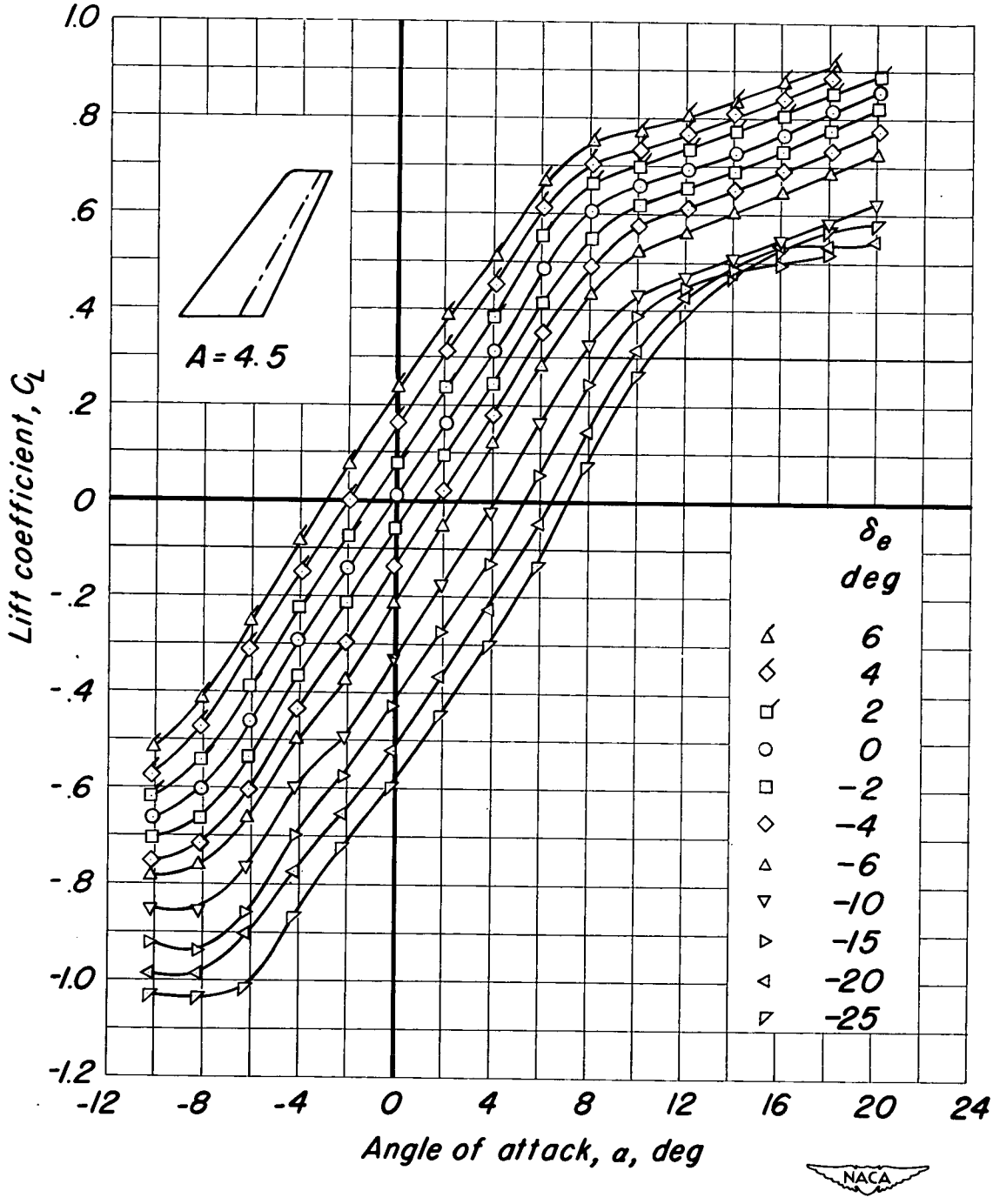

(c) M, 0.85.

Figure 18.- Continued.

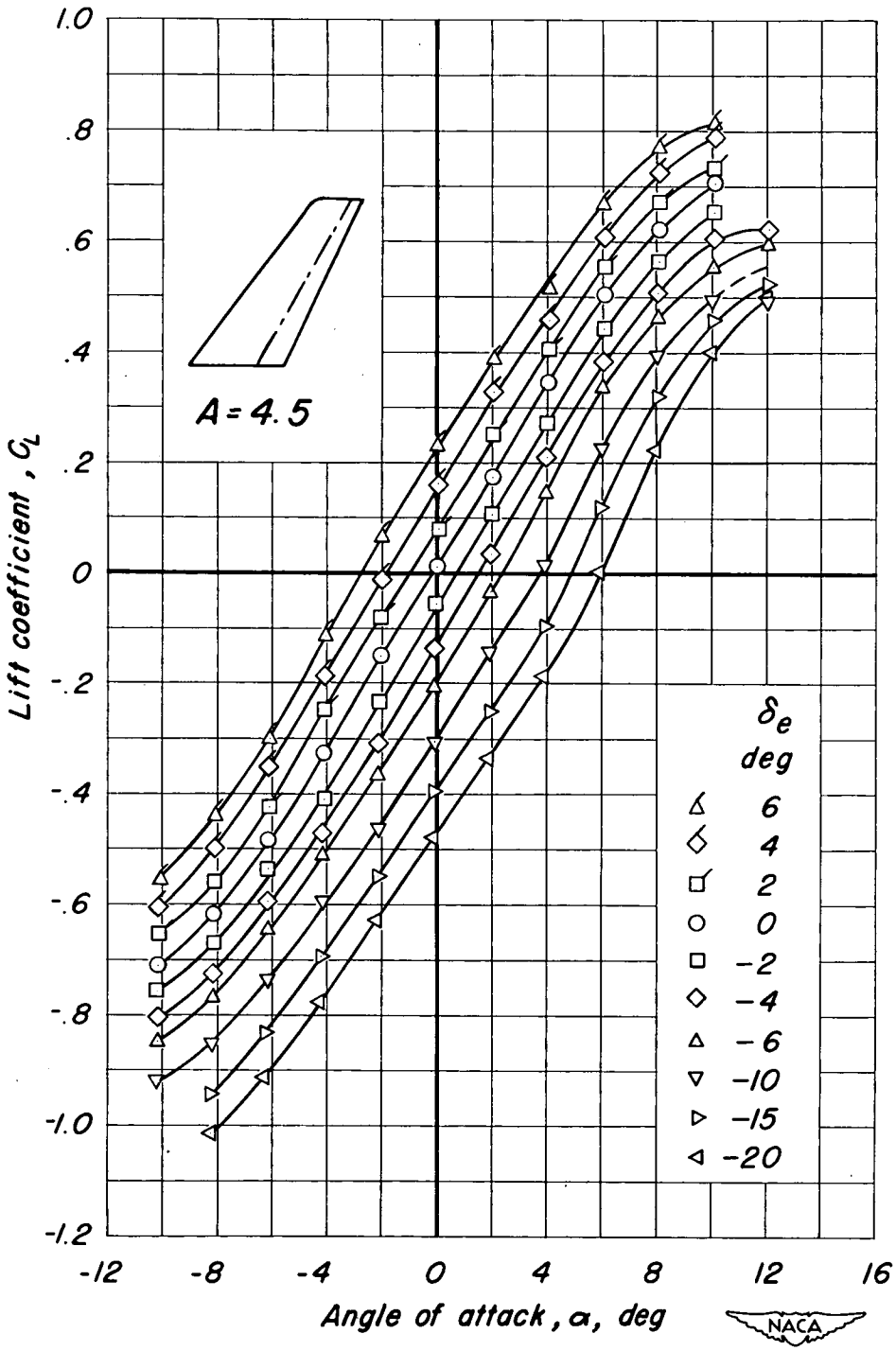

(d) M, 0.90.

Figure 18.- Continued.

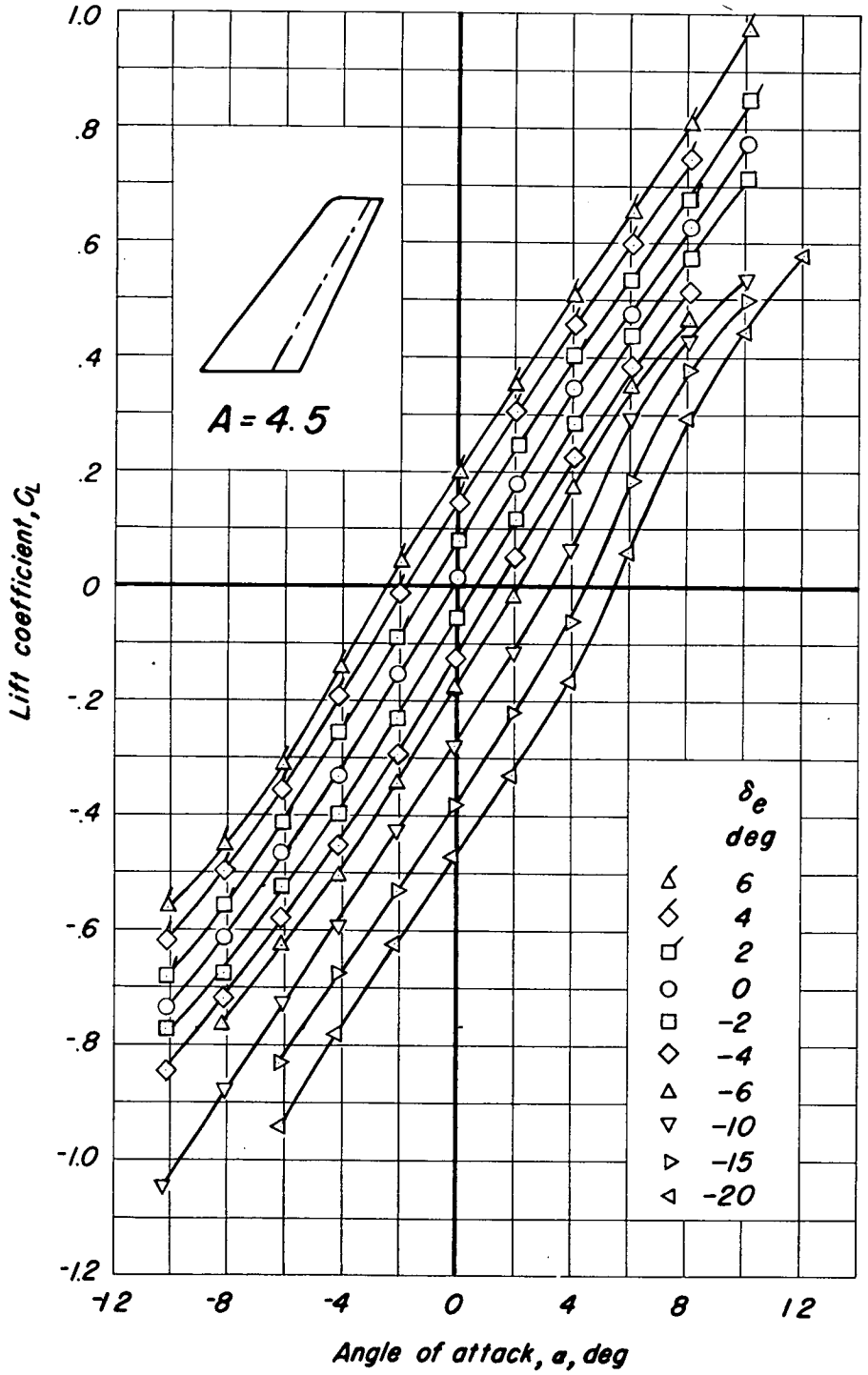

(e) M, 0.93.

Figure 18.—Continued.

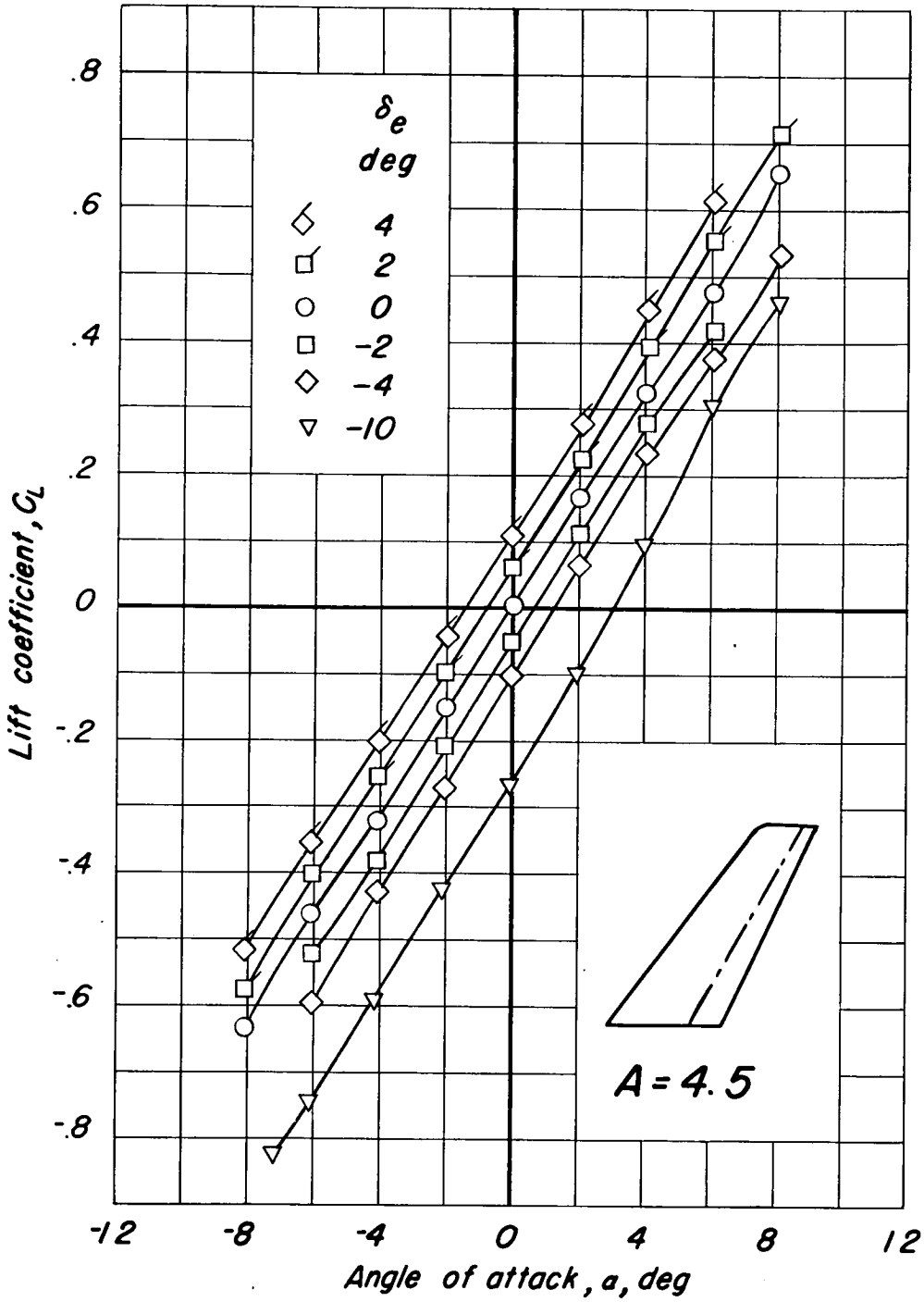

(f) M, 0.94.

Figure 18.- Concluded.

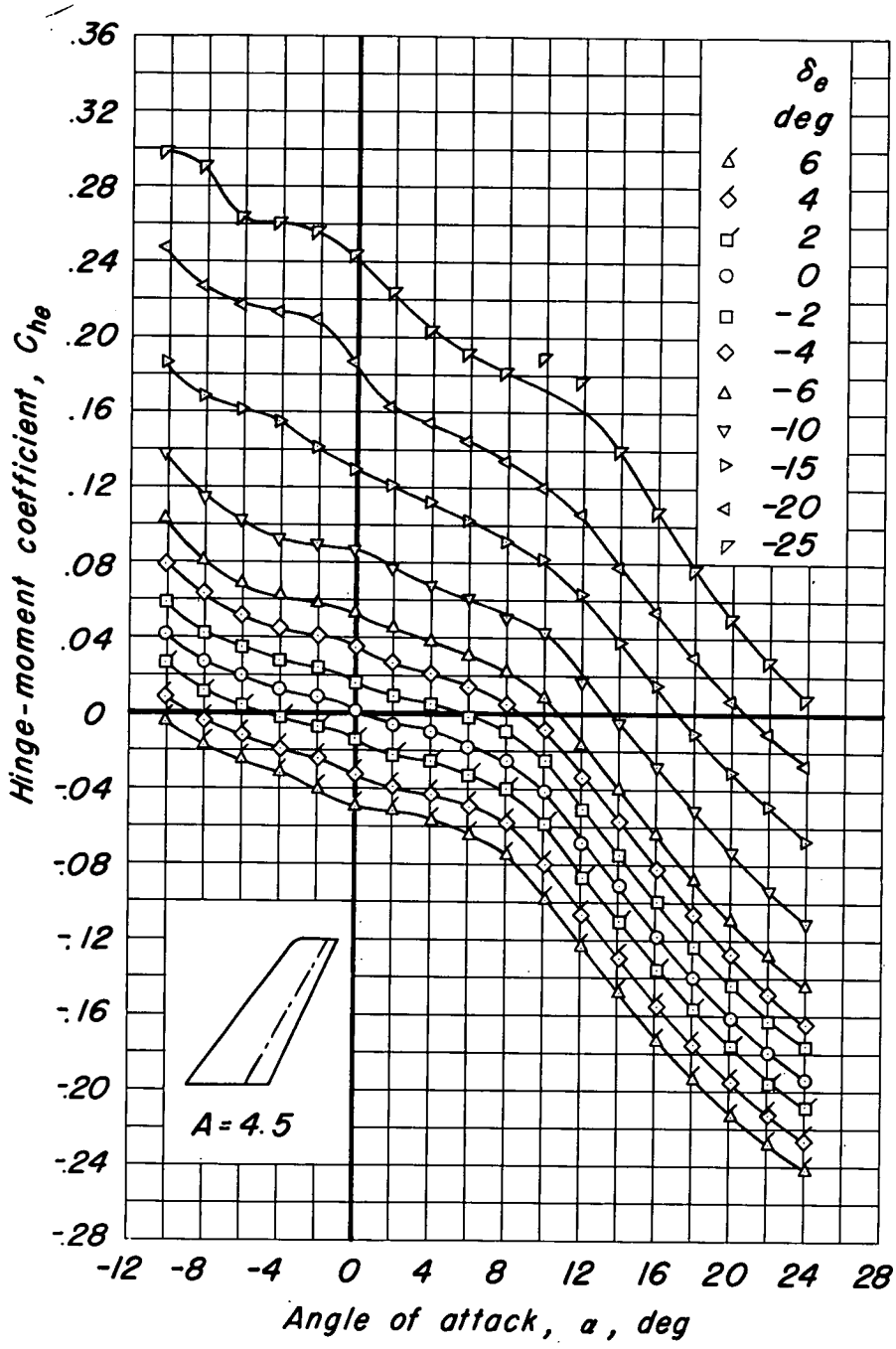

(a) M, 0.21.

Figure 19.- The variation of elevator hinge-moment coefficient with angle of attack for the 35° swept-back model of aspect ratio 4.5. R, 2.0×10^6; $\delta_t = 0°$.

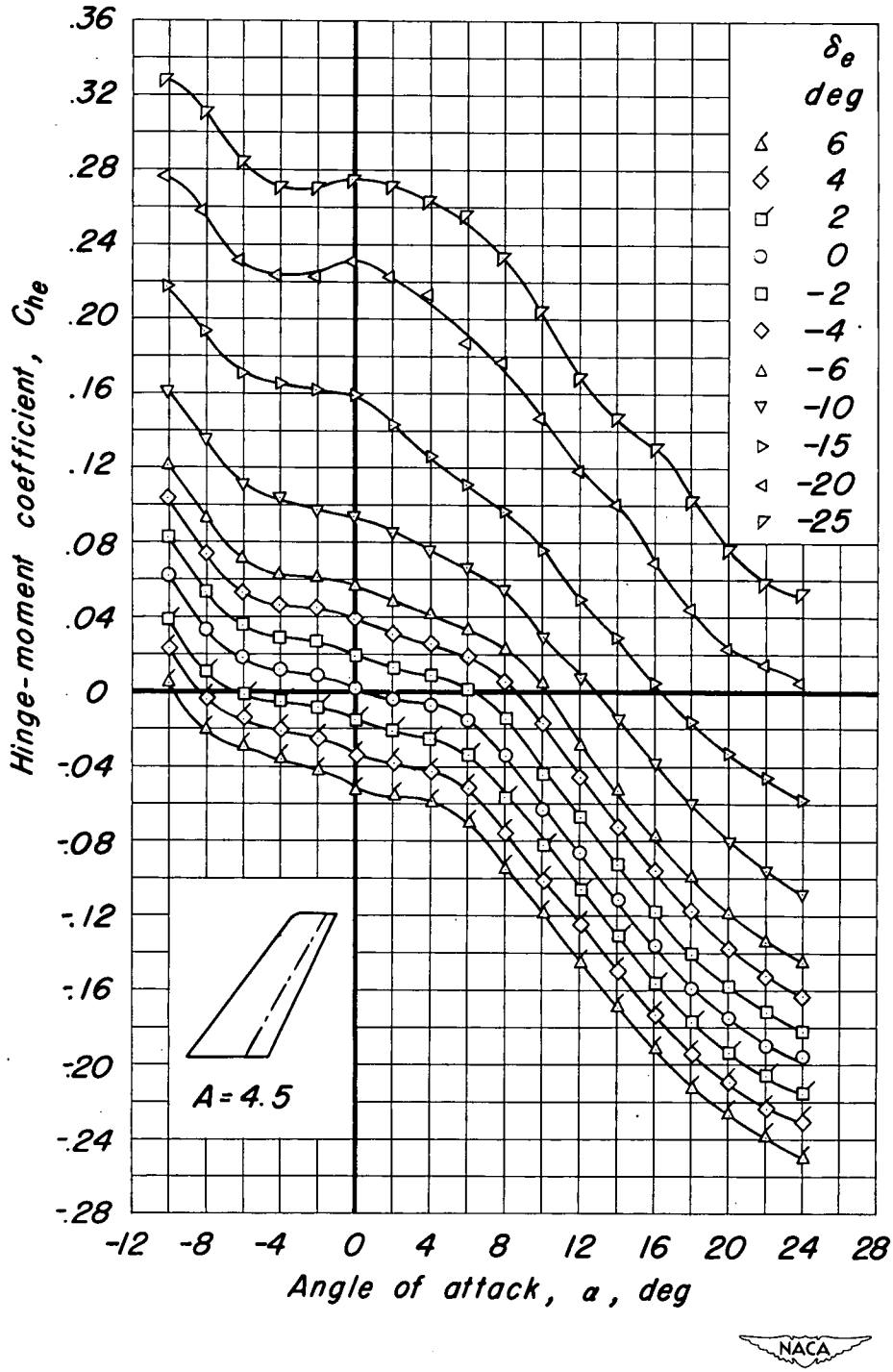

(b) M, 0.60.

Figure 19.-Continued.

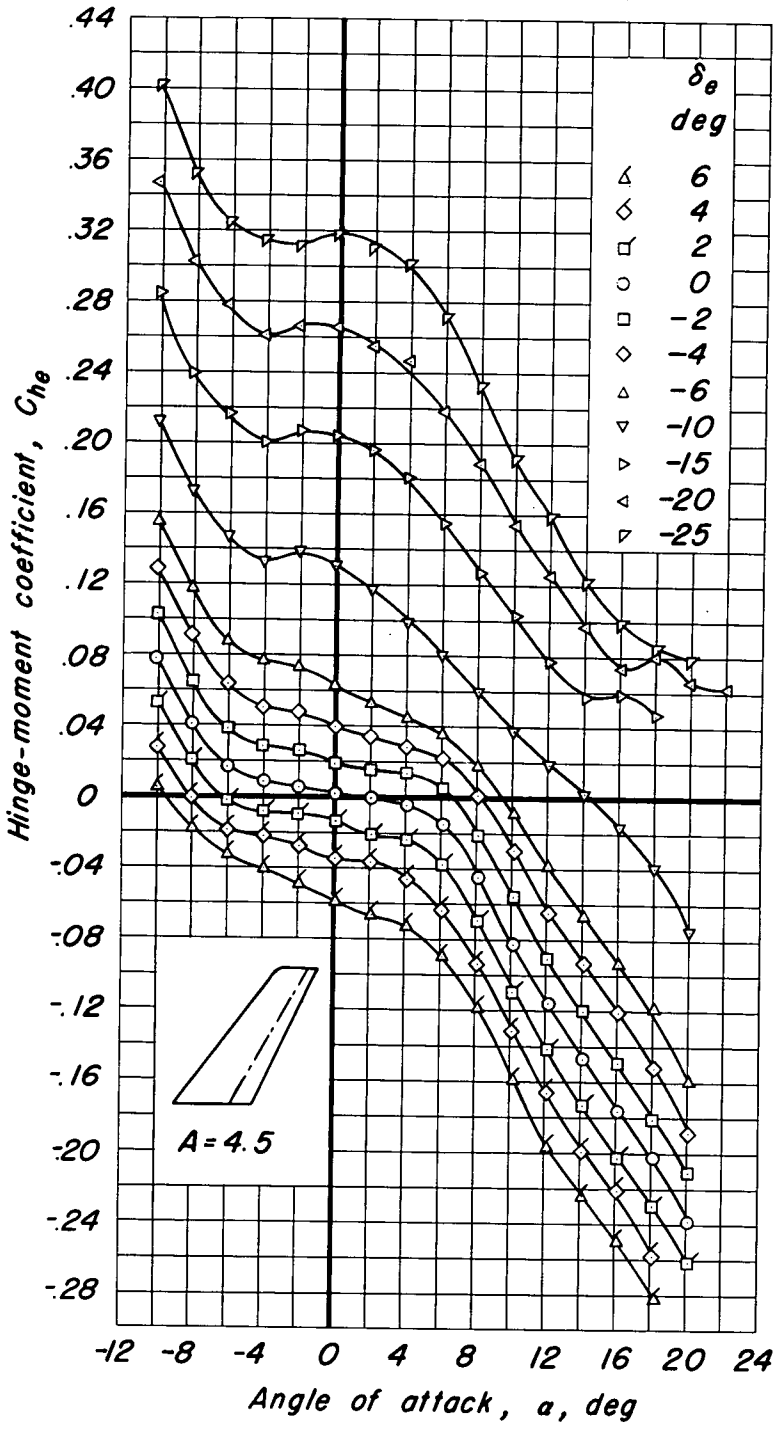

(c) M, 0.85.

Figure 19.—Continued.

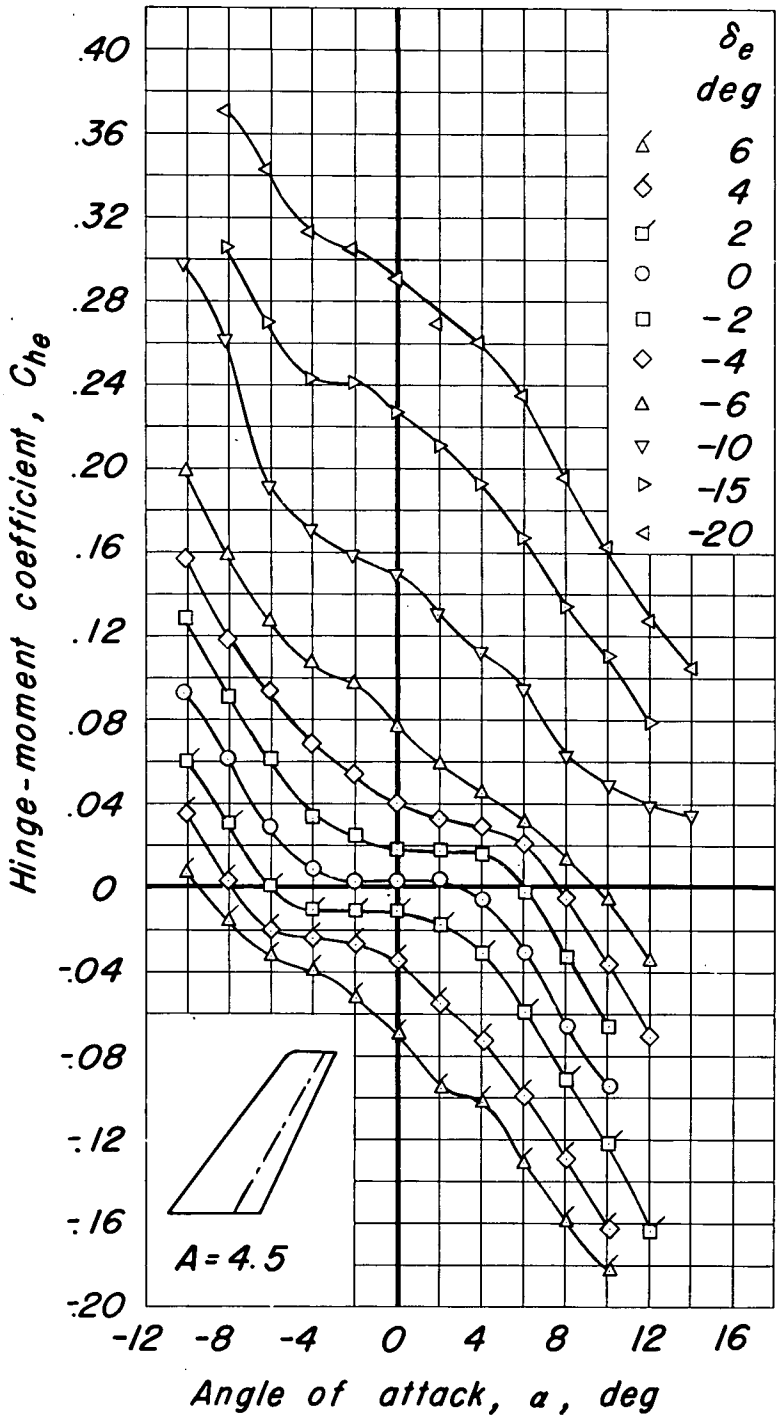

(d) M, 0.90.

Figure 19.- Continued.

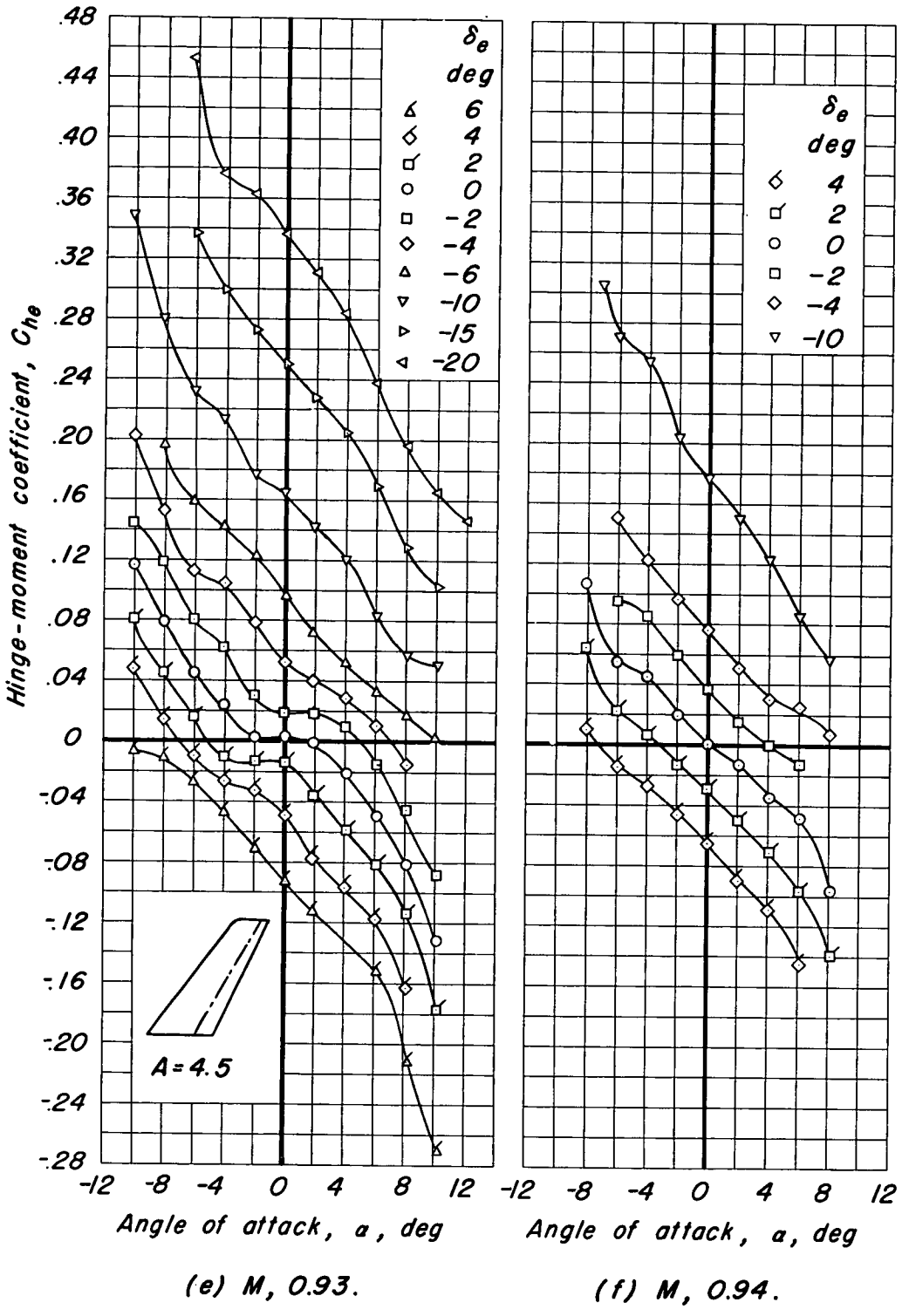

Figure 19.- Concluded.

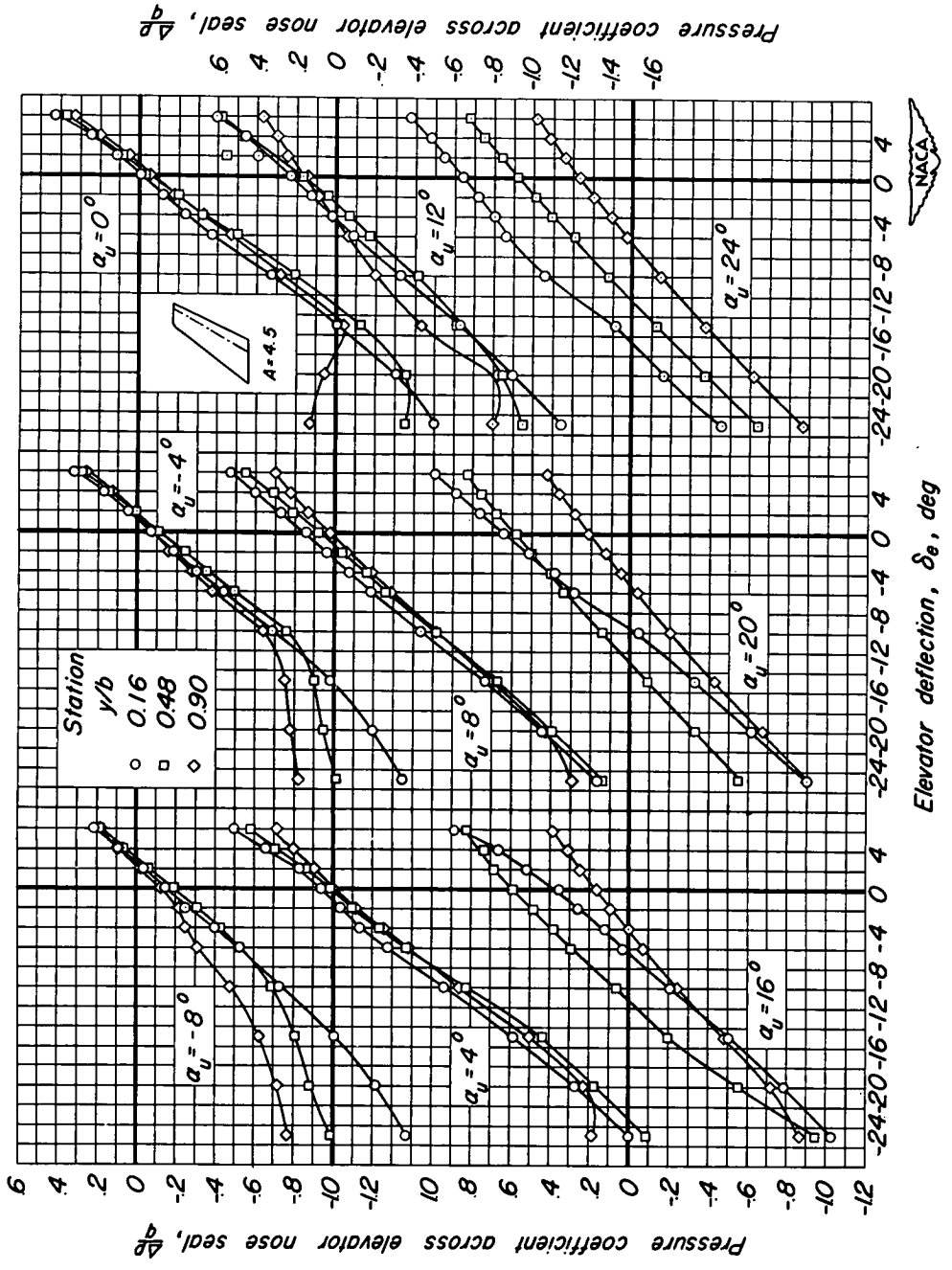

Figure 20.—The variation of pressure coefficient across the elevator nose seal with elevator deflection for the 35° swept-back model of aspect ratio 4.5. $R, 2.0 \times 10^6$; $\delta_t = 0°$.

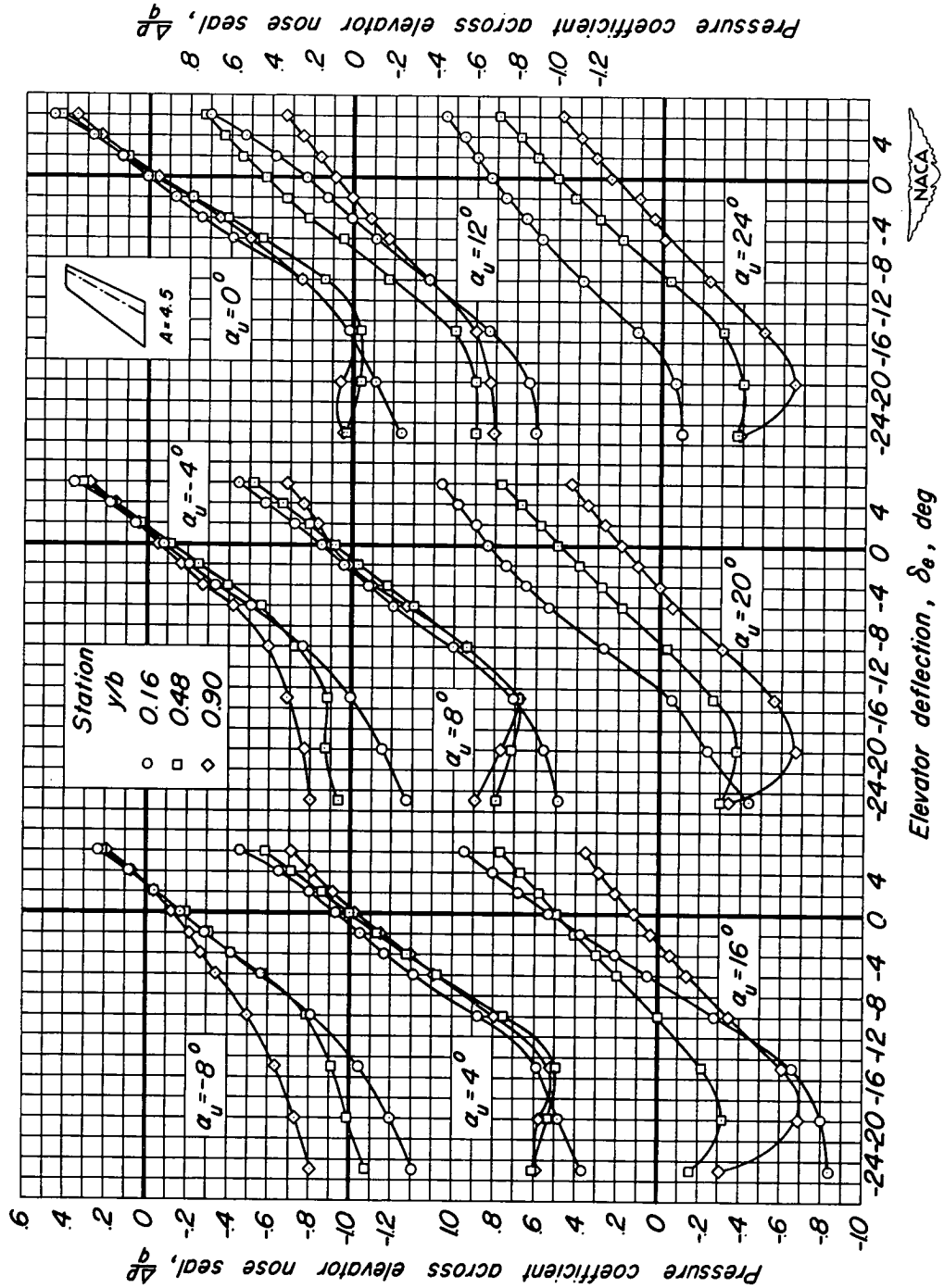

(b) M, 0.60.

Figure 20.- Continued.

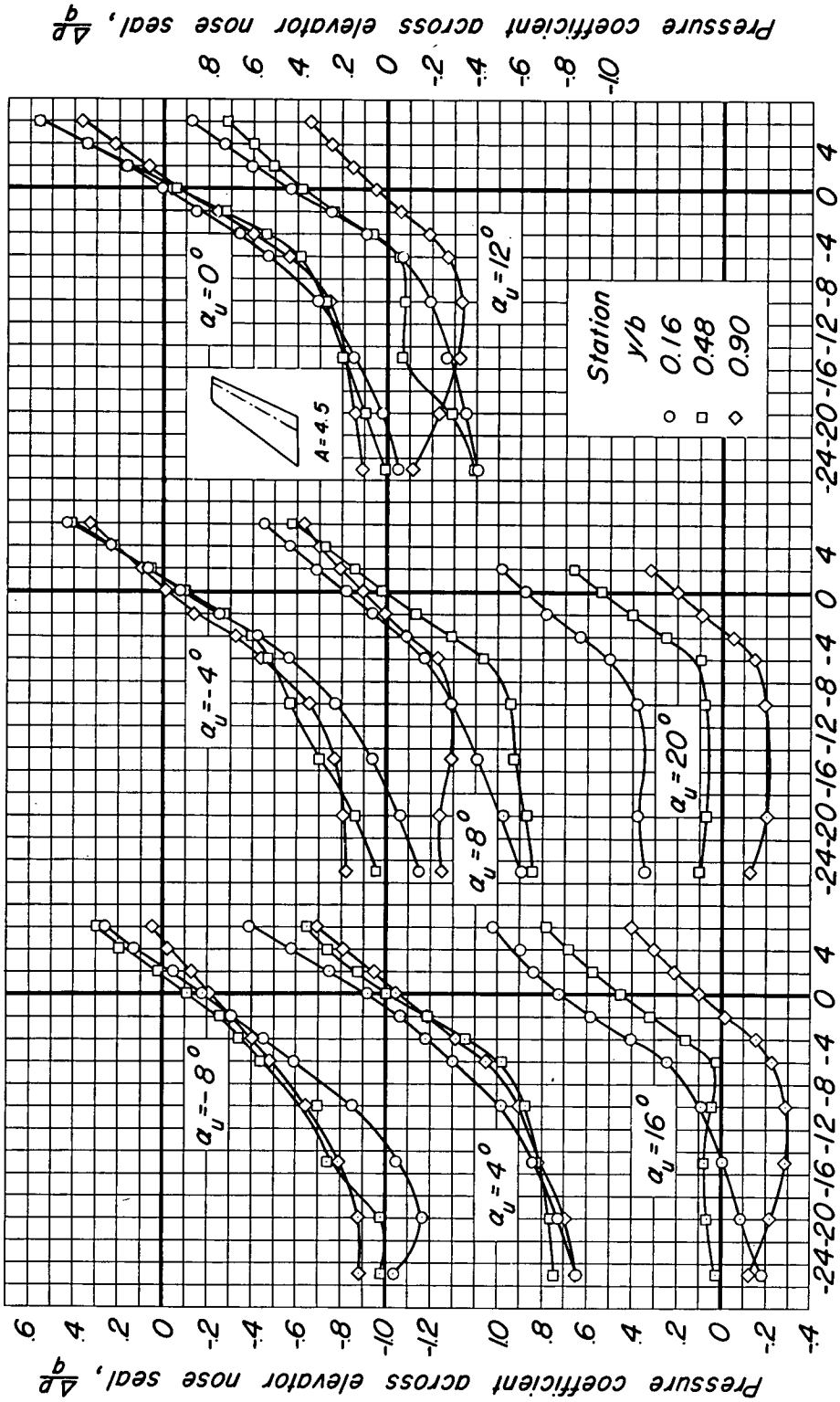

(c) M, 0.85.

Figure 20.- Continued.

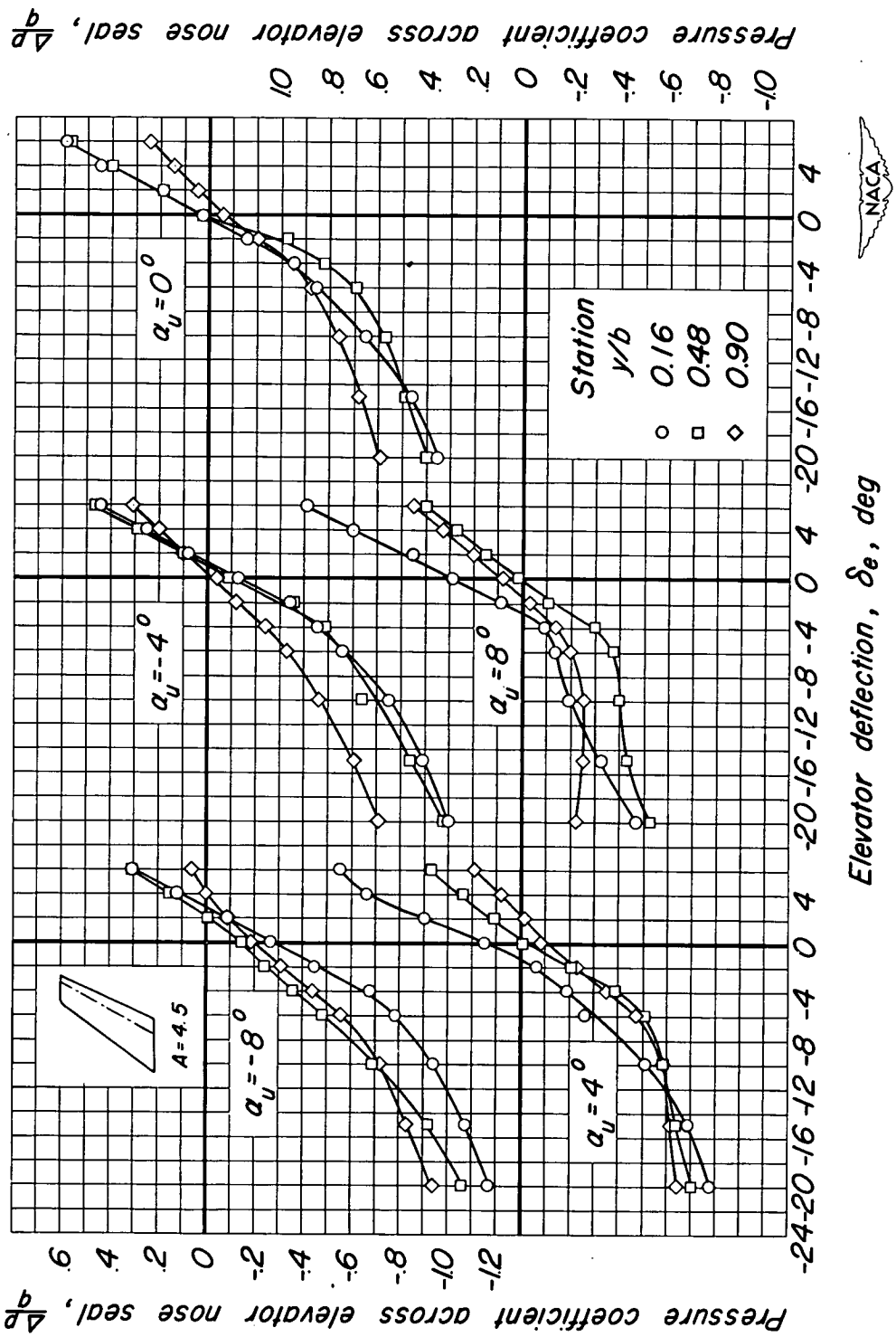

(d) M, 0.90.

Figure 20- Continued.

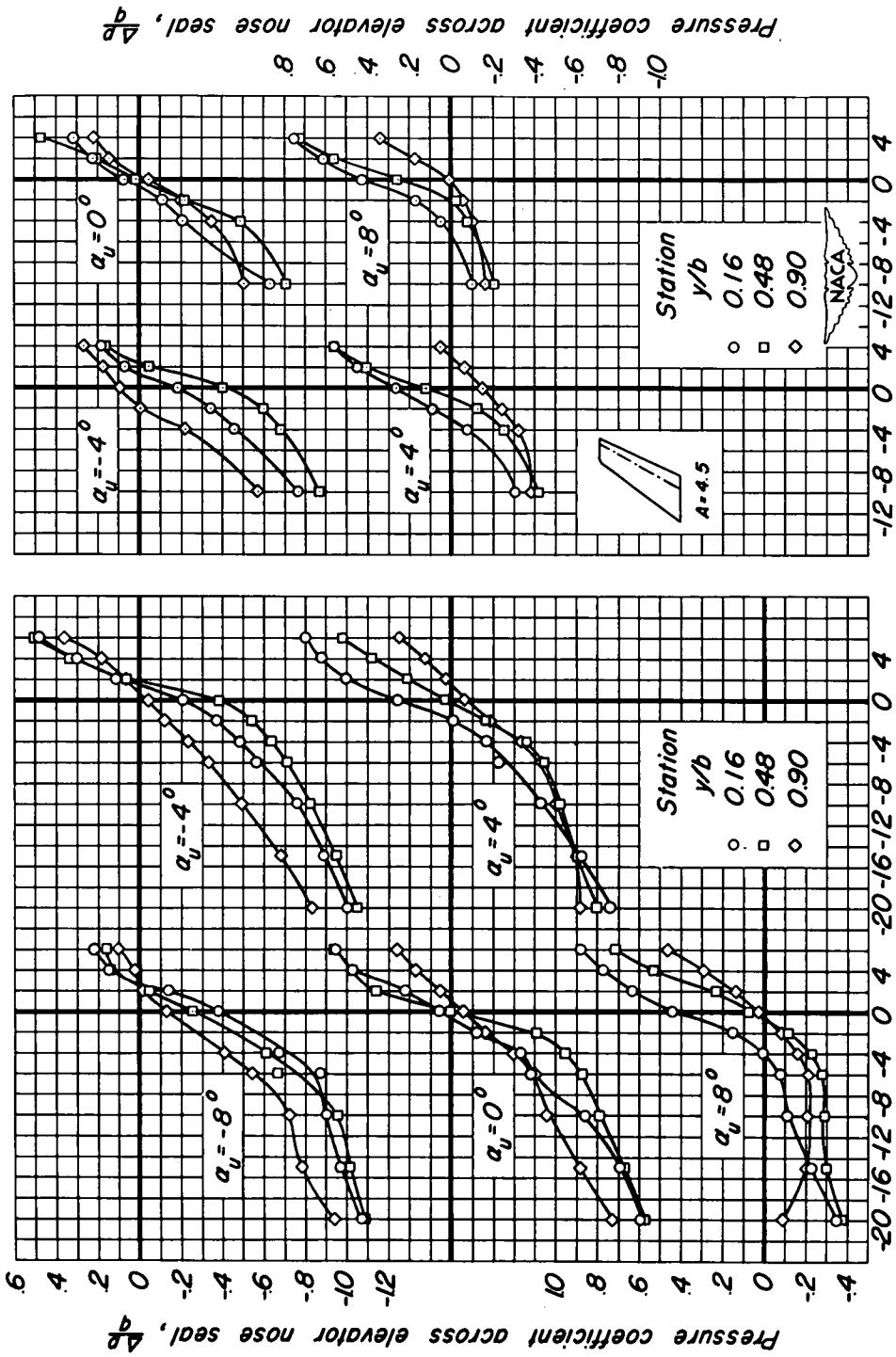

Figure 20.- Concluded.

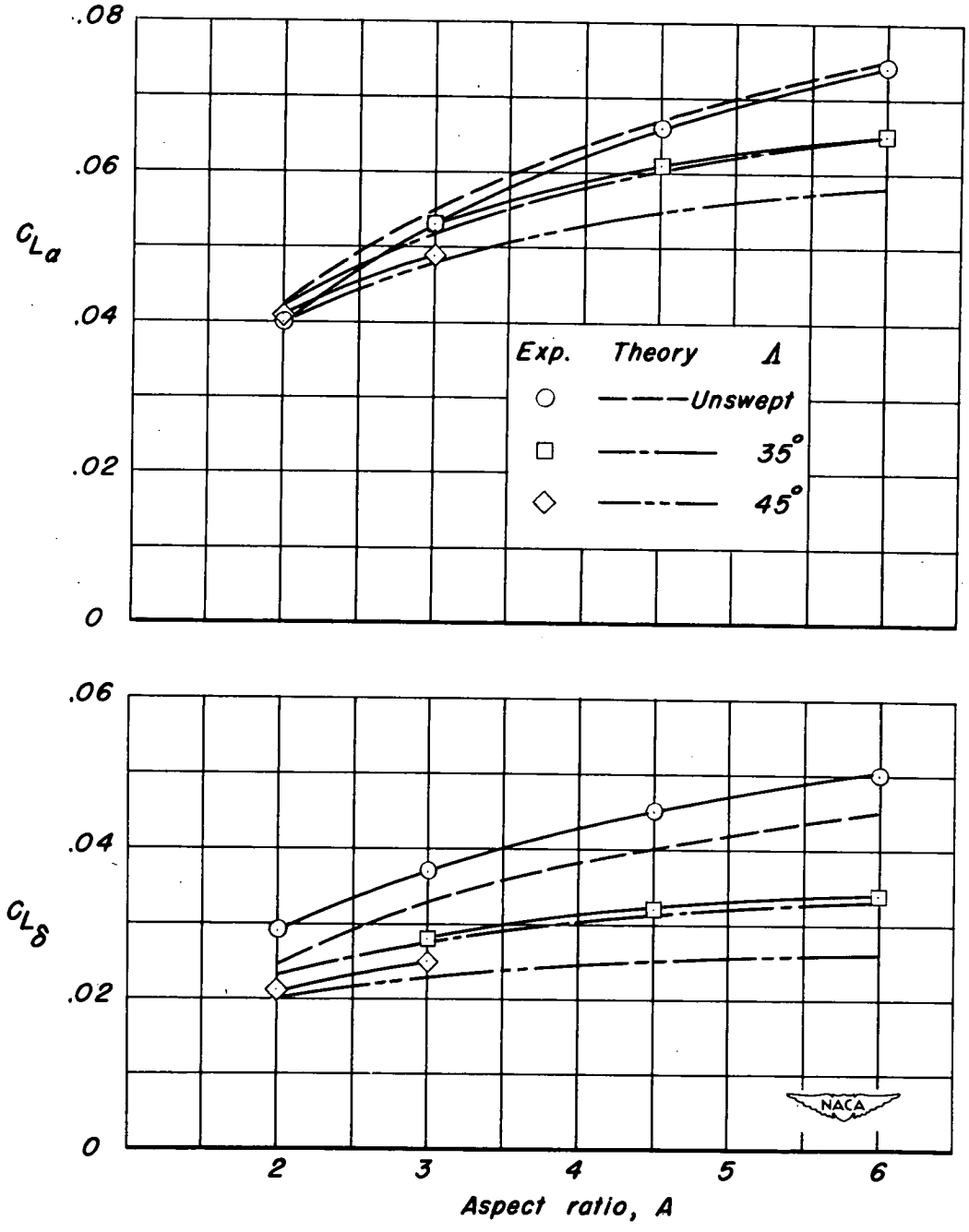

(a) Lift parameters.

Figure 21.— Comparison of the low-speed experimental and theoretical values of the lift and hinge-moment parameters as a function of the aspect ratio. R, 3.0 x 10^6.

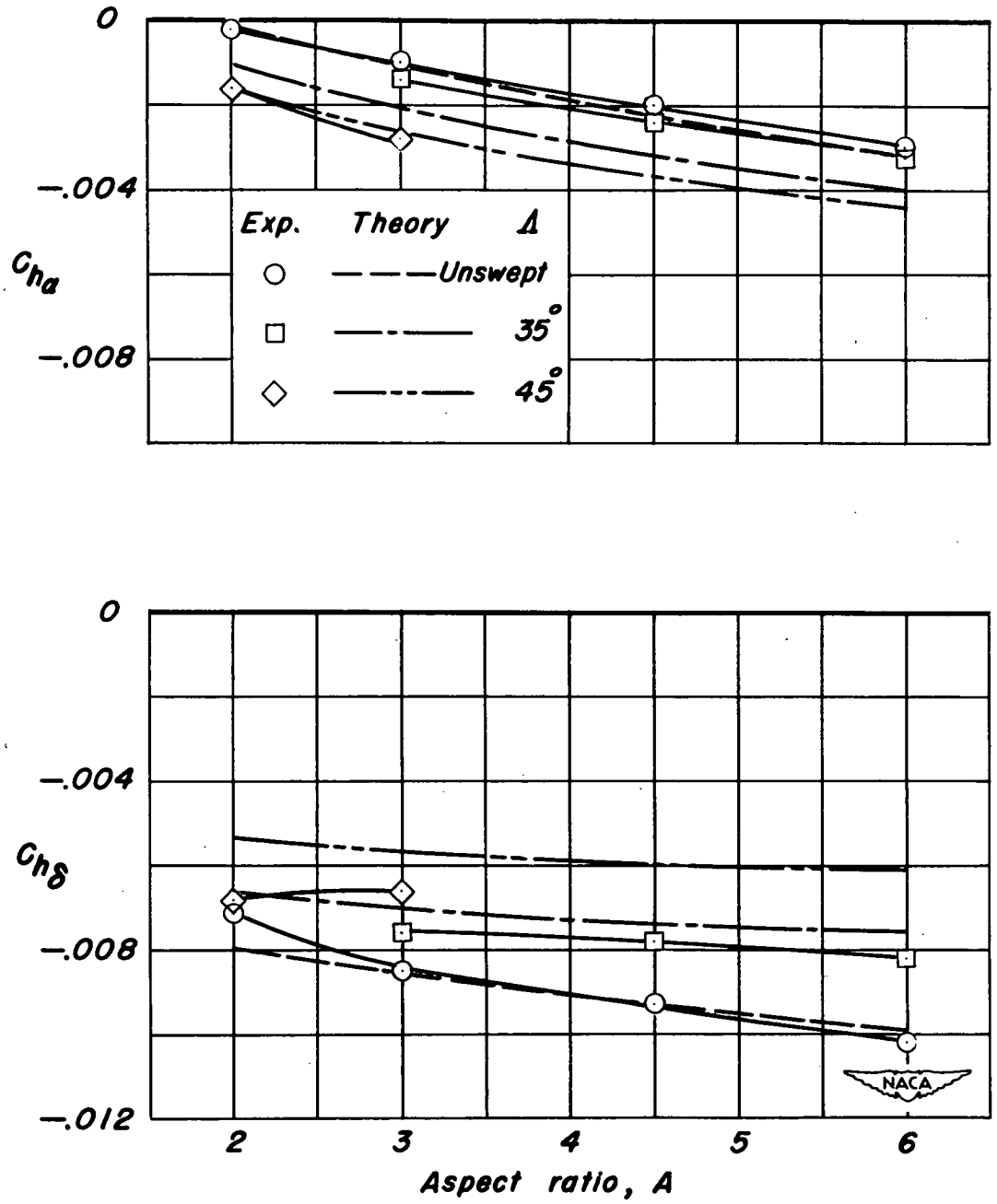

(b) Hinge-moment parameters.

Figure 21.-Concluded.

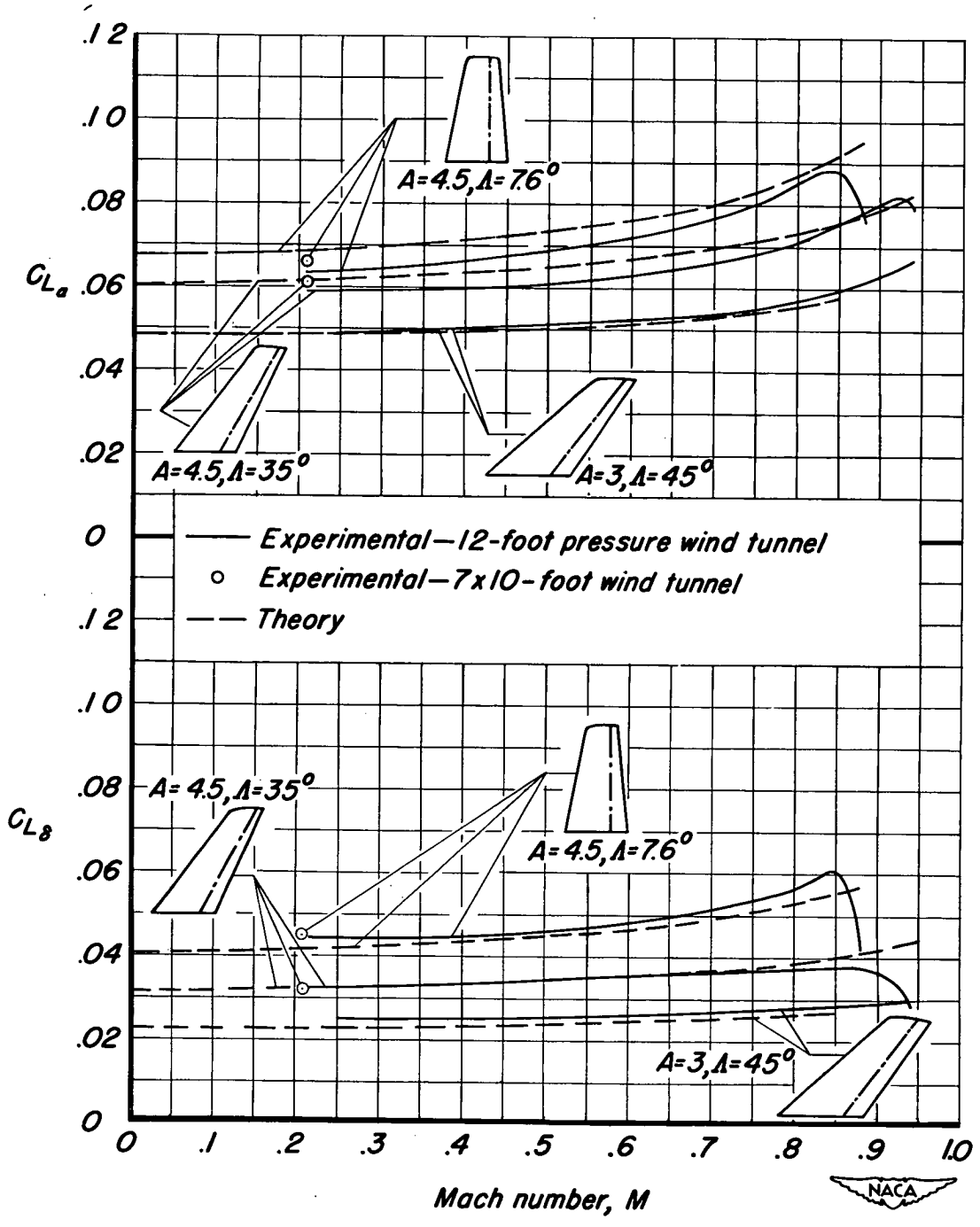

Figure 22.—The variation of the lift parameters C_{L_α} and C_{L_δ} with Mach number.

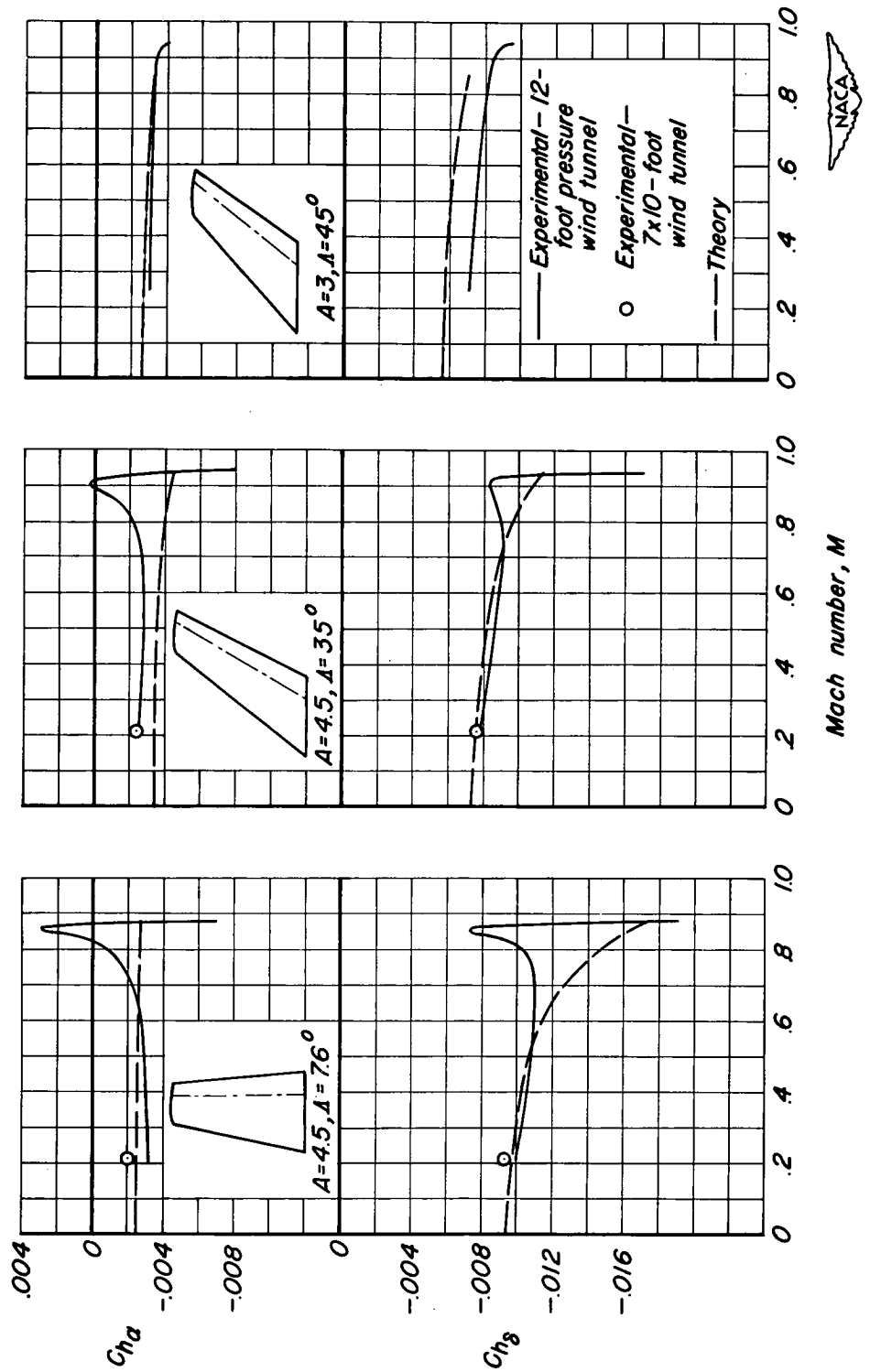

Figure 23.– The variation of the hinge-moment parameters C_{h_α} and C_{h_δ} with Mach number.

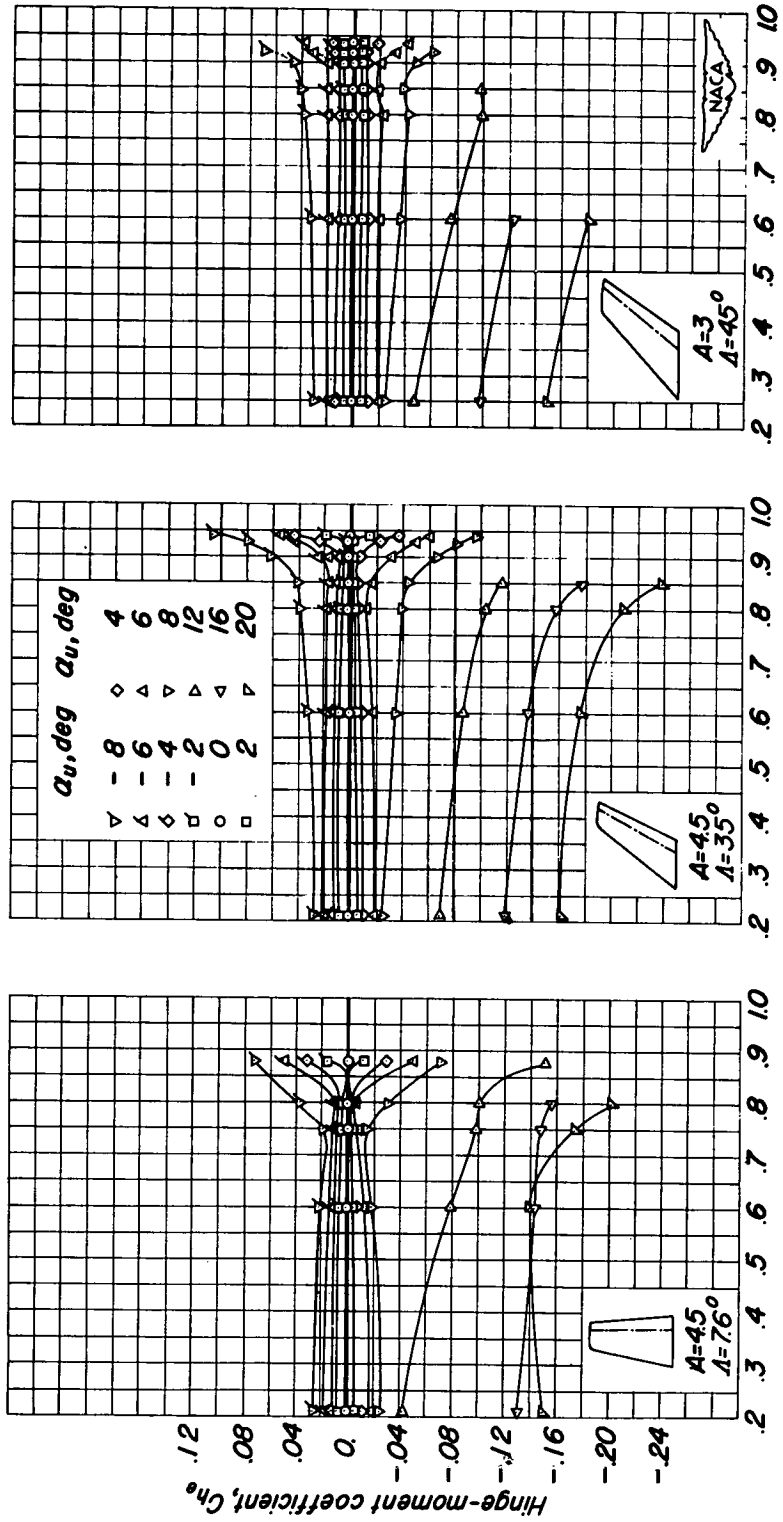

(a) $\delta_e = 0°$.

Figure 24.–The variation of the elevator hinge-moment coefficient with Mach number.

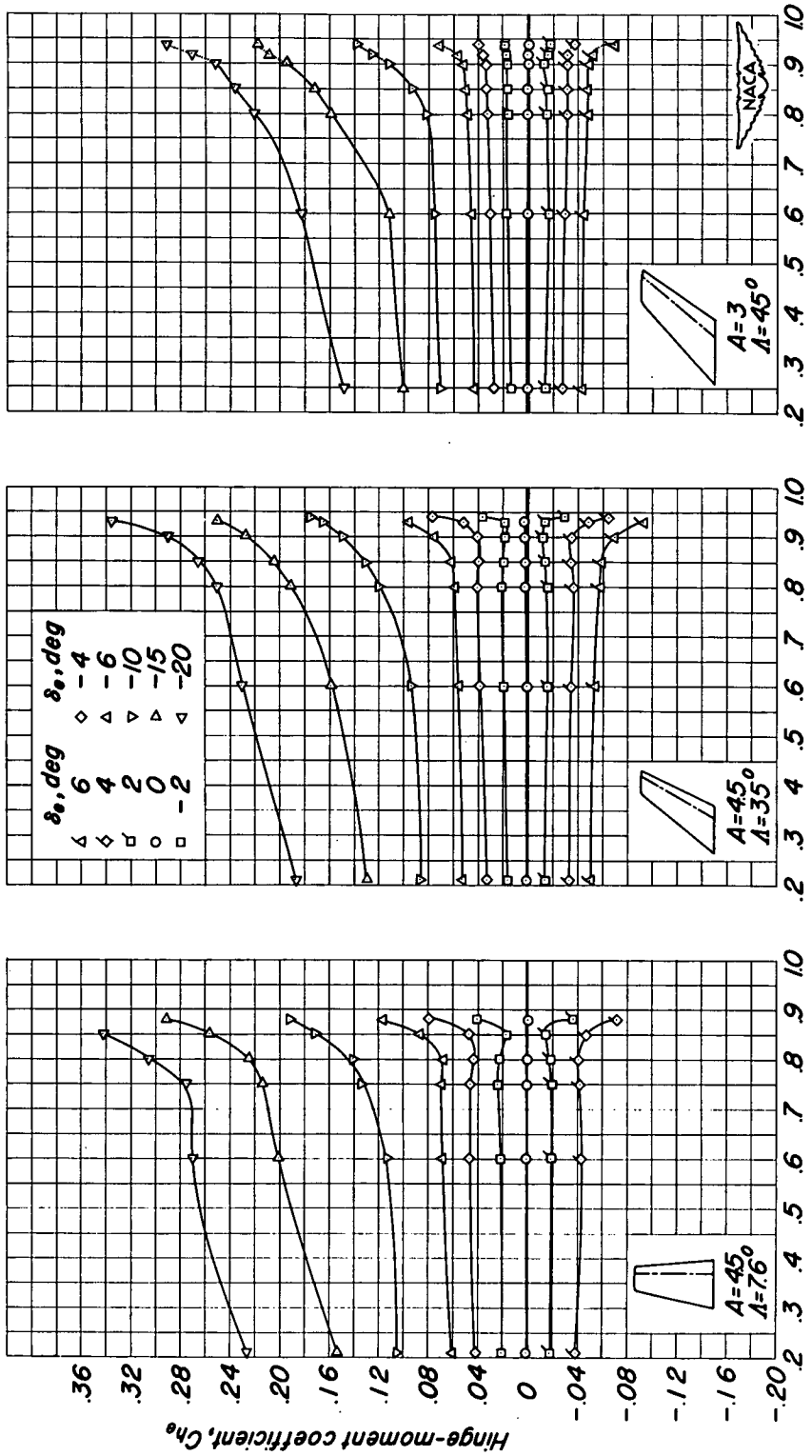

(b) $\alpha = 0°$.

Figure 24.–Concluded.

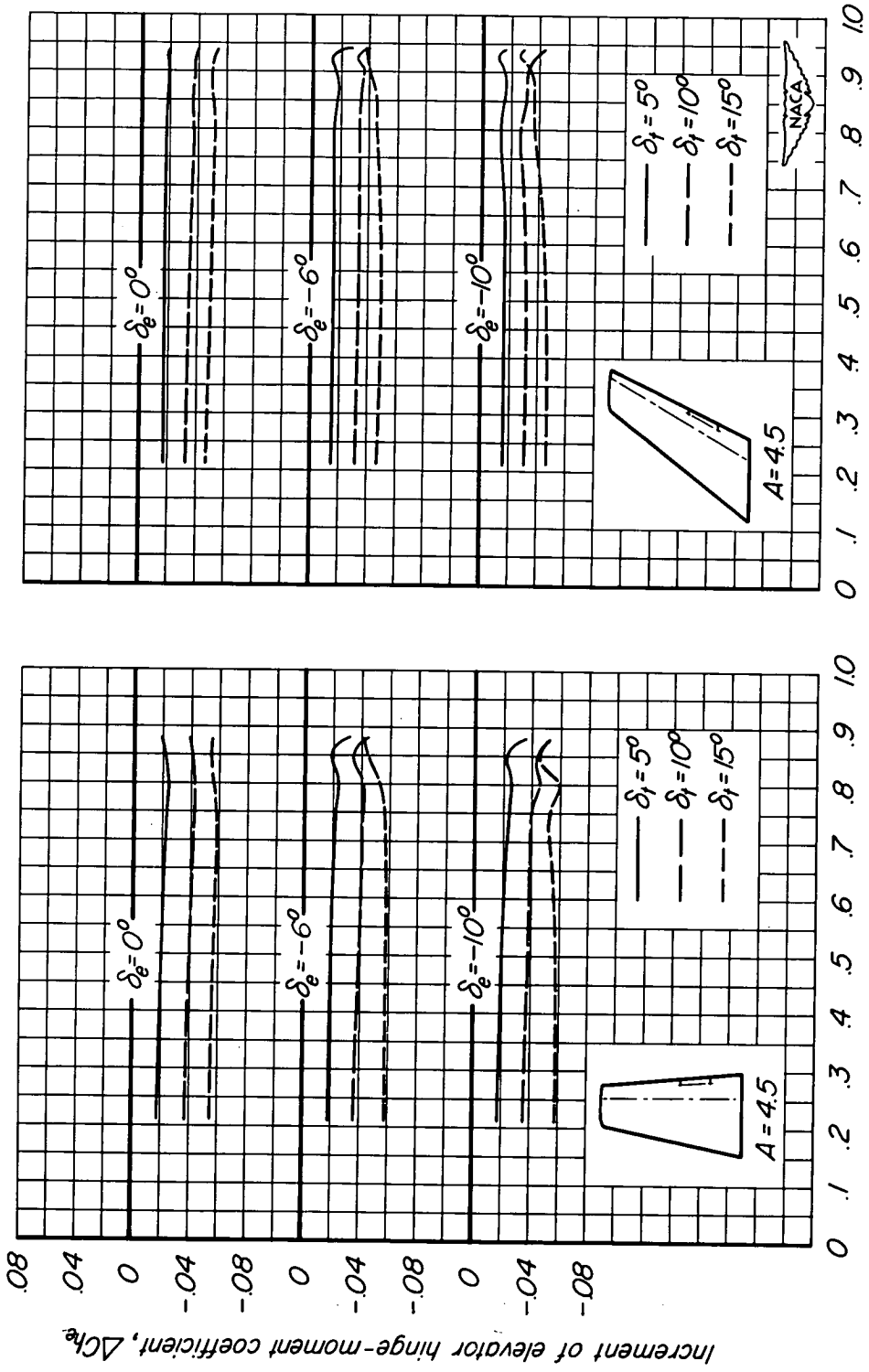

Figure 25.—The variation of the increment of elevator hinge-moment coefficient due to tab deflection with Mach number for the unswept and the 35° swept-back models of aspect ratio 4.5. $\alpha_u = 0°$; R, 2.0×10^6.